MINI REVIEW

Check for updates

Recent advances in hydrogenation of CO_2 into hydrocarbons *via* methanol intermediate over heterogeneous catalysts

Poonam Sharma, Joby Sebastian, Sreetama Ghosh, Derek Creaser and Louise Olsson [ID]*

The efficient conversion of CO_2 to hydrocarbons offers a way to replace the dependency on fossil fuels and mitigate the accumulation of surplus CO_2 in the atmosphere that causes global warming. Therefore, various efforts have been made in recent years to convert CO_2 to fuels and value-added chemicals. In this review, the direct and indirect hydrogenation of CO_2 to hydrocarbons *via* methanol as an intermediate is spotlighted. We discuss the most recent approaches in the direct hydrogenation of CO_2 into hydrocarbons *via* the methanol route wherein catalyst design, catalyst performance, and the reaction mechanism of CO_2 hydrogenation are discussed in detail. As a comparison, various studies related to CO_2 to methanol on transition metals and metal oxide-based catalysts and methanol to hydrocarbons are also provided, and the performance of various zeolite catalysts in H_2, CO_2, and H_2O rich environments is discussed during the conversion of methanol to hydrocarbons. In addition, a detailed analysis of the performance and mechanisms of the CO_2 hydrogenation reactions is summarized based on different kinetic modeling studies. The challenges remaining in this field are analyzed and future directions associated with direct synthesis of hydrocarbons from CO_2 are outlined.

1. Introduction

Global warming and dwindling fossil fuels have been a huge and growing recent concern for the human community. The excessive use of fossil fuels increases the emissions of CO_2 into the atmosphere and contributes to global warming.[1–3] Therefore, the conversion of CO_2 to value-added products is a very attractive method to use a non-toxic, renewable and abundant source of carbon[4] (Fig. 1). The synthesis of electrofuels also offers the possibility to produce carbon-based fuels from CO_2 and H_2O using renewable electricity as the primary source of energy.[5] There are two main sources of CO_2 emissions: 1) biogenic sources and 2) fossil sources. Biogenic emissions are from either natural or human harvesting, combustion, fermentation and decomposition of biomaterials. It involves carbon that is already in the biosphere and is thus part of the natural carbon cycle. Fossil carbon is derived from largely human driven combustion and processing of fossil resources, like natural gas, coal, and petroleum, and involves an unsustainable transfer of carbon that has been stored in the earth's crust for hundreds of millions of years into the biosphere.[6,7]

Carbon capture is the main technology to obtain CO_2 from different sources before and after its release into the atmosphere. The captured CO_2 can thereafter be either stored, *i.e.* carbon capture and storage (CCS), or utilized further in carbon capture and utilization (CCU). Pre-combustion, post-combustion, and oxyfuel combustion are the three main CO_2 capture systems related to different combustion processes.[8,9] Out of them, the post-combustion technology offers a way to capture CO_2 from flue gases that come from the combustion of fossil fuels. There are many separation technologies such as wet scrubbing, dry

Competence Centre for Catalysis, Chemical Engineering, Chalmers University of Technology, SE-412 96 Gothenburg, Sweden. E-mail: louise.olsson@chalmers.se
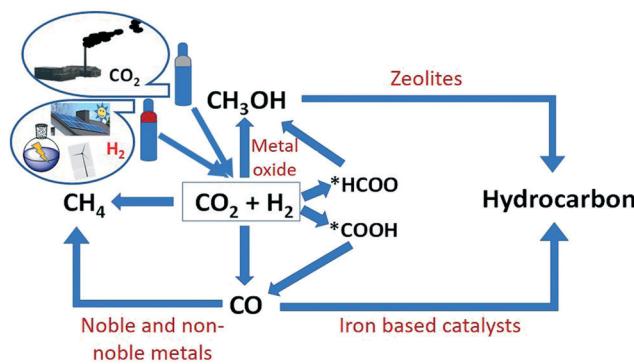
Fig. 1 Pictorial representation of regeneration of CO_2 to value-added products *via* hydrogenation.

This journal is © The Royal Society of Chemistry 2021

Catal. Sci. Technol., 2021, **11**, 1665–1697 | **1665**

regenerable adsorption, membrane separation, cryogenic distillation, pressure and temperature swing adsorption that can be used to isolate CO_2 from flue gases.[8] CCS could face many challenges concerning transportation and storage of CO_2, as there is a possibility for leakage and contamination of groundwater if geological storage is used.[10]

The utilization of CO_2 after capturing is an attractive way to mitigate CO_2 emissions. There are several processes where CO_2 can be utilized such as enhanced oil recovery,[11] mineralization,[12] and conversion into value-added chemicals and fuels.[13] However, CCU needs a large amount of energy for the conversion of CO_2 due to its kinetic inertness and thermodynamic stability, but it could function as a part of the sustainable natural carbon cycle in the biosphere, if the cost of the produced materials is equal to the cost of their production as well as possible offset costs for emissions while reducing the excess CO_2 emitted into the atmosphere.[14] The second main reagent for CO_2 transformation is hydrogen. Hydrogen itself is a renewable source of energy if it is produced from water splitting and using electricity from resources like wind, hydro and solar at low cost[15] but its handling, storage, and transportation are challenging, considering its explosiveness and low-energy density. It is therefore a large advantage to use hydrogen for the reduction of CO_2 and in this way to store energy in the form of chemicals and fuels, which are easier to store and transport. Therefore, the current focus of this review is the production of chemicals like CH_3OH (methanol) and value-added hydrocarbons such as lower olefins, gasoline, aromatics and petroleum gas from the hydrogenation (HYD) of CO_2.

The hydrocarbon synthesis could be possible *via* direct and indirect routes (Scheme 1).[16]

1. Indirect CO_2 hydrogenation to hydrocarbons
2. Direct CO_2 hydrogenation to hydrocarbons

There are two main routes in indirect synthesis of hydrocarbons from CO_2 which are (i) synthesis of CH_3OH and subsequent transformation into hydrocarbons (olefins, gasolines, aromatics, alkanes, and so on) in different stages and (ii) synthesis of CO *via* reverse water gas shift (RWGS) and then formation of hydrocarbons using a modified Fischer–Tropsch synthesis (FTS) process based on two reactor

$$CO_2 + 3H_2 \rightleftharpoons CH_3OH + H_2O \quad \Delta H = -49.5 \text{ kJ mol}^{-1} \quad (1) \text{ CO}_2 \text{ HYD}$$
$$CO + 2H_2 \rightleftharpoons CH_3OH \quad \Delta H = -90.4 \text{ kJ mol}^{-1} \quad (2) \text{ CO HYD}$$
$$CO_2 + H_2 \rightleftharpoons CO + H_2O \quad \Delta H = +41.5 \text{ kJ mol}^{-1} \quad (3) \text{ RWGS}$$
$$CO_2 + 4H_2 \longrightarrow CH_4 + 2H_2O \quad \Delta H = -165.0 \text{ kJ mol} \quad (4) \text{ Methanation}$$
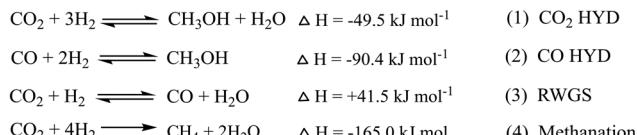
Scheme 2 Possible reaction between CO/CO_2 and H_2.

stages. Hydrocarbons can be synthesized by a direct route which could be more economically favourable and environmentally benign compared to indirect routes.[17,18] The direct route also includes two routes: (i) hydrocarbon synthesis over bifunctional catalysts in which CO_2 is first hydrogenated into CH_3OH and then hydrocarbon, and (ii) reduction of CO_2 to CO *via* the RWGS reaction followed by hydrogenation of CO to hydrocarbons *via* FTS. There are various possible reactions between CO/CO_2 and H_2 (Scheme 2), which could occur during CO/CO_2 hydrogenation.

Some reviews have explored the catalytic hydrogenation of CO_2 including various factors related to catalyst activity, selectivity and conversion of CO_2.[19–21] These reviews mainly focus on various aspects of CO_2 hydrogenation over noble and non-noble metal catalysts.[19–25] In this review, the objective is to focus on recent advances in CO_2 hydrogenation to hydrocarbons *via* methanol as an intermediate. In recent studies, CO_2 hydrogenation over bifunctional catalysts was found to be an efficient method to synthesize hydrocarbons. In addition, metal and metal oxide-based catalysts have been developed for the synthesis of CH_3OH and hydrocarbons directly from CO_2 reduction. Thus, this review includes these recent studies where hydrocarbons are synthesized directly from CO_2 in a single step combining CO_2 to methanol, and methanol to hydrocarbons reaction steps. The mechanisms, catalyst preparation methods, and proximity effects are discussed based on results from *in situ* experiments and DFT studies over bifunctional catalysts to understand the one-step process for the synthesis of hydrocarbons. To gain a flavor of how each process performs separately, detailed studies of CO_2 to methanol and methanol to hydrocarbons are also discussed in this review. More specifically, for the
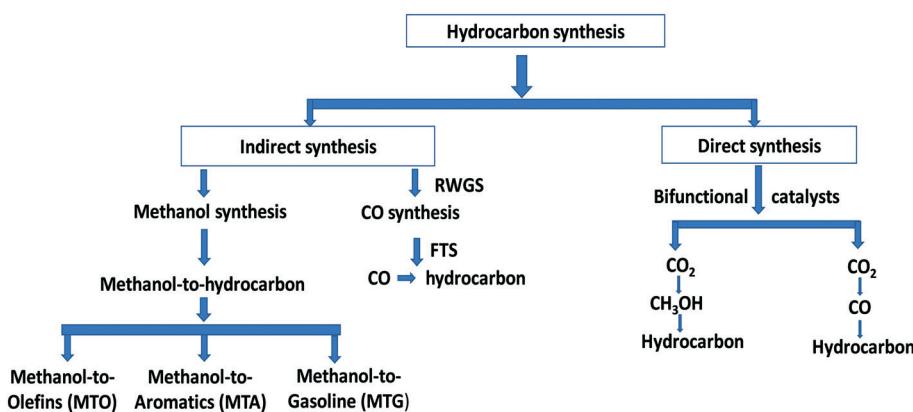
Scheme 1 A schematic overview of hydrocarbon synthesis.

1666 | *Catal. Sci. Technol.*, 2021, **11**, 1665–1697

This journal is © The Royal Society of Chemistry 2021

methanol to hydrocarbons process, we review the process from the perspective of the CO_2 to hydrocarbons process itself. Thus, the performance of catalysts in the presence of H_2, CO_2, and H_2O (the reactants and byproducts of the direct conversion of CO_2 to hydrocarbons process) is discussed in detail. Furthermore, this section also incorporates a review of the methanol to hydrocarbons process, reaction mechanism based on experimental evidence, shape selectivity, catalyst deactivation, and regeneration pathways for a better understanding of the direct conversion of CO_2 to hydrocarbons process discussed in detail in the following section. In addition, this review also provides an outline of various aspects like catalyst synthesis, catalytic activity and reaction mechanisms from experiments, DFT calculations, and a kinetic modeling section discussing the reaction kinetics for the conversion of CO_2 to methanol and methanol to hydrocarbons using advanced heterogeneous catalysts.

Thus, this review consists of four major sections which cover (1) CO_2 to methanol, (2) methanol to hydrocarbons, (3) CO_2 to hydrocarbons, and (4) kinetic modeling.

2. Indirect CO_2 hydrogenation

A variety of chemicals such as CH_3OH, dimethyl ether (DME), formic acid, ethanol, and hydrocarbons like methane, liquid fuels, aromatics and lower olefins are the products of CO_2 hydrogenation. There are many reports and reviews on the synthesis of these products from CO_2.[24,26] For example, Yang *et al.* reported the catalytic hydrogenation of CO_2 to value-added hydrocarbons.[20] Recently, Li *et al.* reviewed the recent advances in CO_2 hydrogenation to CH_4 and C_{2+} hydrocarbons over Ni, Co, Ru, Ir, Fe and Rh catalysts and discussed the metal–support interaction, effect of metal particle size, process integration, reaction mechanism, and catalyst deactivation during CO_2 hydrogenation.[27] This review section covers the indirect route of CO_2 hydrogenation into hydrocarbons which includes (1) CO_2 hydrogenation to CH_3OH and (2) CH_3OH to hydrocarbons (MTH). A detailed study of catalyst performance and reaction mechanisms is discussed below.

2.1 CO_2 hydrogenation to CH_3OH

This section gives an overview of the various reports on CH_3OH synthesis (Table 1). Methanol has been synthesized by heterogeneous and homogeneous catalysis, as well as electrochemical and photocatalytic processes.[28–34] In earlier studies, syngas was the main source for the production of CH_3OH as it can be produced from various sources such as biomass, natural gas, coal, and wastes, but in recent studies, CO_2 transformation into value added chemicals is found to be an important theme to use surplus CO_2 present in the environment. The main chemical reactions include direct CO_2 hydrogenation to CH_3OH according to:

$$CO_2 + 3H_2 \rightleftharpoons CH_3OH + H_2O, \quad \Delta H_{298K} = -49.5\,\text{kJ mol}^{-1} \quad (5)$$
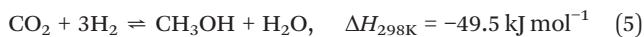
and the competing RWGS reaction:

$$CO_2 + H_2 \rightleftharpoons CO + H_2O, \quad \Delta H_{298K} = 41.5\,\text{kJ mol}^{-1} \quad (6)$$

From the above chemical reaction, it can be seen that CH_3OH synthesis from CO_2 and the direction of the reaction depends upon temperature, pressure and reactant ratio as the CO_2 hydrogenation to CH_3OH reaction is exothermic (eqn (5)), whereas the competitive RWGS reaction is endothermic (eqn (6)). Generally, a lower reaction temperature and higher reaction pressure favor the synthesis of CH_3OH. However, a high reaction temperature is helpful for CO_2 activation whereas the lower temperature is thermodynamically favorable for CH_3OH formation and this condition may create a kinetic limitation for the reaction. Under the reaction conditions, there are other competing reactions that occur in addition to RWGS that can produce many side products like methane, formaldehyde, and formic acid.[32] The water vapor and other side products inhibit the reaction and may cause catalyst deactivation.[35–37] To avoid the formation of side products and increase the stability of the catalyst, an efficient catalyst system is required.

$Cu/ZnO/Al_2O_3$ catalysts have been used and studied for the synthesis of CH_3OH from syngas at the industrial scale while at the laboratory scale, the Cu–ZnO system with various support materials has been studied extensively for CH_3OH synthesis.[38–40] A number of research groups have developed a wide variety of heterogeneous catalysts for the synthesis of CH_3OH from CO_2 hydrogenation. There are various reports in which Cu, Pd, Ag and Pt have been used as active catalysts and as promotors, and oxygen-deficient materials like In_2O_3 have been employed as active catalysts.[41–44]

2.1.1 Transition metal-based catalysts for methanol synthesis. Numerous reports and reviews based on transition-metal-catalyzed CH_3OH synthesis have been published as shown in Table 1.[22,23,25,45] Transition metals have been used for CO_2 hydrogenation due to their considerable activity and selectivity. Most of the studies have employed Cu-based systems, such as Cu–ZnO-based composites, that have demonstrated good activity for CH_3OH synthesis. In these studies, Al_2O_3 (alumina) and ZrO_2 (zirconia) have appeared as the most popular support materials.[46–48] Other than Cu, Pd-based catalysts with Ga_2O_3, CeO_2 and SiO_2 as supports have been screened for CH_3OH synthesis.[49–51] Bimetallic combinations like Co–Cu, Ni–Ga, Au–Cu, and Pd–Cu have been tested for CH_3OH synthesis from CO_2 hydrogenation.[52–56]

At the industrial scale, BASF was the first to produce CH_3OH from syngas.[57,58] The $Cu/ZnO/Al_2O_3$ catalyst, which was developed by ICI (Imperial Chemical Industries), allowed for industrial operation under milder reaction conditions.[59–61] In many reports, Cu has been used as an active catalyst and later it was modified with other metals and non-metal promoters. Activity and selectivity for CO_2 hydrogenation over Cu alone were not enough for large scale CH_3OH synthesis; thus appropriate changes were made to increase the activity and selectivity of catalysts.[62,63] No doubt, the achievable activity and

Table 1 Catalytic performance of transition metal-based catalysts in CO_2 hydrogenation to CH_3OH

Catalysts	P (MPa)	Preparation method	T (K)	GHSV (h^{-1})	CO_2 conv. (%)	CH_3OH select. (%)	Ref.
Cu/ZrO_2	1.7	Co-precipitation	493	—	6.0	67.0	46
Cu–ZnO	5	Co-precipitation	523	—	11.7	36.1	51
$Cu/ZnO/Al_2O_3$	4.9	Co-precipitation	523	—	19.7	48.1	47
Cu/ZrO_2	1.7	Sequential precipitation	623	—	6.9	70.0	48
Cu/ZrO_2	2	Deposition–precipitation	513	5400	6.3	48.8	64
$Cu/Zn/Ga/SiO_2$	2	Co-precipitation	543	—	5.6	99.5	83
Cu/Ga/ZnO	2	Co-precipitation	543	—	6.0	88.0	84
$Cu/YDC/\gamma-Al_2O_3$	3	Co-precipitation	523	—	na	78.6	87
Cu/ZnO/ZnO	2	Gel co-precipitation	513	7200	17.3	32.4	88
$Cu–ZnO–ZrO_2$	8	Co-precipitation	493	3300	21.0	68.0	81
$Mn–Cu/Zn/ZrO_2$	10	Thermal decomposition	553	3400	16.0	91.0	85
$Cu/Ga/ZrO_2$	2	Deposition–precipitation	523	2500	13.7	75.5	86
$Cu/B/ZrO_2$	2	Deposition–precipitation	523	2500	15.8	67.2	86
$Cu/Zn/Ga/ZrO_2$	8	Co-precipitation	523	3300	na	75.0	55
$Cu/Zn/Al/ZrO_2$	4	Co-precipitation	513	9742	18.7	47.2	89
$Cu–ZnO–Al_2O_3$	5	Co-precipitation	443	—	14.3	54.8	90
$Cu–ZnO–ZrO_2$	1.0–3.0	Co-precipitation	473	8800	5.8	55.2	91
$Cu–ZnO–ZrO_2$	3	Co-precipitation	503	—	15.2	35.1	82
$Cu/Zn/ZrO_2$	3	Co-precipitation	523	—	19.4	29.3	82
$Cu/Zn/ZrO_2$	3	Urea–nitrate combustion	513	3600	17.0	56.2	92
$Cu/Zn/ZrO_2$	3	Glycine–nitrate combustion	493	3600	12.0	71.1	93
$Cu/plate\ ZnO/Al_2O_3$	4.5	Precipitation	543	—	10.9	72.7	69
$Cu/Ga_2O_3/ZrO_2$	3	Ion exchange/impregnation	523	20 000	1.3	74.0	54
Cu/Al_2O_3	95	Impregnation	553	11 900–25 000	30.0	80.0	78
$Cu–ZnO–ZrO_2$	4	Co-precipitation	513	4000	na	na	94
$Cu–ZnO–Al_2O_3$	36	Co-precipitation	533	10 471	65.8	77.3	79
$Cu/ZnO/Al_2O_3$	3	Co-precipitation	503	—	18.3	43.0	80
$Cu/ZnO/ZrO_2/Al_2O_3$	3	Co-precipitation	503	—	23.2	60.3	80
$Cu–ZnO–ZrO_2$	3	Co-precipitation	513	3600	12.1	54.1	95
$Cu–ZnO–ZrO_2$	5	Co-precipitation	553	10 000	23.0	33.0	96
Cu/ZrO_2	3	Impregnation	553	—	12.0	32.0	97
Cu/ZrO_2	0.1	Deposition–precipitation	493	—	0.53	19.8	98
$Cu–ZnO–ZrO_2$	5	Co-precipitation	553	10 000	21.0	34.0	99
$Cu–ZnO–Al_2O_3$	44.2	Co-precipitation	553	10 000	65.3	91.9	77
$Cu–ZnO–ZrO_2$	3.9	Co-precipitation	473	7800	3.9	70.0	100
Pd/SiO_2	0.95	Incipient wetness	548	—	0.8	9.5	49
Pd/CeO_2	3	Impregnation	533	—	5.2	84.7	50
Pd/SiO_2	5	Co-precipitation	523	—	0.05	100	51
Pd/Ga_2O_3	5	Co-precipitation	523	—	19.6	51.5	51
PdZn/h-CNTs	3	Impregnation	523	1800	na	99.6	101
$Pd/\beta-Ga_2O_3$	3	Incipient impregnation	523	—	0.9	52.0	102
$PdGa/(\beta-Ga_2O_3)$	0.7	Incipient wetness impregnation	523	—	≤1	5.2	103
$Pd/plate\ Ga_2O_3$	5	Deposition	523	—	17.3	51.6	104
$PdGa/(rod-Ga_2O_3)$	5	Impregnation	523	—	11.0	41.3	105
$Pd–Cu/SiO_2$	4.1	Impregnation	573	3600	6.6	34.0	52
Pd/ZnO	2	Sol-immobilization	523	—	10.7	60.0	106
PdZnAl/hydrotalcite	3	Co-precipitation	523	—	0.6	60.0	107
$Au/ZnO/ZrO_2$	8	Co-precipitation	493	3300	1.5	100	81
$Au/Cu–ZnO–Al_2O_3$	1–6	Co-precipitation	533	7000–13 200	28.0	55.0	56
Au/ZnO	0.5	Deposition–precipitation	493	—	0.2	56.2	108
Au/ZnO	0.5	Deposition–precipitation	513	—	1.0	70.0	109
Ni_5Ga_3/SiO_2	1	Impregnation	483	6000	na	na	110
PtW/SiO_2	3	Impregnation	473	—	2.6	92.2	111
Re/ZrO_2	1	Impregnation	433	—	na	73.2	112
Rh/TiO_2	1	Impregnation	513	2400	na	60.7	113
Rh/SiO_2	5	Impregnation	473	—	0.5	6.8	114
Rh/TiO_2	2	Incipient wetness impregnation	543	3000–6000	7.9	0.8	53
$Rh–Fe/TiO_2$	2	Incipient wetness impregnation	543	3000–6000	9.2	1.2	53
$Ag/ZnO/ZrO_2$	8	Co-precipitation	493	3300	2.0	97.0	81
La–Zr–Cu–ZnO	5	Sol–gel	523	3600	13.0	52.5	115

na = not available.

selectivity depend on other factors as well like the catalyst composition, catalyst preparation method and reaction conditions which also affect the surface structure of the catalyst.[64] ZnO has been found to be most preferably combined

with Cu, as it facilitates the dispersion and stability of the active Cu sites by providing a close contact between itself and the Cu phase.[23,25,65] The interface between Cu and ZnO plays a crucial role in preparing a highly active catalyst and it can be optimized by various factors like temperature, hydrogen partial pressure, and heating rate.[66,67] In addition, the exposed phase of ZnO which is in contact with Cu regulates the catalytic activity of the Cu/ZnO system.[68,69] Lei et al. studied the morphology effect of ZnO and found that the (002) face of ZnO gave good results in CH_3OH synthesis due to its higher concentration of oxygen vacancies.[68] Several efforts have been made to increase the activity of the Cu/ZnO system by fabricating new structures of the catalyst like a core–shell design of Cu–ZnO, graphitic-like ZnO and nano-alloy layers of Cu–Zn.[66,67,70,71] Further, Cu/ZnO-based catalysts have been modified with promotors and stabilizers to increase the activity and stability.[72,73] Later, it has been reported that the addition of Al_2O_3 increases the stabilization of the Cu active site.[74] Another method to increase activity is to focus on the synthesis process. The conventional synthesis process for $Cu/ZnO/Al_2O_3$ is co-precipitation in which the synthesis of hydroxycarbonates of Cu, Zn and Al_2O_3 is a crucial stage. This stage can alter the surface area of Cu and the interaction between ZnO and Cu that are the important factors to define/change the activity of the catalysts.[29,75] The synthesis of the hydroxycarbonates can be controlled by pH, temperature and precipitate washing.[76]

Gaikwad et al. studied the effect of pressure, temperature, and GHSV (gas hourly space velocity) on CO_2 hydrogenation to CH_3OH over a commercial $Cu/ZnO/Al_2O_3$ catalyst.[77] Excellent results were observed at 44.2 MPa with a low GHSV in the range of 533–553 K (Table 1). In this study, the authors achieved the highest CH_3OH selectivity compared to the other $Cu/ZnO/Al_2O_3$-based studies mentioned in Table 1 along with high CO_2 conversion. Cu/Al_2O_3 has also been screened for CH_3OH synthesis at 95 MPa to get a higher product yield and CO_2 conversion.[78] Tidona et al. reported a higher space-time yield at 95 MPa compared to 3 MPa.[78] In both studies, it can be noted though that the extreme pressures which are thermodynamically favorable played an important role in obtaining higher conversion and selectivity rather than the catalyst performance. To get higher CH_3OH selectivity, Bansode and Urakawa reported the effect of high H_2 partial pressure by decreasing the molar ratio of CO_2/H_2 from 1:3 to 1:10 and they found good CH_3OH selectivity and CO_2 conversion with excess CO_2.[79] Li et al. doped Zr into commercial $Cu/ZnO/Al_2O_3$ catalysts and studied the activity, stability and poisoning effect of water on the active sites of the catalysts.[80] The authors found excellent performance for the Zr-doped catalyst compared to the commercial catalyst with excellent tolerance for water vapor. Considering the positive effect of Zr in CO_2 hydrogenation, Al_2O_3 has been replaced with ZrO_2 in recent years. Słoczyński et al. synthesized a series of catalysts in which crystalline ZnO and amorphous ZrO_2 were co-precipitated with Cu, Ag, and Au.[81] The Cu-containing ZnO/ZrO_2 catalyst exhibited higher activity than Ag and Au. The effect of suspension ageing on a co-precipitated $Cu/ZnO/ZrO_2$ catalyst

was studied by Raudaskoski et al. and as a result, they found higher CO_2 conversion and selectivity to CH_3OH with increasing ageing time. With a longer ageing time, a fine crystallite structure of the catalyst was obtained with a high surface area and less sodium content as Na_2CO_3 was used as the precipitating agent. The longer ageing time also helped in the reduction of Cu.[82]

In addition, different modifiers are used to increase the activity and stability of the Cu-based system. Toyir et al. prepared a Ga-promoted Cu-based system in which SiO_2 and ZnO were used as supports. The hydrophilic nature of SiO_2 along with smaller particles of Ga_2O_3 enhanced the catalytic activity. The hydrophilic support increased the dispersion of the catalyst whereas the small Ga_2O_3 particles favor the formation of Cu^+.[83] Further, the same group studied the influence of metallic precursors on the catalytic performance of the Ga-promoted Cu-based system and found that the use of methanolic solutions of methoxide–acetic acid precursors in the Ga-promoted catalyst preparation played a key role in obtaining a high performance catalyst in CO_2 hydrogenation to CH_3OH.[84] Lachowska and Skrzypek investigated the effect of Mn as a promoter on Cu/Zn/Zr systems.[85] Later from the same group, Słoczyński et al. studied the effect of metal and metal oxides (Mn, B, In, Ga, Gd, Y, and Mg oxides) on the stability and activity of $Cu/ZnO/ZrO_2$ systems.[55] Among the various oxides, the Ga_2O_3 additive with the catalyst gave the highest CH_3OH selectivity. Liu et al. prepared $Cu/Ga_2O_3/ZrO_2$ and $CuO/B_2O_3/ZrO_2$ catalysts and in this study, they discussed the effect of the nanocrystalline Zr size on the catalytic performance.[86] It was observed that the nanocrystalline Zr changed various properties of the catalyst such as the electronic structure and the interaction between the metal and support, leading to more corner defects, facile reduction, and more oxygen vacancies on the surface, and all these changes were found to be beneficial for CH_3OH synthesis. Fornero et al. synthesized $Cu–GaO_x/ZrO_2$ catalysts and observed higher CH_3OH selectivity with a high Ga/Cu atomic ratio.[54] Besides Cu, other transition metals have been used for CH_3OH synthesis. In the literature, Pd-based catalysts are the most commonly studied for hydrogenation of CO_2 to CH_3OH after Cu. Erdöhelyi et al. reported various Pd-based catalysts supported on SiO_2, TiO_2, Al_2O_3, and MgO and concentrated on the surface species during the reaction.[49] It was observed that the dispersion of Pd plays an important role in controlling the direction of the $CO_2 + H_2$ reaction. Pd catalysts supported on CeO_2, SiO_2, Ga_2O_3 and carbon nanotubes (CNTs) were used for CH_3OH synthesis.[50,51] Bahruji et al. prepared Pd/ZnO catalysts by different methods and screened them for hydrogenation of CO_2. Their study includes the structure–activity relationship and they found the PdZn alloy to be the active site, where a high surface area, smaller alloy size, and less metallic Pd surface are favorable conditions to increase the selectivity for CH_3OH.[106] Liang et al. developed PdZn alloys supported on multiwalled CNT catalysts for CH_3OH synthesis where CNTs function as a promoter and catalyst support.[101] Pd–ZnO/CNT

This journal is © The Royal Society of Chemistry 2021

Catal. Sci. Technol., 2021, 11, 1665–1697 | 1669

catalysts were successful in providing a micro-environment with a higher concentration of active H-adspecies at the surface, whereas herringbone-type CNTs helped in the promotion of the catalysts.

Collins et al. studied Ga_2O_3 supported Pd catalysts and explained the function of Ga_2O_3 and Pd.[102] It is proposed in this catalytic system that gallium oxide provides a surface for adsorption of CO_2 as carbonate species and Pd dissociates the hydrogen molecule to hydrogen atoms that spillover to the oxide surface converting the adsorbed carbonate to formate species. Further, the same function and interaction between Pd and Ga were identified using quasi-in situ transmission electron microscopy by the same group.[103] The effect of the shape of Ga_2O_3 on interactions was explained by Zhou et al., where the (002) surface of Ga_2O_3 was found to be highly unstable, which readily provided more O-defect sites and electrons in the conduction band than other surfaces. It gave higher metal dispersion that led to the formation of $PdGa_x$ which was found to be more active for CH_3OH production.[104,105] In another metal series, Ni, Rh, Re, and Pt have been used for CH_3OH selectivity as they have higher activity towards the hydrogenation reaction.[53,112,113] Studt et al. explored the activity of Ni-based alloys (NiGa, Ni_3Ga and Ni_5Ga_3) for hydrogenation of CO_2 at ambient pressure.[110] Importantly, these alloys were superior to the $Cu/ZnO/Al_2O_3$ catalyst due to their ability to reduce the RWGS activity and favor CH_3OH production.[116,117] The structure effect of the alloys on the reaction was studied by Sharafutdinov et al.,[118] where a series of Ni–Ga catalysts were prepared with different compositions. Later, the catalysts were screened, and it was found that the reactivity depended on the catalysts' intermediate phase, particle size or structure. The Ni_5Ga_3 composition was found to be more active for CH_3OH selectivity among the various compositions.[110]

Many studies have reported the high reactivity of Au and Ag towards CH_3OH selectivity.[81,108,119] Hartadi et al. studied the pressure and CO effect over Au/ZnO catalysts and observed that high temperature and pressure inhibit the activity of the RWGS reaction and improve the product selectivity, whereas an increase in the CO concentration decreases the formation of CH_3OH.[119] Słoczyński et al. prepared Au and Ag-based catalysts with a support composition of $3ZnO–ZrO_2$ and studied the morphology, surface composition and activity of the catalysts for CH_3OH synthesis from CO_2.[81] In the $Au–Cu/ZnO/Al_2O_3$ system, the hydrogen spillover on the Au–Cu surface reduced the reaction selectivity towards CO.[56] Hartadi et al. reported about various Au supported catalysts (Au/Al_2O_3, Au/ZnO, Au/TiO_2, and Au/ZrO_2) and studied their activity for CH_3OH synthesis.[108] The Au/ZnO system was found to be more selective for CH_3OH synthesis and the authors extended this study to examine the effect of the catalyst size, total pressure, support, and influence of CO on the reaction activity.[119]

Frauenheim and Xiao reported first principles calculations for CO_2 hydrogenation on the ZnO supported Ag (111) monolayer.[120] The CO_2 adsorption on the pristine and stretched surface of Ag (111) was weak and the ZnO support increased the binding ability of CO_2 and catalytic activity due to a strong metal–support interaction. Furthermore, the phase diagram for the Ag-doped ZnO surface was investigated under hydrogen and oxygen atmospheres and found stable in a hydrogen atmosphere. Also, the Zn impurities do not affect the reactivity for CO_2 adsorption and reduction.

2.1.1.1 Reaction intermediates and mechanism over Cu-based systems. Since many reports are based on Cu-based systems, the reaction mechanism has been more explored on Cu-containing catalysts by means of experiments, analytical techniques, and DFT calculations.[89,121–124] Many studies have reported two key intermediates formed during the synthesis of CH_3OH.[125,126] Some research groups found the formate (HCOO*) intermediate[127,128] whereas others the hydrocarboxyl species (COOH*) on the surface of the catalysts. These intermediate species divide the mechanism into two routes: (1) formate route and (2) hydrocarboxyl route.[129,130] Scheme 3 below illustrates different possible reaction intermediates and steps during the hydrogenation of CO and CO_2 into CH_3OH over Cu.[131] Here, we will only elaborate on the intermediates that formed during CO_2 hydrogenation. Nakatsuji and Hu explained the formation of formate on Cu (100) and Zn/Cu (100) surfaces employing ab initio calculations and found that CO_2 reacts with surface hydrogen to form formate via either a Langmuir–Hinshelwood (LH) or an Eley–Rideal (ER) mechanism.[132] In the formate route, first CO_2 reacts with atomic hydrogen to form HCOO*. Further, this species again hydrogenates to HCOOH* (ref. 63) which is further hydrogenated making H_2-COOH* followed by cleavage into H_2CO* and *OH. Further, the subsequent hydrogenation of this species forms H_3COH. In the above route, the first atomic hydrogen attached with carbon (HCOO*) and the second hydrogen has two ways to attach: (A) it could attach again to carbon and form H_2COO* (ref. 40) and (B) it could bind with oxygen to make HCOOH* (ref. 133) which further could take hydrogen on the carbon atom whereas H_2COO* could take hydrogen on the oxygen atom before cleavage. Larmier et al. determined the surface intermediates on the surface of $Cu–ZrO_2$ using kinetics, in situ IR, NMR, and DFT.[121] The combined results showed the formation of the HCOO* intermediate and the $Cu–ZrO_2$ interface plays a crucial role in converting HCOO* to CH_3OH. Kattel et al. identified the same intermediate by kinetic Monte Carlo simulations, DFT, and X-ray photoemission spectroscopy (XPS) on the Cu–ZnO synergic interface.[129]

The second route favors the first attachment of atomic hydrogen with an oxygen of the CO_2 molecule rather than carbon to form *COOH. Further, the second atomic hydrogen also binds with the second oxygen of CO_2 followed by the formation of *OH and *COH. Then the third, fourth and fifth hydrogen atoms bond with carbon to finally yield CH_3OH.[126] In this route, there is one more possibility for successive hydrogenation. In this possible alternative, *COOH (cis-COOH) first dissociates into CO and OH and a further hydrogen atom binds with carbon to form methoxy which

Catalysis Science & Technology

Mini review
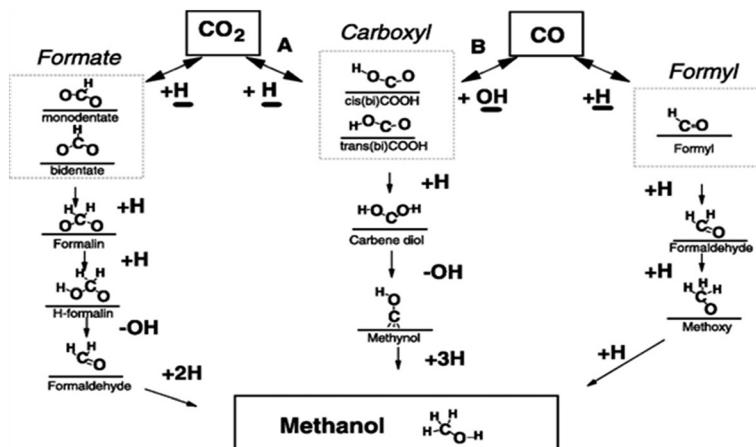
Scheme 3 Mechanistic pathways for conversion of CO and CO_2 to CH_3OH over Cu. Reprinted from *J. Catal.*, 298, Y. Yang, C. A. Mims, D. Mei, C. H. Peden and C. T. Campbell, Mechanistic studies of methanol synthesis over Cu from $CO/CO_2/H_2/H_2O$ mixtures: the source of C in methanol and the role of water, page no. 10–17, Copyright (2013), with permission from Elsevier.

then forms CH_3OH by the addition of hydrogen with oxygen. This intermediate was observed on Cu (111) and proposed based on a DFT study. The authors claimed based on their DFT calculations that CO_2 hydrogenation to methanol on Cu (111) *via* the hydrocarboxyl (*trans*-COOH) intermediate is kinetically more favorable than formate in the presence of H_2O *via* a unique hydrogen transfer mechanism. It was reported that the formate intermediate on Cu (111) is not feasible due to the high activation barriers for some of the elementary steps.[126]

Instead of the above two intermediates, Grabow *et al.* presented a model for CH_3OH synthesis that includes reaction intermediates such as hydroxymethoxy (CH_3O_2) and formic acid (HCOOH) on a commercial $Cu/ZnO/Al_2O_3$ catalyst.[133]

2.1.2 Metal and metal oxide-based catalysts for methanol synthesis. Most of the studies reported so far are on noble and non-noble metal systems.[129,134–136] Recently, oxide-based catalysts have been investigated for CO_2 hydrogenation apart from transition metal-based catalysts (Table 2). Oxide-based catalysts have different active sites than traditional metal catalysts with different reaction mechanisms. Recently, In_2O_3

was found to be a highly reported oxide for CH_3OH synthesis. The activity of In_2O_3 was studied for the RWGS reaction.[137–139] Moreover, some studies theoretically demonstrated the activity of In_2O_3 towards CH_3OH synthesis.[140,141] Sun *et al.* confirmed the previous theoretical studies and demonstrated with micro-kinetic modeling that the formation rate of CH_3OH increases with increasing reaction pressure.[44] Martin *et al.* synthesized ZrO_2 supported In_2O_3 which was found to be more stable (1000 h on stream) and more selective for CH_3OH synthesis (100% selectivity) than a reference $Cu–ZnO–Al_2O_3$ catalyst.[142] In addition, oxygen vacancies in In_2O_3 are considered to be active sites and the number of vacancies can be regulated by CO feeding and due to effective electronic interaction with the ZrO_2 support. Recently, In_x/ZrO_2 (x = 0.1–5 wt%) catalysts were screened for CH_3OH under industrially relevant conditions and a highly tunable selectivity for CH_3OH in CO_2 hydrogenation was observed.[143] With a loading of 2.5–5 wt.% of In, the catalysts have shown 70–80% CH_3OH selectivity between 523 and 553 K, whereas 0.1% loading of In exhibited a CO selectivity of up to 80%. It is observed that the

Table 2 Catalytic performance of oxide-based catalysts in CO_2 hydrogenation to CH_3OH

Catalysts	Preparation method	T (K)	P (MPa)	GHSV (h^{-1})	CO_2 conv. (%)	CH_3OH select. (%)	Ref.
In_2O_3	Calcination	543/603	4	15 000	1.1/7.1	54.9/39.7	44
In_2O_3/ZrO_2	Impregnation	573	5	16 000	5.2	99.8	142
$ZnO–ZrO_2$	Co-precipitation	588	5	24 000	>10	91.0	147
Pd/In_2O_3	Incipient wetness impregnation	573	5	>21 000	>20	>70	146
$Pd–P/In_2O_3$	Impregnation	498/573	5	—	3/20	6.01/27.81	146
In_5/ZrO_2	Impregnation	553	5	24 000	na	60.0	143
$Cu–In–Zr–O$	Co-precipitation	523	2.5	18 000	1.48	79.7	148
$Ga_{0.4}In_2–xO_3$	Co-precipitation	593	3	—	12.5	26.4	149
$In : Pd$ (2 : 1)/SiO_2	Incipient wetness impregnation	573	5	—	na	61.0	150
$Pd–In_2O_3$	Co-precipitation	553	5	—	na	78.0	151
Pt/In_2O_3	Impregnation	303	0.1	—	37.0	62.6	152
$Pd/In_2O_3/SBA-15$	Wetness impregnation	533	4	—	12.6	83.9	153

na = not available.

This journal is © The Royal Society of Chemistry 2021

Catal. Sci. Technol., 2021, **11**, 1665–1697 | **1671**

distribution of products depends on the interfacial structure of ZrO_2 and In_2O_3.

Luo et al. developed a porous 3D hierarchical indium-based catalyst for selective CO_2 reduction via electrodeposition and they showed that it exhibits an extremely high HCOO production rate and excellent selectivity with high stability.[144] The reduction of CO_2 to formate is explained by DFT calculations. In this study, Pd/In-nano particles (NP) having different compositions were screened in the liquid phase hydrogenation of CO_2 and they were found to have higher CH_3-OH synthesis activity than $Cu/ZnO/Al_2O_3$, Pd (0) and In_2O_3. Microkinetic modeling and DFT calculations were conducted to examine the reaction mechanism on the Pd_4/In_2O_3 catalyst.[145] They found that the strong interaction between In_2O_3 and Pd occurs during reduction and forms bimetallic species that change the nature of interfacial sites which were found detrimental to CH_3OH synthesis. Later, Rui et al. used a Pd loaded In_2O_3 catalyst for CH_3OH synthesis in which they used a Pd–peptide composite to prevent the formation of Pd–In bimetallic species during mixing with In_2O_3.[146] The peptide templates bond to Pd ions through electrostatic interaction between peptide sites (negative charge) and Pd^{2+}, which control the facet and size of catalysts under mild conditions. After confinement of Pd NPs on In_2O_3, the peptide composite was removed by thermal treatment. Recently, Frei et al. reported a different method to stop the formation of Pd–In bimetallic species, in which the Pd clusters were anchored on the In_2O_3 lattice by coprecipitation and stabilized by Pd atoms which were embedded into the In_2O_3 matrix.[151] This preparation method helped to modify the electronic properties of the catalyst which increased the formation and dispersion of Pd atoms. The CH_3OH formation rate on this catalyst was found to be higher than $Pd-P/In_2O_3$.[146] García-Trenco et al. prepared unsupported PdIn (Pd : In = 1 : 1) intermetallic nanoparticles using a thermal decomposition method for liquid phase CH_3-OH synthesis under the reaction conditions of 5 MPa at 483 K with a ratio of 3 : 1 of $H_2 : CO_2$.[42] The catalyst exhibited around 70% higher CH_3OH rates and higher stability than the conventional $Cu/ZnO/Al_2O_3$ catalyst. Recently, the promotional effect of Pd on the In_2O_3 catalyst was investigated using in situ X-ray spectroscopy, microkinetic modeling, and ex situ characterization.[150] Silica (SiO_2) supported catalysts were prepared and tested for CH_3OH synthesis by varying In : Pd ratios on SiO_2 (0 : 1, 1 : 0, 1 : 1, 2 : 1, 1 : 2). Out of the various catalysts, the In : Pd catalyst having a 1 : 2 ratio on SiO_2 showed the highest activity and selectivity towards CH_3OH. It was observed from characterization that the catalyst has an In_2O_3 phase and In–Pd intermetallic compounds gave the highest CH_3OH formation. Further, DFT and experimental results suggested that the active phases were formed due to the synergistic interaction between the In_2O_3 phase and a bimetallic In–Pd particle.

The authors found a similar composition–activity behavior in the case of In–Ni systems.[150] Recently, Men et al. prepared Pt NP incorporating In_2O_3 catalysts for CH_3OH synthesis using a dielectric barrier discharge plasma reactor.[152] The

catalyst presented good activity and selectivity to CH_3OH at 303 K and 0.1 MPa. A composition of Cu–In–Zr–O was reported by Yao et al. to act as a bifunctional catalyst, where defective In_2O_3 adsorbs CO_2 and Cu-sites adsorb and provide active hydrogen to adjacently adsorbed CO_2.[148] Commercial CH_3OH synthesis occurs in a temperature range of 473–533 K but recently, Akkharaphattawon et al. reported CH_3OH synthesis over $Ga_xIn_{-x}O_3$ at a higher temperature range (593–673 K).[149] Fan's group reported various multiple-metal catalysts including In_2O_3, like $Ni-In-Al/SiO_2$ and $La-Ni-In-Al/SiO_2$ for the synthesis of CH_3OH at low-pressure.[154,155] Wang et al. synthesized a $ZnO-ZrO_2$ catalyst for CH_3OH synthesis which showed good CH_3OH selectivity and sulfur resistance.[147] In addition, the high CH_3OH selectivity was due to the synergetic effect between Zr and Zn sites.

2.1.2.1 Reaction intermediates and mechanism over oxide-based catalysts. Before methanol synthesis, In_2O_3 and its composites have been studied for CH_3OH steam reforming, dehydrogenation of propane[156] and other chemical transformations.[157–159] In this section, a plausible reaction mechanism based on DFT and in situ infrared Fourier transform spectroscopy DRIFT studies over In-based catalysts is discussed. Ghuman et al. investigated the role of surface hydroxy groups and oxygen vacancies in the photochemical and thermal reduction of CO_2 to CO on In-based catalysts (Fig. 2a).[160] The kinetic study, in situ spectroscopy, and DFT calculations showed that the oxygen vacancies and hydroxy groups both assist the RWGS reaction (Fig. 2a). The activation energy estimated for the RWGS reaction was 86 kJ mol^{-1} for photochemical reduction whereas it was 107 kJ mol^{-1} for thermal reduction. This study has opened a way to understand the surface conditions that can increase the activity of the catalyst towards the RWGS reaction, which is a concurrent reaction in the case of CH_3OH synthesis. A similar activity towards the RWGS reaction was reported by other groups.[137,138,161] Ye et al. investigated the adsorption and hydrogenation of CO_2 on the (110) surface of In_2O_3 via DFT calculations.[140] Later, the same group found that the oxygen vacancy on the surface of In_2O_3 could act as an active site for CH_3OH synthesis via computational modeling.[141] A mechanism was proposed from various reports as shown in Fig. 2b by Tsoukalou et al.,[162] in which oxygen vacancies termed as V_o sites were formed on the In_2O_3 surface. The presence of V_o sites was verified by various experiments based on electron paramagnetic resonance spectroscopy (EPR), X-ray photoelectron spectroscopy (XPS), and temperature-programmed desorption (CO_2-TPD) of In_2O_3-based catalysts.[140–142,159] These V_o sites assisted CO_2 hydrogenation and activation by stabilizing the HCOO*, H_2COO* and H_2CO* species and the hydrogenation of H_2CO* was found to be the rate determining step. It was observed that these sites could be recovered during hydrogenation of CO_2. Later, Sun et al. experimentally confirmed the activity of In_2O_3 and reported 54.9% CH_3OH selectivity at 543 K.[44] It was observed that CO_2 conversion increases and CH_3OH selectivity decreases with rising

1672 | Catal. Sci. Technol., 2021, 11, 1665–1697

This journal is © The Royal Society of Chemistry 2021
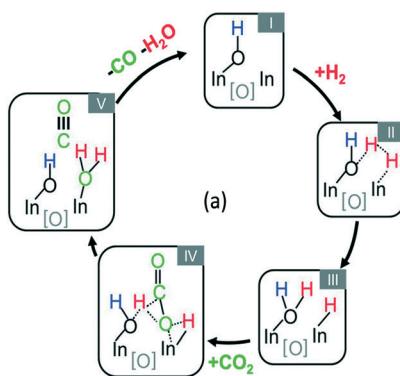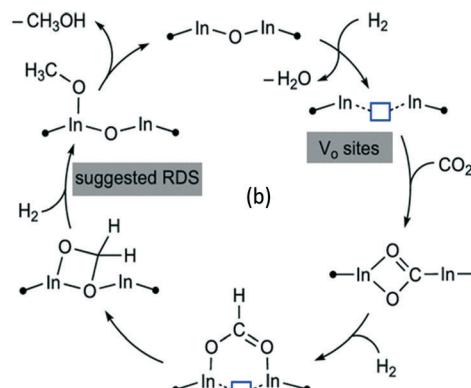
Fig. 2 A proposed mechanism for (a) the $CO_2 + H_2 \rightarrow CO + H_2O$ reaction on $In_2O_{3-x}(OH)_y$. Reproduced from ref. 160 with permission from the Royal Society of Chemistry. (b) The hydrogenation of CO_2 to CH_3OH on V_o sites of In_2O_3. Reprinted (adapted) with permission from A. Tsoukalou, P. M. Abdala, D. Stoian, X. Huang, M.-G. Willinger, A. Fedorov and C. R. Müller, *J. Am. Chem. Soc.*, 2019, **141**, 13497–13505. Copyright (2019) American Chemical Society.

temperature. Oxygen vacancies were found to be the active sites which were generated using thermal treatment or diluted hydrogen by the Pérez-Ramírez group.[142] It was reported that thermally-induced oxygen vacancies had a higher CH_3OH space time yield (STY) than H_2-induced vacancies and it was found that hydrogen treatment reduced the surface area of In_2O_3. In addition, operando diffuse reflectance (DRIFTS) showed that adsorbed CO_2 bridges with two In-atoms around thermally induced oxygen vacancies and hydrogenated intermediates formed thereof. The CH_3OH selectivity was also increased by Cu addition to In_2O_3 where it was proposed that Cu helped to generate atomic hydrogen which was transferred to CO_2 adsorbed on the surface of In_2O_3.[148] In some reports, oxygen vacancy formation was increased by CO co-feeding and introducing Pd nanoparticles.[142,145,146] Recently, a few reports discussed the positive synergetic effect between Pd and In for CH_3OH synthesis.[42,150] The adsorption, reactivity of hydrogen, defect formation, and bonding on different In_2O_3 samples were studied and as a result, the surface reduction, bonding of hydrogen, and formation of oxygen vacancies were observed after exposure to hydrogen at 573 K.[163]

A DFT study proposed a mechanism for CO_2 hydrogenation on In_2O_3 where oxygen vacancies were created on the indium surface which aided the heterolytic cleavage of hydrogen. Further, the hydrogen atom was transferred to chemisorbed CO_2 to start the hydrogenation and formation of various intermediates. According to this study, the route for CH_3OH synthesis on In_2O_3 is shown below:[140,141] (eqn (7))

$$CO_2 \rightarrow *HCOO \rightarrow *H_2CO \rightarrow *H_3CO \rightarrow CH_3OH \qquad (7)$$
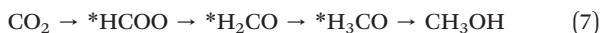
The proposed intermediates were $*HCOO$, $*H_2COO$ and $*H_3CO$. The stability of the intermediates was explained based on a kinetic study. Chen *et al.* reported the stability and bonding strength of these intermediate species on the In_x/ZrO_2 catalyst system during CO_2 hydrogenation and how the loading of In affects the product selectivity.[143] Fig. 3 shows that CH_3OH was

the main product in the case of 2.5 wt% loading of In on ZrO_2 while 0.1 wt% In loading gave CO as the main product. The authors found *via* a DRIFTS study that among the various intermediates, $*HCOO$ was the most abundant and stable with low loading of In on ZrO_2 ($In_{0.1}/ZrO_2$). $*HCOO$ formed on the $In–ZrO_2$ interfaces and further hydrogenation was difficult due to the lack of active dissociated H_2 from $In_{0.1}$, which led to
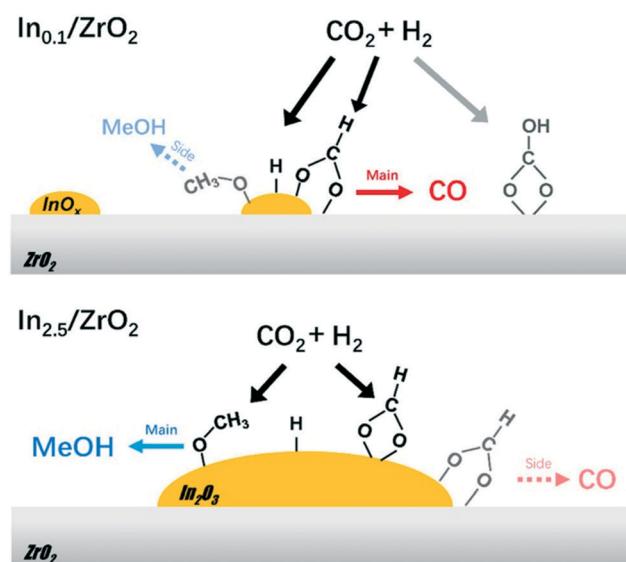
Fig. 3 CO_2 hydrogenation pathways and schematic–structure–performance relationships over In_x/ZrO_2. Reprinted (adapted) with permission from T.-y. Chen, C. Cao, T.-b. Chen, X. Ding, H. Huang, L. Shen, X. Cao, M. Zhu, J. Xu and J. Gao, *ACS Catal.*, 2019, **9**, 8785–8797. Copyright (2019) American Chemical Society.

This journal is © The Royal Society of Chemistry 2021

Catal. Sci. Technol., 2021, **11**, 1665–1697 | **1673**

subsequent decomposition to CO. Meanwhile with 2.5 and 5 wt% In loading, stepwise hydrogenation of the *HCOO intermediate occurred forming *H_3CO, and leading to CH_3OH on the catalyst. In addition, the STY of CH_3OH and CO varies with the loading percentage of In over ZrO_2. Apart from the conventional theory that oxygen vacancies are the most active sites for methanol synthesis on In_2O_3, Posada-Borbón and Grönbeck showed that oxygen vacancies may have only a minor role in facilitating CO_2 adsorption.[164] Instead, they have proposed that under reaction conditions the surface of In_2O_3 (110) is hydroxylated by either H_2 or water adsorption and largely vacancy free and as a result it is this hydroxylated surface that plays a significant role in methanol synthesis for CO_2 activation.

2.2 Methanol to hydrocarbons (MTH)

One of the earliest discoveries of the conversion of methanol to hydrocarbons (MTH) was reported by Mobil researchers in the late 1970s.[165,166] A zeolite-based catalyst (ZSM-5) was used for the reaction. This was then followed by the second oil crisis in 1979 which initiated extensive and systematic

research on the conversion of methanol to hydrocarbon-range product molecules, eventually leading to the commissioning of a methanol to gasoline (MTG) plant by 1985 in New Zealand (14 500 barrels per day).[166,167] Methanol can also be utilized as the starting chemical for the synthesis of light olefins (methanol to olefins, MTO process), branched alkanes, aromatics (methanol to aromatics, MTA process), etc., generally designated as the methanol to hydrocarbons (MTH) process. The choice of a given product depends largely on the selection of catalyst and the operating conditions, usually in the temperature range of 623 to 773 K and atmospheric pressure. The selectivity to olefins increases with a decrease in pressure (kinetic effect) and an increase in temperature (partly thermodynamic). The conventional starting material for methanol is coal and natural gas; however, nowadays sustainable resources like biomass and CO_2 are of increasing interest. Since the MTH process is a mature field of research, many excellent reviews are available in the literature covering the various aspects of the process including fundamental understanding, catalysts, structures, etc.[168–173] Here we attempt to provide a description of the
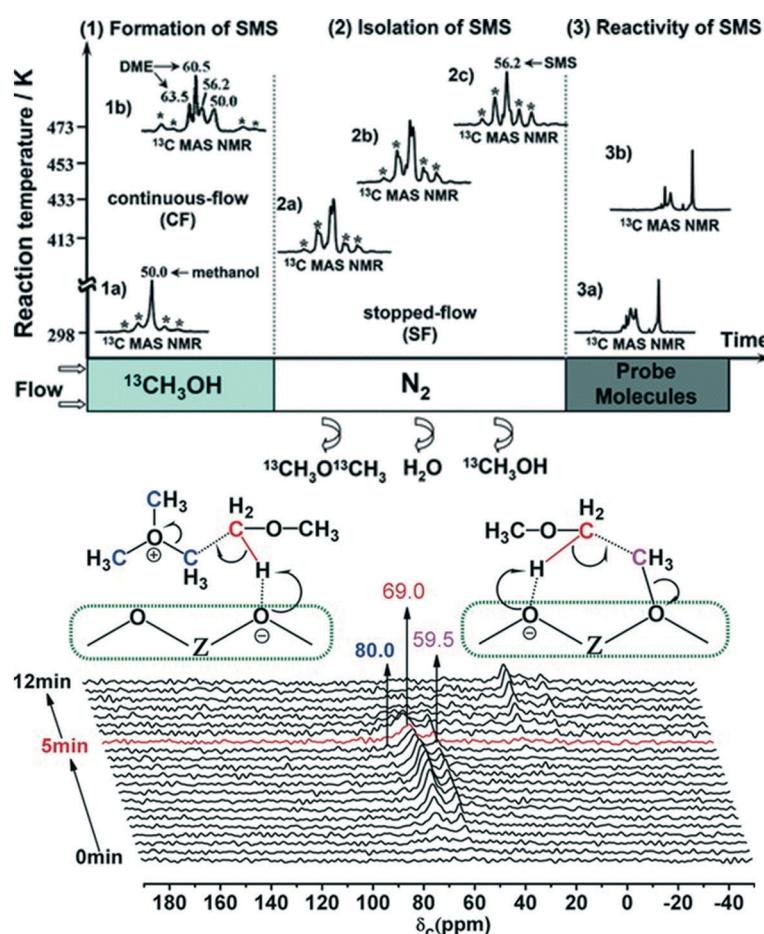
Fig. 4 Experimental evidence for surface methoxy species in different reaction environments (top panel), reprinted (adapted) with permission from W. Wang and M. Hunger, Acc. Chem. Res., 2008, 41, 895–904, Copyright (2008) American Chemical Society, and the first C–C bond formation route involving the trimethoxy oxonium species (bottom panel), Copyright (2017) Wiley, used with permission from X. Wu, S. Xu, W. Zhang, J. Huang, J. Li, B. Yu, Y. Wei and Z. Liu, Direct mechanism of the first carbon–carbon bond formation in the methanol-to-hydrocarbons process, Angew. Chem. Int. Ed., 2017, 56, 9039–9043, Wiley. 55, 15840–15845, Wiley.

1674 | Catal. Sci. Technol., 2021, 11, 1665–1697

This journal is © The Royal Society of Chemistry 2021

MTH process in the context of the direct conversion of CO_2 to hydrocarbons (CTH process, both direct and indirect) as it represents an intermediate and final step of the CTH process itself. Therefore, in this section, we limit our focus to an introduction to the reaction mechanism of the MTH process as a preamble solely based on experimental evidence, shape selectivity of zeolites in the MTH reaction, and performance of catalysts and their deactivation trends in the presence of CO_2, H_2 and H_2O as these molecules are involved in the CTH process. Moreover, a brief guide to the various approaches to regenerate the deactivated catalysts is also presented.

2.2.1 Mechanism of methanol to hydrocarbons. The reaction mechanism of the MTH process is highly complex. Researchers have reported more than 20 different pathways since its discovery.[168,169] Here, we discuss a few selected literature reports providing theoretical and experimental evidence for the presence of transient reaction intermediates involved in the first C–C bond formation from methanol, and the successive formation of higher hydrocarbons.

2.2.1.1 Experimental evidence for the first C–C bond formation mechanism. Brønsted acid sites on the zeolite catalyst are the active sites for the MTH process. The reaction initiates by the adsorption of methanol on these acid sites generating the surface methoxy species. The presence of these surface methoxy species has now been experimentally verified with the help of *in situ* MAS NMR spectroscopy (Fig. 4).[174,175] The next step is the generation of trimethyl oxonium ions. These can be generated by the reaction of surface methoxy species/methanol with dimethyl ether, formed *via* the dehydration of two methanol molecules at the Brønsted acid sites. Wu et al.,[176] with the help of the *in situ* solid-state ^{13}C MAS NMR spectroscopic technique, identified the presence of trimethoxy oxonium species on the catalyst surface (Fig. 4 (bottom panel)). Both the surface methoxy species and trimethoxy oxonium species can act as potential methylating agents *via* the carbene ylide mechanism. They can methylate dimethyl ether with the help of the Lewis acidic surface oxygen atom of the zeolite framework to generate the first C–C bond, *i.e.*, a surface adsorbed methoxyethane (Fig. 4 (bottom panel)). The methoxyethane's further transformation through the elimination of methanol generates the first C–C bond containing the ethene molecule. The surface methoxy species and trimethyl oxonium ion can also methylate methanol to form a surface adsorbed ethanol molecule, which upon further dehydration can also generate the ethene molecule.[176]

According to Li et al.,[177] the mechanism of the first C–C bond formation over SAPO-34 occurs through the formation of the methoxymethyl cation intermediate ($^+CH_2OCH_3$). The cation intermediate is formed from surface methoxy species and dimethyl ether. The methoxymethyl cation then reacts with another molecule of dimethyl ether or methanol to form 1,2-dimethoxyethane and 2-methoxyethanol, respectively, the compounds containing the first C–C bonds. The formation of the methyl cation was both theoretically and experimentally verified (Fig. 5).[177]
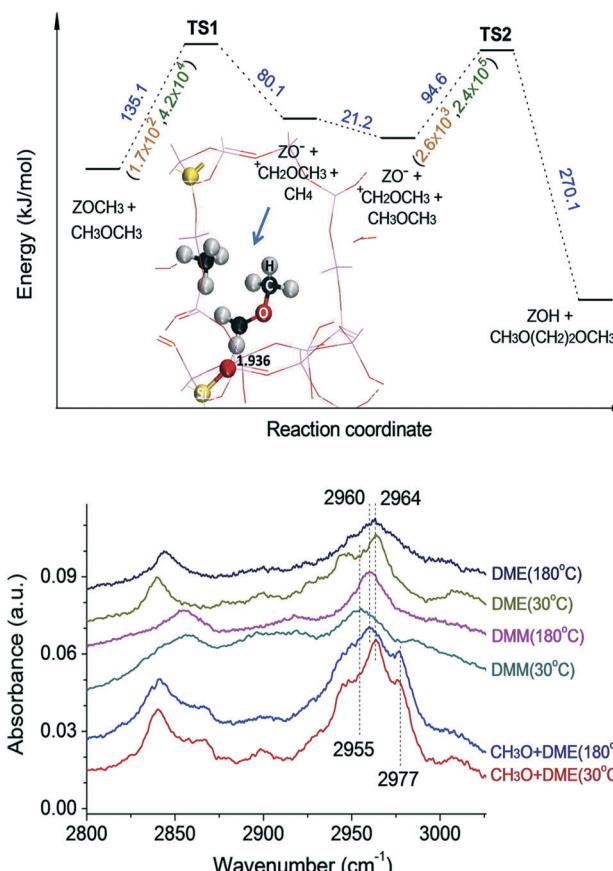

Fig. 5 Theoretical (top panel) and experimental (bottom panel) evidence for the methoxymethyl cation route, the band at 2960 cm^{-1} is assigned to the CH_2 group in CH_3OCH_2O-zeolite, DME = dimethyl ether, CH_3O = surface methoxy species, DMM = dimethoxymethane. This article was published in *Journal of Catalysis*, J. Li, Z. Wei, Y. Chen, B. Jing, Y. He, M. Dong, H. Jiao, X. Li, Z. Qin, J. Wang, and W. Fan, A route to form initial hydrocarbon pool species in methanol conversion to olefins over zeolites, *J. Catal.*, 2014, **317**, 277–283, Copyright Elsevier (2014).

Chowdhury et al.[178] presented experimental (MAS NMR) evidence for the involvement of acetate species in the first C–C bond formation over the SAPO-34 catalyst. In the proposed mechanism, the surface methoxy species undergo carbonylation (CO being derived *via* the decomposition of methanol) to form a surface-bound acetate species (the first C–C bond) which upon addition of a methanol molecule generates a surface adsorbed methyl acetate species (Fig. 6).[178]

2.2.1.2 Dual (arene and alkene) cycle mechanism – the hydrocarbon pool (HCP) mechanism. The dual cycle mechanism deals with the formation of reaction products (selectivity) after the first C–C bond formation. According to Dessau et al.,[179] various aliphatic and aromatic hydrocarbons in the MTH reaction can be considered to generate through the consecutive methylation by methanol as shown in Fig. 7 (top left panel). In principle, ethylene is methylated to form propylene. Further methylation of propylene yields butylene and the process carries on generating higher

This journal is © The Royal Society of Chemistry 2021

Catal. Sci. Technol., 2021, **11**, 1665–1697 | **1675**
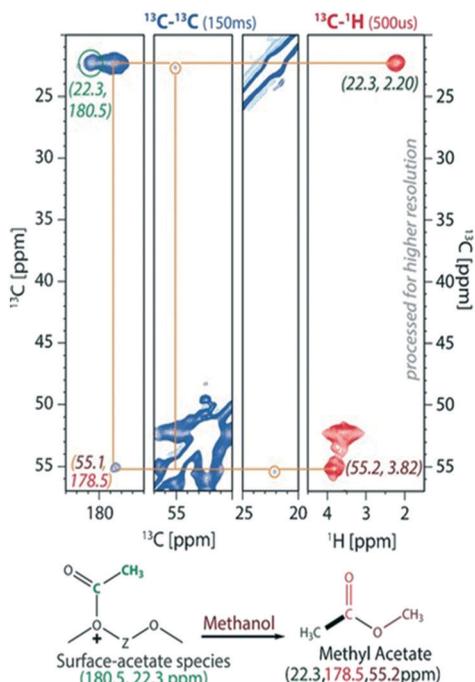
Fig. 6 Experimental evidence for the acetate route and the reaction pathway for the first C–C bond formation involving acetate species, Copyright (2016) Wiley, used with permission from A. D. Chowdhury, K. Houben, G. T. Whiting, M. Mokhtar, A. M. Asiri, S. A. Al-Thabaiti, S. N. Basahel, M. Baldus and B. M. Weckhuysen, Initial carbon–carbon bond formation during the early stages of the methanol-to-olefin process proven by zeolite-trapped acetate and methyl acetate, *Angew. Chem., Int. Ed.*, 2016, **55**, 15840–15845, Wiley.

hydrocarbons. Cyclization of the C_6 alkenes and further methylation produces various substituted aromatics.

Dahl et al.[180] used ^{13}C labeled methanol and ^{12}C labeled ethene over a SAPO-34 catalyst to verify the probable routes to higher hydrocarbon formation. The authors considered two mechanistic pathways; the first one was the previously suggested consecutive methylation path, and the second one was the "hydrocarbon pool" (HCP) type mechanism. The HCP is a pool of adsorbates having many characteristics similar to ordinary coke, represented as $(CH_x)_n$ with $0 < x < 2$. In the latter mechanism, methanol is continuously added to the pool of $(CH_x)_n$ species, causing their growth. The $(CH_x)_n$ species also undergo splitting/cracking to generate the product molecules (Fig. 7, top right panel). According to the experimental results (^{13}C and ^{12}C), only a minor part of propylene was formed from ethene and methanol, indicating that the HCP mechanism is more prevalent than the consecutive mechanism.

Arstad et al.[181] also supported the HCP mechanism, suggesting that the reaction proceeds through penta- and hexamethyl benzene intermediates (the hydrocarbon pool). ^{13}C labelled methanol and detailed analysis of the trapped molecules inside the SAPO-34 catalyst were used to verify the reaction route. In the early stages of the reaction, methylated benzenes were formed inside the large cavities of SAPO-34. Because of their large molecular size, they could not diffuse through the small pore openings, hence

undergoing cracking to form smaller hydrocarbons such as ethylene and propylene – called the aromatic or arene cycle.[181] In addition, higher alkenes are formed *via* the methylation of lower alkenes and their interconversions (methylation, water-assisted hydrogen transfer, alkyl transition, and olefin liberation) – called the alkene or olefin cycle.[182] In short, the olefins meet with methylation and cracking in the alkene cycle, and the aromatics meet with methylation and dealkylation in the aromatic cycle. These two cycles are interconnected by the dealkylation of aromatics to olefins and dehydrocyclization of olefins to aromatics.[183] Among these steps, the methylation step is regarded as the most difficult step and hence the rate-determining step of the entire process.
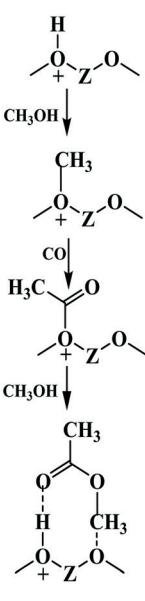
2.2.1.3 Control over arene versus alkene cycles. There are various factors that influence which cycle operates for product generation. For instance, the position of Al in the zeolite can control the alkene and aromatic cycles. Kim et al.[184] reported a larger amount of Al in the straight channels of their hierarchical mesoporous ZSM-5 than in the microporous ZSM-5. Free energy calculations showed that over the hierarchical ZSM-5, olefins were generated mainly through the alkene cycle (largely propylene) whereas, on the microporous ZSM-5, both alkene and aromatic cycles contributed almost equally to the olefins (both ethylene and propylene) (Fig. 7, bottom panel).

The pore diameter of the zeolites also influences the alkene and aromatic cycles. For instance, small-pore zeolites like SSZ-13 and SSZ-39 having large cages follow the aromatic cycle, only permitting the effusion of small hydrocarbons in the range of C_2–C_4. In contrast, the medium and large-pore zeolites, FER and BEA, respectively, favor the concurrent propagation of both the olefin cycle and the aromatic cycle, also favoring the effusion of C_4^+ hydrocarbons through their pore mouth.[185]

Over time, the olefin and aromatic cycles start to produce polycyclic compounds that no longer serve as reaction intermediates for the generation of hydrocarbons but stay as spectators (a nonactive hydrocarbon pool). With reaction time, they polymerize to form macromolecules that block the accessibility of reactant molecules to the active sites. This situation, which is unavoidable, leads to the deactivation of the catalyst.

2.2.1.4 Effect of zeolite topology on product selectivity. A small pore zeolite, SAPO-34 (CHA topology) having ellipsoidal cavities (10.4 × 12.0 Å) interconnected *via* narrow 8-membered ring apertures (3.8 × 3.8 Å), allows only the effusion of small chain molecules. The large cavities in it cause the HCP mechanism (arene cycle) to prevail, permitting only small molecules to escape through the pore aperture at the same time retaining the bulky reaction intermediates (the hydrocarbon pool). Therefore, it gives high selectivities to smaller olefins for instance ethylene and propylene. The effect of cavity sizes with the same ring apertures has also been reported. Bhawe et al.[186] chose zeolites with LEV, CHA, and AFX topologies for this investigation. These zeolites have different cavity sizes (LEV < CHA < AFX) with the same

1676 | *Catal. Sci. Technol.*, 2021, **11**, 1665–1697

This journal is © The Royal Society of Chemistry 2021
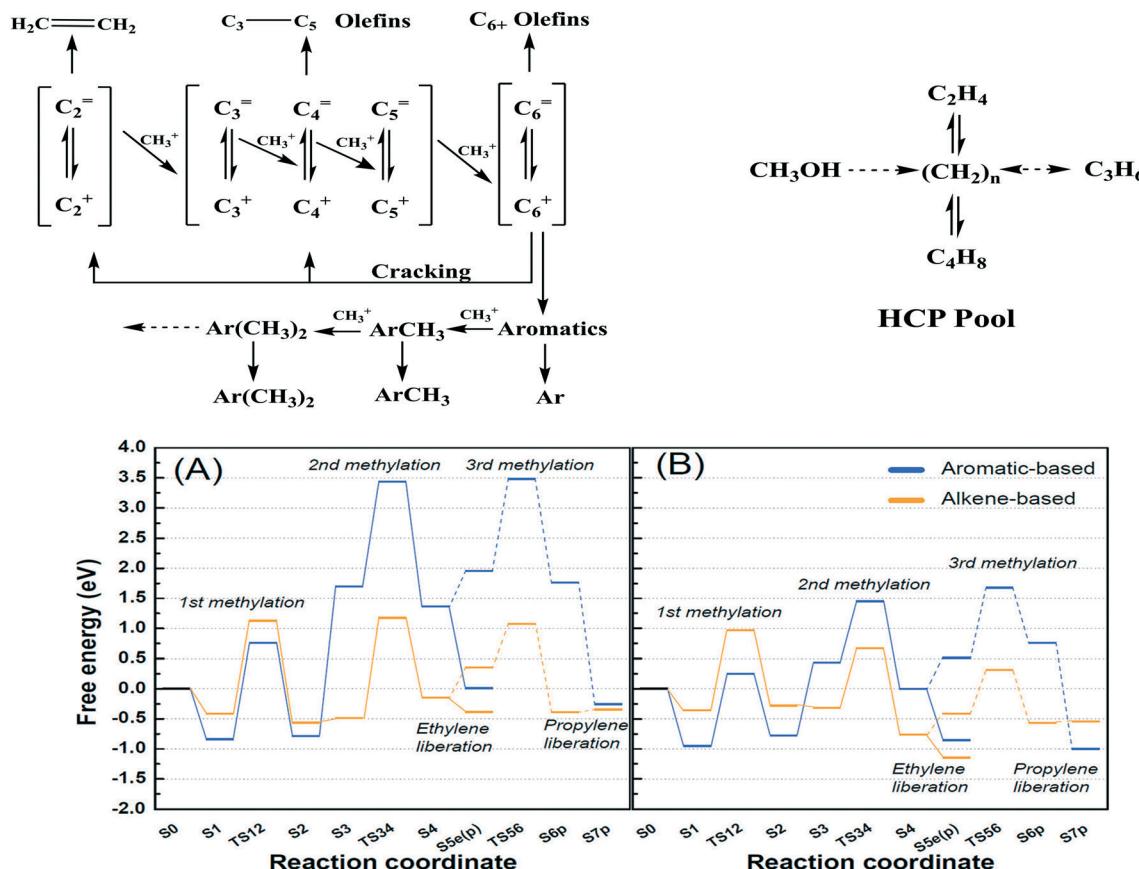
Fig. 7 Top left panel: Consecutive methylation scheme for higher hydrocarbons, this article was published in *Journal of Catalysis*, R. Dessau and R. LaPierre, On the mechanism of methanol conversion to hydrocarbons over HZSM-5, 1982, **78**, 136–141, Copyright Elsevier (1982). Top right panel: The HCP pathway, this article was published in *Journal of Catalysis*, I. M. Dahl and S. Kolboe, On the reaction mechanism for hydrocarbon formation from methanol over SAPO-34: I. Isotopic labeling studies of the co-reaction of ethene and methanol, *J. Catal.*, 1994, **149**, 458–464, Copyright Elsevier (1994). Bottom panel: Free energies of alkene- and aromatics-based MTO reactions at Al atoms situated at the straight channel – alpha position (A), and those situated at the channel intersection – beta position (B) of ZSM-5 zeolite,[169] reprinted (adapted) with permission from S. Kim, G. Park, M. H. Woo, G. Kwak and S. K. Kim, *ACS Catal.*, 2019, **9**, 2880–2892, Copyright (2019) American Chemical Society.

8-membered ring apertures. It was found that the ethylene selectivity decreased with increased cavity size. However, the CHA topology gave higher selectivity to propylene than AFX. The AFX material showed the lowest carbon yield. An
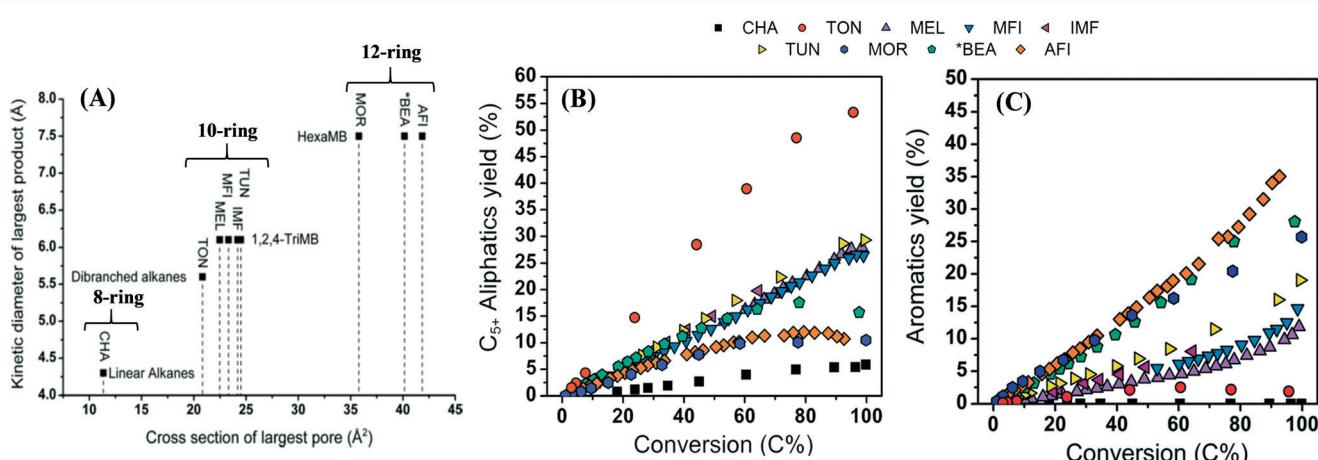
Fig. 8 (A) Cross-section of the largest pore of zeolites *versus* kinetic diameter of the largest product. (B) C_5^+ aliphatic yield over various zeolites as a function of conversion, 423 K, *P* (methanol) = 0.01 MPa. (C) Aromatics yield over various zeolites as a function of conversion, 423 K, *P* (methanol) = 0.01 MPa,[174] Bleken, S. Svelle, K. P. Lillerud and U. Olsbye, *Catalysis*, 2014, **26**, 179–217, reproduced by permission of The Royal Society of Chemistry.

increase in cavity dimension leads to the formation of larger polyaromatics *via* successive methylation, which no longer serve as active intermediates in the HCP mechanism, but leads rather to deactivation of the catalyst by polymerization to coke.[187] An intermediate cavity size appeared to be ideal for high olefin selectivity.[186]

On the other hand, a medium pore zeolite, ZSM-5 (MFI topology) with channel dimensions 5.3 × 5.6 Å (straight) and 5.1 × 5.5 Å (sinusoidal) having 10-membered ring apertures, can allow the effusion of larger molecules. Therefore, it can yield both lower olefins and gasoline range olefins.[188]

The large pore zeolite BEA (7.7 × 6.6 Å, 12-membered ring aperture) can give products ranging from C_2 alkanes/alkenes to C_{12} aromatics. This induces a limitation to the selectivity. Therefore, 12-ring aperture zeolites show little or no product shape selectivity in the MTH reaction.[189]

Fig. 8 shows a relation between the largest pore cross-section of zeolite *versus* the kinetic diameter of the largest hydrocarbon product, and the product distribution at various conversions. Zeolites with an 8-membered ring aperture give only linear alkanes during the reaction. If the ring aperture size is made up of 10-membered rings, the zeolite can give branched alkanes and/or aromatics. A further increase in the aperture size to 12-membered rings could produce heavily methylated benzenes. Bulky polymethyl benzene favors the formation of propene and butene, rather than ethene. The situation becomes more complex if the cavity size and the dimensionality of the pore system are taken into consideration.[169,189]

2.2.2 Effect of reaction environments and catalyst composition on deactivation. The main reason for the deactivation of zeolites during the MTH reaction is coke (polycyclic aromatic compounds) deposition. Fig. 9A shows the composition of occluded organic species in a deactivated SAPO-34 catalyst. These compounds are thus considered to be the precursors for coke formation. The catalytic or non-catalytic transformation (oligomerization, cyclization, hydrogen transfer and alkylation) of these precursors leads to the formation of coke of different kinds based on the catalyst structure and experimental conditions. Since coke formation is initiated at the acid sites, its adsorption at areas surrounding these sites inhibits the accessibility of acid sites to reactant/intermediate molecules. The position of coke could be on the internal surface of the micropores (called soft/internal coke) blocking the accessibility to the active sites or as a coating on the outer surface of the zeolite crystal (called external coke) blocking the entrance to the internal pores.[190,191] The growth of coke species inside the internal pore is limited by the size and shape of the pore. No such spatial limitation is anticipated for the external coke. The role (chemical nature, amount, and composition) of internal and external coke in deactivation was studied by Lee *et al.*[190] They chose MFI zeolites with different crystallite sizes. Regardless of the crystallite size and the reaction time, the
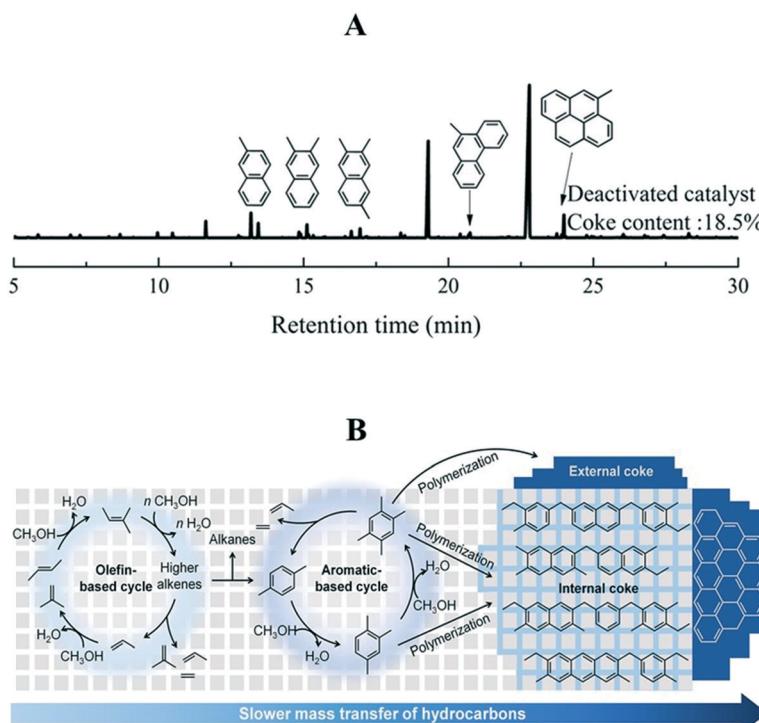
Fig. 9 (A) GC-MS chromatogram of organic species occluded in the deactivated SAPO-34 catalyst, reprinted (adapted) with permission from X. Zhao, J. Li, P. Tian, L. Wang, X. Li, S. Lin, X. Guo and Z. Liu, *ACS Catal.*, 2019, **9**, 3017–3025, Copyright (2019) American Chemical Society. (B) Internal and external coke formation mechanism, 673 K, *P* (methanol) = 0.025 MPa, WHSV = 6.46 to 86.1 h^{-1}, this article was published in *Journal of Catalysis*, S. Lee and M. Choi, Unveiling coke formation mechanism in MFI zeolites during methanol-to-hydrocarbons conversion, *J. Catal.*, 2019, **375**, 183–192, Copyright Elsevier (2019).

1678 | *Catal. Sci. Technol.*, 2021, **11**, 1665–1697

This journal is © The Royal Society of Chemistry 2021

chemical nature of both internal coke and external coke was found to be the same in all zeolites, only their amount was different. The internal coke had an H/C elemental ratio of 1.26 (density is 1.0 g cm^3) and the external coke had a ratio of 0.28 (density is 1.5 g cm^3).[190] Based on these values, the internal coke was proposed to be composed of polymeric structures of methylated acenes (benzene, naphthalene, and anthracene), and the external coke was composed of highly polyaromatic fused rings. Moreover, the internal coke contributed greater to catalyst deactivation than the external coke. Fig. 9B shows a proposed mechanism of internal and external coke formation during the MTH process.[190]

Deactivation by coke demands frequent regeneration of the catalyst by burning off the coke. Therefore, it is highly recommended to increase the lifetime of catalysts either by modifying the reaction environments or *via* the catalyst design.

2.2.2.1 Effect of co-feeding H_2, H_2O, and CO_2 on catalyst lifetime. Arora *et al.*[192] investigated the effect of H_2 co-feeding (0.4–3 MPa) on catalyst lifetime (SAPO-34) during the MTH reaction (673 K and 0.013 MPa of methanol). Almost 2.8 to 70 times greater catalyst lifetime was observed in the presence of H_2. Similar catalyst stability was also observed when ZSM-5 and SSZ-13 catalysts were used (3 and 4.5 times increase in stability for ZSM-5 and SSZ-13, respectively). It was rationalized that H_2 participated in the hydrogen transfer reactions to intercept the pathways promoting the formation of polycyclic compounds inside the zeolite cage. For instance, the intermediate 1,3-butadiene can undergo hydrogenation in the presence of H_2, thus limiting its chances to form aromatic and polycyclic compounds susceptible to coke formation.[185] Zeolites have been reported to perform the hydrogenation/dehydrogenation reactions to a limited extent.[193,194] At a certain methanol partial pressure, the dehydrogenation of methanol to formaldehyde can occur. Formaldehyde can undergo Prins condensation with olefins and aromatics in the HCP to generate inactive polycyclic aromatic species. Co-feeding of H_2 is presumed to reduce the formaldehyde induced polycyclic aromatics formation. Analysis of the occluded reaction species in the completely deactivated SAPO-34 showed that H_2 co-feeding did not change the composition of chemical species (pyrene species), but only delayed the deactivation rate.[192] This delayed deactivation behavior caused by H_2 co-feeding was also observed by others when other zeolite catalysts such as SSZ-39, FER, and BEA were used for the reaction.[185] The only detrimental effect of H_2 co-feeding is the formation of saturated products when used at very high pressures.[192]

The effect of co-feeding of both H_2 and H_2O was reported by Zhao *et al.*[195] The authors reported a synergetic effect of H_2O and H_2 in improving the lifetime of the SAPO-34 catalyst (Fig. 10A). Protonation of H$^+$ sites by H_2O generates H_3O^+ ions.[196] These H_3O^+ ions have been reported to reduce the activation energy for hydrogenation reactions.[197] As a result, the carbenium ions generated from the aromatics, confined in SAPO-34, can easily undergo hydrogenation, inhibiting the coke formation, at the same time, hydrogenating the heavy
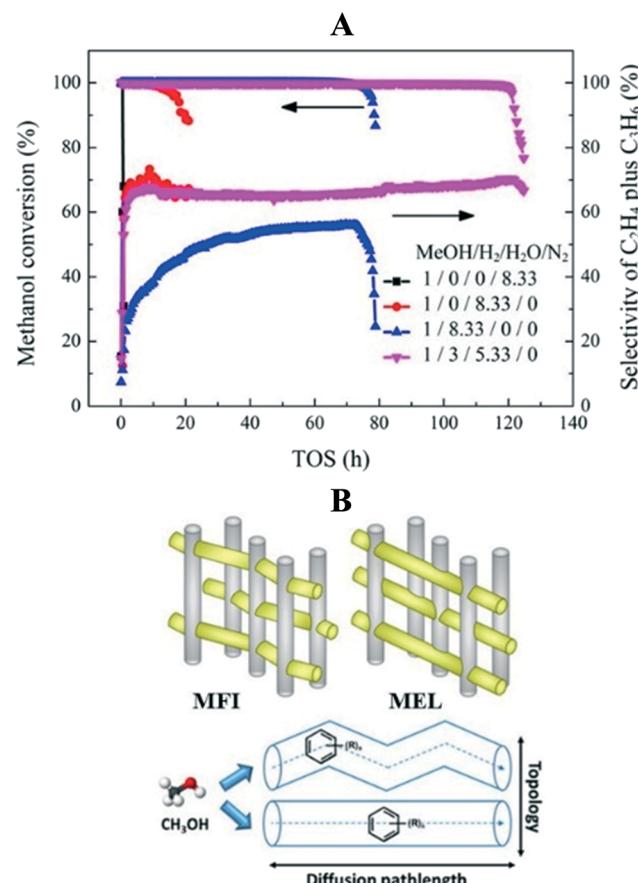
Fig. 10 (A) Effects of different reaction environments (N$_2$, H$_2$, H$_2$O, and H$_2$–H$_2$O mixture, 723 K, 4 MPa, methanol WHSV = 4.0 h^{-1}, GHSV = 13 069 h^{-1}) on the lifetime of a SAPO-34 catalyst, reprinted (adapted) with permission from X. Zhao, J. Li, P. Tian, L. Wang, X. Li, S. Lin, X. Guo and Z. Liu, *ACS Catal.*, 2019, 9, 3017–3025, Copyright (2019) American Chemical Society. (B) Effect of diffusion path length on catalyst lifetime, reprinted (adapted) with permission from Y. Shen, T. T. Le, D. Fu, J. E. Schmidt, M. Filez, B. M. Weckhuysen, and J. D. Rimer, *ACS Catal.*, 2018, 8, 12, 11042–11053, Copyright (2018) American Chemical Society.

aromatic deposits to active aromatic intermediates (HCP mechanism), thereby increasing the catalyst lifetime. The main advantage of co-feeding H_2O along with H_2 is that the propylene selectivity could be improved.[195] And the main disadvantage of H_2O co-feeding is that, at a high amount of H_2O, the zeolite can undergo dealumination leading to irreversible deactivation.[198,199]

Zachariou *et al.*[200] also found the positive effect of H_2O in improving the catalyst lifetime. The authors used methanol and dimethyl ether as reactants. Rapid deactivation was observed when dimethyl ether was used as a reactant. The deactivation was delayed when methanol was used instead of dimethyl ether. This was ascribed to the presence of H_2O that aided the regeneration of acid sites required for the methylation of aromatic compounds (HCP mechanism). The composition of coke also changed in the presence of H_2O. In its presence, the ratio of aromatic to aliphatic species in the coke was found to be lower.[200]

This journal is © The Royal Society of Chemistry 2021

Catal. Sci. Technol., 2021, 11, 1665–1697 | 1679

The effect of CO_2 co-feeding (0.1 MPa) during the MTH reaction has also been reported. Magzoub et al.[201] employed a 3D-printed monolith ZSM-5 catalyst doped with various elements like Ga, Cr, Cu, Zn, Mo, and Y. The CO_2 co-feeding slightly improved the lifetime of the catalysts (673 K, WHSV = 0.35 h^{-1}), probably via the reverse Boudouard reaction. A consequence of CO_2 co-feeding is that it promoted cracking and dehydrocyclization, leading to the production of light alkanes (methane and ethane) and benzene–toluene–xylene compounds.[201]

Overall, the co-feeding of H_2, CO_2, and H_2O was found to be conducive in delaying the deactivation rate thereby improving the catalyst lifetime. Hence during the CTH process, these gases (CO_2 and H_2) and H_2O are anticipated to impart a positive effect on the catalyst lifetime.

2.2.2.2 Effect of catalyst structure and composition on deactivation. An alternative approach to improve the catalyst lifetime is to modify the catalyst structure, for instance, introduce mesoporosity. Kim et al.[184] reported the use of hierarchical ZSM-5 with intracrystalline mesopores for the MTO reaction. In the synthesized catalyst, the Al atoms were predominantly positioned in the straight channels as compared to the conventional ZSM-5 catalyst, where the Al atoms are found in the intersections between sinusoidal and straight channels. The lifetime of the catalyst with hierarchical mesopores was almost 3 times longer than the microporous ZSM-5 catalyst (673 K, WHSV = 4.75). The presence of mesopores served as a carbon reservoir to accommodate the coke and thus minimize the blockage of micropores.[184] The presence of mesopores enhanced the diffusion of coke precursors out of the micropores, allowing the zeolite to accommodate more coke with large structures, and thereby increasing its lifetime.

Another factor contributing to the deactivation of zeolite catalysts during industrial applications is the presence of binders (non-zeolitic materials used to improve the mechanical properties of the zeolite catalysts). Binders can block the pore accessibility, thereby accelerating the propensity of intermediate molecules to form coke precursors.[202] To circumvent this issue, Bingre et al.[203] introduced pore-forming agents (surfactants) to a boehmite binder before extruding it with ZSM-5. Calcination of the extrudate catalyst burned off the pore-forming agents leaving meso/macro pores within the extrudate. These meso/macropores solely existed in the binder leaving the zeolite structure intact. Meso/macro pores in the binder favored improved mass transfer of molecules and were able to trap and hold larger quantities of coke as compared to the conventional extrudate catalyst (723 K, WHSV = 2.0). The coke's ideal position in the meso/macro pores was beneficial to retain the exposure of active sites of the zeolite for a longer reaction time, thus indirectly improving the catalyst lifetime to almost double.[203]

In the case of the ZSM-5 catalyst, the coke deposition is usually observed at the outer rim of the zeolite crystal because aromatic products diffusing out the micropores are condensed at the external surfaces of the crystals. Over time, the pore entrance becomes blocked by the coke, causing the accumulation of hydrocarbons at the channel intersections completely limiting access to internal active sites. Acid sites on the external surface of the zeolites deactivate more quickly than those located inside the crystals due to a lack of shape selectivity. Therefore, to improve the catalyst lifetime, Goodarzi et al.[191] attempted a surface passivation technique involving the introduction of an inert porous shell of silicalite-1 with a thickness of 15 nm on the surface of a mesoporous ZSM-5 catalyst, thus replicating a core–shell structure. In comparison to the mesoporous ZSM-5 without the protective shell, the one with the protective shell had 10 times longer catalyst lifetime extending up to 70 hours of reaction as compared to 7 hours, and 12 times higher conversion capacity based on the acid sites (from 27 to 63%).

To unravel the effect of catalyst composition on deactivation, Chowdhury et al.[204] compared the performance of Ca-modified and unmodified ZSM-5 in the MTH reaction (773 K, WHSV = 8 h^{-1}). The Ca-modification significantly improved the lifetime of the catalyst. This was attributed to the fact that the Lewis acid site may promote (imparted by Ca-incorporation) suppression of the aromatic cycle. The Ca-incorporation isolated the Brønsted acid sites, thereby inhibiting the carbene/ylide species.

In order to investigate the effect of framework topology and diffusion path length on deactivation, Shen et al.[205] used a series of ZSM-5 and ZSM-11 catalysts with different crystallite sizes for the reaction (623 K, WHSV = 9 h^{-1}). As compared to ZSM-5 with a sinusoidal micropore structure, the ZSM-11 with straight micropore structure had almost a two-fold improved catalyst stability (from 4.5 to 8.5 hours) due to higher diffusivity (Fig. 10B). When the crystallite size of ZSM-11 was reduced from 750 nm to 150 nm, an 8-fold increase in catalyst lifetime was observed (from 1.7 to 13.5 hours), owing to the decrease in the diffusion path length. An increase in diffusion limitation favors the aromatic cycle to produce ethylene as the major product.[205] A general conception regarding the effect of zeolite topology on catalyst lifetime is that the shorter the diffusion length or the smaller the crystallite size, the longer the catalyst lifetime.[206–211]

2.2.3 Regeneration of deactivated catalysts. In general, the coke deactivated catalyst is regenerated by high-temperature thermal calcination treatment in the presence of air or oxygen to burn off the coke. The regeneration conditions are normally much more severe than the reaction conditions. The main disadvantages of this approach are the high energy consumption and long time required for coke combustion. Also, care must be taken while selecting the regeneration conditions in order to preserve the catalyst structure, its activity, and selectivity by avoiding irreversible deactivation. Irreversible deactivation of the catalysts is mainly due to changes in textural properties and loss of acidity (dealumination).[212] Other ways to regenerate the deactivated catalyst have also been reported in the literature.

Zhang et al.[213] applied room temperature methanol leaching as a regeneration technique for the deactivated ZSM-5 catalyst. After 2 hours of methanol leaching, the regenerated catalyst

showed textural properties similar to the fresh ZSM-5 catalyst. However, the authors found that regeneration by calcination was more efficient in removing the coke than methanol leaching. One of the main disadvantages of methanol leaching in practical application is the requirement of cooling down the reactor for the leaching process.[213]

Li et al.[212] introduced a rejuvenating process to the ZSM-5 catalyst bed during the MTH process to reactivate the catalyst. Toluene or H_2O was fed to the reactor under the same experimental conditions for a certain period. After this, the methanol feeding was continued. The rejuvenation process decreased the pore volume and surface area (textural properties), and the acidity of the catalyst. Rejuvenation by toluene had generated new polyalkylbenzene species in the catalyst. These species could act as HCP intermediates to partially recover the activity of the catalyst. When H_2O was used, the catalyst was found to be less effective, mainly due to the loss of acidity by dealumination.[212] Altogether, the most efficient way to regenerate a deactivated catalyst is the calcination process and it is successfully practiced in industry via the use of fluidized bed reactors.[169]

3. Direct hydrogenation of CO_2 to hydrocarbons

Hydrocarbons from CO_2 have been synthesized using two processes; the first is a CO-mediated process and the second is a CH_3OH-mediated process (Fig. 11). The focus here will be on the CH_3OH-mediated process, as the CO-mediated process is out of scope of this review. Generally, CO-based hydrocarbon synthesis, called the Fischer–Tropsch process (FT), produces hydrocarbons with a statistical distribution, named Anderson–Schulz–Flory (ASF). The maximum selectivity for a desired hydrocarbon is limited by the ASF model. Apart from this route, the CH_3OH-mediated hydrocarbon synthesis process has the advantage that the hydrocarbon yield does not follow the ASF model. In recent years, many studies report on the direct conversion of CO_2 to hydrocarbons in a one stage reactor via a CH_3OH-mediated process (Table 3). Direct CO_2 hydrogenation is an efficient way to produce hydrocarbons using bifunctional catalysts. Bifunctional catalysts are a combination of CH_3OH synthesis and CH_3OH to hydrocarbon (MTH) catalysts. Up to now,

various Cu, Pd, and oxide-based catalysts (In_2O_3 and ZnO) have been used for CH_3OH synthesis from CO_2, and different types of zeolites have been used for the synthesis of hydrocarbons from CH_3OH.[17,214,215] The direct route would be more economically and energy-efficient compared to the indirect two-stage route. In the case of the two-stage process, two reactors need to operate separately and in addition to the extra capital costs for another reactor stage there is a need to carry out separation processes between stages to separate the undesired intermediates from the process which requires additional energy. There are also efficiency advantages that a single stage process can offer since the equilibrium limitation of methanol synthesis is alleviated by the fact that methanol is directly converted to hydrocarbon products. CO is a major byproduct from CO_2 hydrogenation, but in a one stage CO_2 hydrogenation process, the selectivity for CO can be reduced since the methanol removal will be positive for the equilibrium limitation for the methanol synthesis from CO_2, as will be explained below in greater detail. Inui et al. investigated the synthesis of gasoline with lower olefins from CO_2 + H_2 via the CH_3OH route in a two stage reactor.[216,217] In the first reactor, CO_2-rich syngas was converted to CH_3OH on Cu–Zn–Cr–Al-oxides; further the total reaction mixture was directly fed to a second reactor connected in series, packed with a protonated Fe-silicate crystalline catalyst. Gasoline with 50% selectivity was formed in the second reactor from the CH_3OH synthesized in the first reactor. As a side product, lower olefins were produced with gasoline, which could be an intermediate compound during gasoline synthesis.

There are various reports on the synthesis of lower olefins (butylenes, propylene, and ethylene) which are used industrially as chemical intermediates and also produced from the dehydration of lower alkanes[218] and cracking of hydrocarbon feedstocks.[219] At the lab scale, lower olefins have been synthesized using two stage processes and as a carbon source, syngas is used for CH_3OH synthesis and further converted to lower olefins. Meanwhile in the case of CO_2 to CH_3OH, the formation of water is unavoidable which can lead to deactivation of both catalysts (for CO_2 to CH_3OH catalysts as well as CH_3OH to olefin catalysts like zeolite). In addition, water can cause zeolite dealumination if present in too large quantities; however, as mentioned in section 2.2.2.1 of this review, it also prolongs the lifetime of the MTO catalysts by preventing coke deposition. Thus, it is a challenging task to synthesize hydrocarbons from CO_2 in one stage.

Recently, In_2O_3-based catalysts have shown their excellent activity for CH_3OH synthesis in the temperature range of 473–573 K (ref. 44, 142 and 143) (Table 2). While in this temperature range, zeolites are not active for C–C coupling. Generally, it is found that high temperature is more kinetically favorable for C–C coupling from methanol. For the synthesis of lower olefins from methanol, the temperature range of 673–723 K was found optimal over SAPO-34 which is a more favorable temperature range for the RWGS reaction too, but not for methanol yield (Tables 1 and 2).[171,220] Thus, the big challenge is how to combine the two processes, which
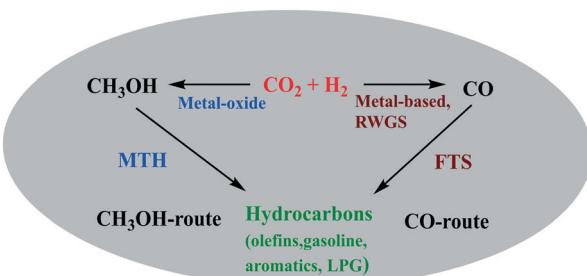

Fig. 11 Pictorial representation of CH_3OH-mediated or CO-mediated routes for direct hydrocarbon synthesis.

This journal is © The Royal Society of Chemistry 2021

Catal. Sci. Technol., 2021, **11**, 1665–1697 | **1681**

Table 3 Catalytic performance of bifunctional catalysts for CO_2 hydrogenation to hydrocarbons

Catalysts	$H_2:CO_2$	T (K)	P (MPa)	CO_2 conv. (%)	GHSV (h^{-1})	Major products[a]	Selectivity for major products among hydrocarbons[b] (%)	CO selectivity[c] (%)	$S_{MeOH/DME}$[d] (%)	Ref.
Zr–In$_2$O$_3$/SAPO-34	3	673	3	35.5	9000	C$_2^=$–C$_4^=$	76.4	85.0	0/n.r.	222
Zn–ZrO$_2$/SAPO-34	3	653	2	12.6	3600	C$_2$–C$_4^=$	80.0	47.0	n.r./n.r.	227
In$_2$O$_3$–ZrO$_2$/SAPO-34	3	673	1.5	19.0	3000	C$_2^=$ + C$_3^=$	80–90	>80	n.r/n.r.	225
In$_2$O$_3$/H-ZSM-5	3	613	3	13.1	9000	C$_{5+}$	78.6	<45	0/n.r.	221
ZnGa$_2$O$_4$/SAPO-34	3	643	3	13.0	5400	C$_2^=$–C$_4^=$	86.0	46.0	0/0	229
In$_2$O$_3$–ZrO$_2$/SAPO-34	3	653	3	26.2	9000	C$_2^=$–C$_4^=$	74.5	63.9	0.2/n.r.	223
In$_2$O$_3$–ZrO$_2$/SAPO-5	3	573	3	6.7	4000	C$_2$–C$_4$	83.0	43.0	<0.5/n.r.	226
ZnAlO$_x$/H-ZSM-5	3	593	3	9.1	2000	Aromatics	73.9	57.4	<0.5/<0.2	232
In$_2$O$_3$–ZnZrO$_x$/SAP-34	3	653	3	17.0	9000	C$_2$–C$_4^=$	85.0	54.0	0/n.r.	224
Cu–CeO$_2$–SAPO-34	3	669	2	13.2	5800	C$_2^=$–C$_4^=$	61.8	56.8	n.r./n.r.	231
ZnZrO/HZSM-5	3	593	4	14.1	1200	Aromatics	73.0	44.0	n.r./n.r.	233
Cr$_2$O$_3$/HZSM-5	3	623	3	33.6	1200	Aromatics	70.5	41.2	0/0	234
CuZnZr@Zn–SAPO-34	3	673	2	19.6	3000	C$_2^=$–C$_4^=$	60.5	58.6	n.r./n.r.	228

[a] Major hydrocarbon product among hydrocarbons. [b] Major hydrocarbon product selectivity among hydrocarbons. [c] CO selectivity based on CO_2 feed. [d] Selectivity for methanol and DME based on CO_2 feed, n.r. = not reported.

have different optimum operating conditions while mitigating the undesired side reactions. Many efforts have been made to synthesize such combined catalysts to achieve stable and excellent catalytic performance. Note that in all cases in the following paragraphs the reported selectivities for certain hydrocarbon products (or major hydrocarbon products) are based only among all hydrocarbon products whereas the reported CO/CH$_3$OH/DME selectivities are based on total carbon from the CO_2 feed.

Gao et al. prepared a bifunctional catalyst by mixing In$_2$O$_3$ and zeolite (ZSM-5) that showed 78.6% selectivity towards C$_{5+}$ (based on hydrocarbons) with only 1% selectivity for CH$_4$ at a CO_2 conversion of 13.1%.[221] In addition, less than 45% CO selectivity was observed. Moreover, when using beta zeolite, liquefied petroleum gas products (C$_3$ and C$_4$ paraffins) were formed and an enhanced CO_2 conversion was observed at higher pressure and H$_2$/CO$_2$ ratio while the CO selectivity was decreased. Later, the same group reported 76.4% selectivity for lower olefins (C$_2^=$–C$_4^=$) with ~35% CO_2 conversion over a composite catalyst of In–Zr oxide and SAPO-34 zeolite.[222] However, the CO selectivity over this composite was above 80% under different reaction conditions. The CO_2 activation occurred on the In–Zr oxide, whereas the zeolite was responsible for C–C coupling. The authors studied the effect of reaction pressure and the feed ratio of H$_2$/CO$_2$ and found that CO_2 conversion increased with the H$_2$/CO$_2$ ratio while the selectivity for C$_2^=$–C$_4^=$ decreased with increasing pressure and H$_2$/CO$_2$ ratio. It was also observed that when the space velocity was increased from 4500 to 15 750 mL g$_{cat}^{-1}$ h^{-1}, the selectivity for lower olefins increased from 68% to 84% and the selectivities for C$_{5+}$ and CH$_4$ were decreased.

To understand the role of ZrO$_2$, a series of bifunctional catalysts composed of In–Zr composite oxides having different atomic ratios of In and Zr, and SAPO-34 zeolite were prepared by Dang et al. and screened for direct CO_2 hydrogenation into lower olefins.[223] The catalysts gave 15–27% conversion of CO_2 with 96% selectivity for C$_2$–C$_4$ among the hydrocarbon products (65–80% for C$_2^=$–C$_4^=$ and 13–30% for C$_2^0$–C$_4^0$), and

the selectivity for CH$_4$ was merely 2.5%. The selectivity for CO via the RWGS reaction was less than 70%. The authors demonstrated by combined experimental and computational studies that In$_{1-x}$Zr$_x$O$_y$ mixed oxide was formed after the incorporation of Zr into In$_2$O$_3$. This mixed oxide was found to contain more oxygen vacancies with higher binding energies for the reaction intermediates compared to pure In$_2$O$_3$. Further, the CO_2 adsorption behavior was studied on the mixed oxide using DFT calculations and it was found that the CO_2 and reaction intermediates were adsorbed more strongly on the oxygen vacancy sites which were situated near the Zr dopant than that on pure In$_2$O$_3$. Thus, the presence of a certain amount of Zr in In$_2$O$_3$ (In:Zr = 4:1) increased the selectivity for CH$_3$OH from CO_2 and decreased the RWGS activity. Consequently, the formation of hydrocarbons also increased with the incorporation of Zr. However, it was also observed that an excess amount of Zr in In$_2$O$_3$ significantly decreased the olefin selectivity due to the smaller pore size of the oxides and longer average distance between the metal-oxide and zeolite.

Recently, a composite of In$_2$O$_3$–ZnZrO$_x$ oxides and SAPO-34 was prepared in which In$_2$O$_3$ (8 nm) was supported on ZnZrO$_x$ and mechanically mixed with a series of SAPO-34 zeolites having different crystal sizes and pore structures.[224] The composite catalyst was used for direct CO_2 hydrogenation to lower olefins and a 85% selectivity for C$_2^=$–C$_4^=$ was found among all the hydrocarbons with a CO_2 conversion of 17% and CO selectivity of 54%. It was found that the selectivity for C$_2^=$–C$_4^=$ increased with decreasing pore size. The reason for this was that the diffusion length can be shortened from the surface to the acid sites inside the pores of the zeolite and this helps to provide an efficient mass transfer of intermediate species for C–C coupling to produce lower olefins, whereas the pore structure and the crystal size of the zeolite did not influence the equilibrium of the RWGS reaction. A similar type of composite was synthesized by Gao et al., fabricated from In$_2$O$_3$/ZrO$_2$ and SAPO-34 for direct conversion of CO_2 to light olefins (ethylene and propene).[225] The authors reported the selectivity for light olefins in the

1682 | Catal. Sci. Technol., 2021, 11, 1665–1697

This journal is © The Royal Society of Chemistry 2021

range of 80–90% with ~20% CO_2 conversion. The influence of composition on the selectivity for hydrocarbons and conversion of CO_2 was studied and it was found that equal mass of In_2O_3/ZrO_2 to SAPO-34 gives a relatively high yield of light olefins, whereas higher content of In_2O_3/ZrO_2 in the composite increased the CO_2 conversion and selectivity for CO (>80%) which is a side product during CH_3OH synthesis over In_2O_3/ZrO_2. Recently, Wang et al. reported results for the same type of catalyst in which SAPO-34 was replaced with SAPO-5.[226] This bifunctional catalyst integrated In_2O_3/ZrO_2 and SAPO-5 and exhibited an excellent selectivity towards C_2–C_4 (83%) lower hydrocarbons with a lower yield of CH_4 at 6.7% conversion of CO_2. A comparison study for hydrocarbon selectivity over SAPO-34 and SAPO-5 was carried out and it was found that the total selectivity for C_2–C_4 (83% in hydrocarbons) over SAPO-5 was higher than that over SAPO-34. The selectivity for CO was found to be between 40 and 60% over this composite and it decreased by increasing the space velocity and granule mixing of In_2O_3/ZrO_2 and SAPO-5 while it increased with temperature.

Li et al. fabricated a tandem catalyst that was a composite of ZnO–ZrO_2 and a Zn-modified SAPO-34 and over this catalyst, they found 12.6% CO_2 conversion with 80% selectivity for lower olefins ($C_2^=$–$C_4^=$) which was the highest among all the hydrocarbon products (3% CH_4, 14% C_2–C_4^0, and 3% C_{5+}).[227] It was concluded that the ZnZrO produced CH_3OH from CO_2 hydrogenation and the lower olefins occurred on the SAPO catalyst from CH_3OH with 47% CO selectivity. This catalyst was found to be promising for industrial applications, since it has good sulfur and thermal resistance under the mentioned reaction conditions (Table 3). The highly efficient conversion of CO_2 to lower olefins on tandem catalysts can be attributed to the thermodynamic and kinetic coupling.

To obtain high selectivity towards light olefins from CO_2 hydrogenation, a core–shell structural (CuZnZr)CZZ@SAPO-34 composite catalyst was prepared and compared with CZZ/SAPO-34 which was prepared by physical mixing.[228] CZZ/SAPO-34 (mass ratio of 4:1) gave 9.7% CO_2 conversion with 34.7% olefins selectivity and 58.5% CO selectivity. It was found that the physically mixed CZZ/SAPO-34 with a mass ratio of 4:1 reduced the acidity of the catalyst which is a factor that could increase the selectivity for lower olefins, but surprisingly the catalyst gave lower selectivity to olefins and higher selectivity for CH_4 compared to CZZ/SAPO-34 with a mass ratio of 2:1. This could be due to the strong hydrogenation ability of CZZ at the reported temperature. Meanwhile in the case of the core–shell composite (CZZ@SAPO-34), the higher mass ratio (CZZ@SAPO-34 (4:1)) gave higher selectivity for olefins with lower selectivity for CH_4 compared to the lower mass ratio of CZZ@SAPO-34 (2:1). This is possibly due to the reduced interface between CZZ and SAPO-34, because of the great difference in the particle size of CZZ in CZZ@SAPO-34 and CZZ/SAPO-34 catalysts. In addition, it was stated that the hydrogenation activity was weakened in the case of CZZ@SAPO-34, which was found beneficial for lower olefins as

the selectivity for lower olefins was increased via restraining the secondary hydrogenation reaction. It was also found that the acid density of SAPO-34 affected significantly the selectivity for the product. The authors reduced the acid density and total acidity of SAPO-34 by Zn-modification which then greatly increased the CO_2 conversion and selectivity for lower olefins on the CZZ@Zn–SAPO-34 (4:1) catalyst (see Table 3). No change was observed in CO selectivity due to the interface or the acidity of CZZ@Zn–SAPO-34 (4:1), CZZ@SAPO-34 (2:1), and CZZ/SAPO-34 (4:1).

Another new oxide-based catalyst was reported recently by Liu et al.[229] This bifunctional catalyst was composed of a spinel structure of $ZnGa_2O_4$ and SAPO-34 which gave 86% C_2–C_4 olefins and 46% CO selectivity with a CO_2 conversion of 13%. It was reported that the molar ratio of Zn/Ga in $ZnGa_2O_4$ plays an important role in adsorption, activation and conversion of CO_2 as it influenced the density of oxygen vacancies in the catalyst.[230]

Sedighi et al. reported a new composite for direct hydrogenation of CO_2 to lower olefins ($C_2^=$–$C_4^=$) via CH_3OH as an intermediate.[231] A crystalline hybrid catalyst (CuCe/SAPO-34) was prepared by a physical coating process in which the outside surface of the SAPO-34 powder was covered with Cu/CeO_2. The CO and olefin selectivity were found to be 57.8 and 61.8% (based on hydrocarbons), respectively, with 13.2% CO_2 conversion at 669 K. The CO_2 conversion and CO selectivity were promoted by high temperature.

Several aromatic hydrocarbons have been successfully synthesized by CO_2 hydrogenation. A composite catalyst of $ZnAlO_x$ and H-ZSM-5 was synthesized and tested for CO_2 hydrogenation.[232] The catalyst yielded 57.4% selectivity for CO, 73.9% selectivity for aromatics (among the HCs) with 9.1% CO_2 conversion, and 0.4% CH_4 selectivity. It was found that Zn^{2+} activated the CO_2 hydrogenation in $ZnAlO_x$ whereas Si–H-ZSM-5, containing the composite zeolite, was selective for p-xylene (58.1%), ethylene and propylene. During the reaction, DME, CH_3OH, and olefins were found as reaction intermediates. The RWGS reaction was suppressed by increasing the ratio of H_2/CO_2 and introducing CO without affecting the aromatization.

A tandem catalyst ZnZrO/ZSM-5 was prepared and screened for the hydrogenation of CO_2 to aromatics.[233] The catalyst exhibited 14% conversion of CO_2 with an aromatics selectivity of up to 73% (based on HCs) and 44% CO selectivity. Thermodynamic coupling was observed on the tandem catalyst where CH_xO intermediates were formed on the surface of ZnZrO from CO_2 hydrogenation and then the intermediates transferred to the pores of H-ZSM-5 and produced aromatics. It was found that the presence of H_2O in H-ZSM-5, produced from CO_2 hydrogenation over ZnZrO, helped stabilize the ZnZrO/ZSM-5 catalyst by suppressing the production of polycyclic aromatics.

Wang et al. presented a novel tandem catalytic process for CO_2 hydrogenation to aromatics in a single-step (Fig. 12).[234] A CH_3OH-mediated pathway was found to occur over Cr_2O_3/H-ZSM-5 catalysts, which were prepared by physical mixing of

This journal is © The Royal Society of Chemistry 2021

Catal. Sci. Technol., 2021, 11, 1665–1697 | 1683

Cr_2O_3 and H-ZSM-5. The catalyst yielded 70.5% selectivity for aromatics among all the hydrocarbons and 41% CO selectivity with 33.6% conversion of CO_2. Meanwhile, the selectivity for CH_4 and CO was successfully suppressed to 1.5% and 11.4%, respectively, by co-feeding 5.4 vol% CO in the feed gases whereas the aromatics selectivity and the CO_2 conversion increased up to 75.9 and 34.5%, respectively. In addition, to enhance the selectivity towards benzene, xylene, and toluene, a structural change was carried out to form a core–shell type catalyst. The core–shell structured zeolite catalyst enhanced the selectivity for benzene, toluene and xylene from 13.2% to 43.6% (in aromatics) while the CO_2 conversion was decreased from 34.5 to 27.6%. In addition, by tuning the mass ratio of both components of the tandem catalyst and the acid strength of zeolites, the catalytic performance could be influenced. The developed catalyst exhibited excellent stability for a 100 h reaction run. Most studies discussed the effect of space velocity on selectivity. An enhancement in selectivity to hydrocarbons was observed by increasing the space velocity, whereas the selectivity for CO was suppressed after the combination of zeolite with a metal oxide catalyst. The method used to combine catalysts also affects the catalyst activity and selectivity for products which is termed as proximity and will be discussed in section 3.3. In other words, reducing the contact time between the catalyst bed, feed gas and CH_3OH is favorable for timely diffusion into the zeolite pores for conversion to hydrocarbons.

In most of the studies listed in Table 3, lower olefins are the major products among the hydrocarbons. The synthesis of lower olefins was explained based on the synergic interaction between two catalysts which were responsible for methanol synthesis and the MTO reaction. However, it is challenging to selectively synthesize lower olefins from CO_2 using the reaction coupling strategy, since the MTO reaction is more favorable at higher temperatures (>623 K)[235] whereas the CO_2 to methanol reaction is thermodynamically unfavorable at higher temperature. It was found that after

mixing the two catalysts (methanol synthesis catalyst and MTH catalyst), the bifunctional catalyst shows a unique property which shifts the CH_3OH synthesis equilibrium and decreases the selectivity for CO and CH_4. The immediate conversion of methanol into lower olefins might be a driving force for the higher reactivity to methanol and lower selectivity towards CO. Methanol has been reported as an intermediate in most of the studies (Table 3) while DME was also found with methanol in a few studies. It was observed that methanol and CO were the main products with the metal-oxide catalyst alone, but when the metal oxide was mixed with zeolite, then the selectivity for methanol was found to be near zero or less than detectable under the reaction conditions listed in Table 3, whereas the CO selectivity was also reduced. It means that all produced methanol/DME could be converted into hydrocarbons. In some cases, small amounts of methanol were found unreacted when reaction conditions such as the mass ratio of metal oxide and zeolite catalysts, space velocity, pressure, and temperature were changed. For example, aromatics synthesis was examined on a $ZnAlO_x$/H-ZSM catalyst, and CH_3OH and DME were observed as intermediates.[232] A higher selectivity for methanol (above 98%, excluding CO) was obtained with ZnO alone, whereas the selectivity for CH_3-OH was reduced (to below 60%) after the addition of AlO_x and DME was found with CH_3OH with almost equal selectivity. Further, with the addition of H-ZSM, the selectivity for both CH_3OH and DME dropped. The preparation method and the packing method of $ZnAlO_x$ and H-ZSM also changed the selectivity for CH_3OH and DME. For example, the selectivity for CH_3OH + DME was higher than 0.5% when they were prepared by grinding mixing, whereas the selectivity dropped to below 0.5% when both catalysts were mixed by granule mixing. Only DME was observed when both catalysts were packed in a dual-bed configuration in the reactor with $ZnAlO_x$ upstream from H-ZSM.

The selectivities for CH_3OH and DME were also increased with higher space velocity in the case of the $ZnAlO_x$/H-ZSM catalyst. It was stated that the rate of formation of CH_3OH from CO_2 hydrogenation is higher than the hydrogenation of CO. Thus, there is less chance to obtain CH_3OH from CO over metal oxides.[229] The reason for the lower CO selectivity with combined metal oxide and zeolite catalysts might be because both methanol and CO formation compete for consumption of the same reactants (CO_2 and H_2). At the high temperature used for direct CO_2 hydrogenation to hydrocarbons, methanol synthesis should be strongly equilibrium limited and this reaction is favored by high reactant and low product (methanol and water) concentrations. The progress of the competing CO formation reaction lowers the reactant concentration and increases water, which favors reverse methanol synthesis. However, if methanol is immediately consumed by its conversion into hydrocarbons, then methanol synthesis can proceed with less restrictive equilibrium limitations and the negative effects that CO formation would have on its equilibrium. In
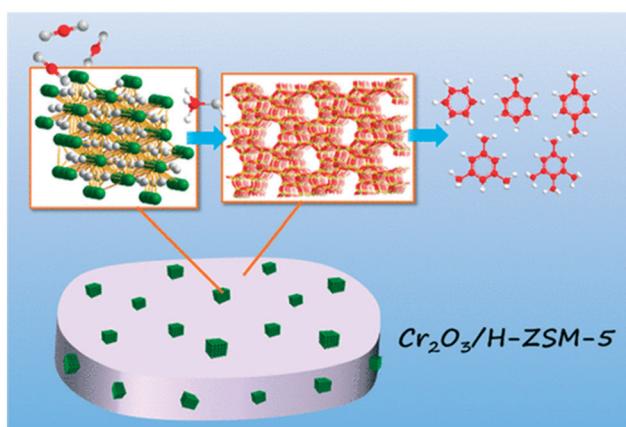
Fig. 12 A pictorial representation on the direct conversion of CO_2 to aromatics over Cr_2O_3/H-ZSM-5. "Reprinted (adapted) with permission from Y. Wang, L. Tan, M. Tan, P. Zhang, Y. Fang, Y. Yoneyama, G. Yang and N. Tsubaki, *ACS Catal.*, 2018, **9**, 895–901. Copyright (2019) American Chemical Society".

1684 | *Catal. Sci. Technol.*, 2021, **11**, 1665–1697

This journal is © The Royal Society of Chemistry 2021

addition, unhindered methanol formation consumes more reactants which reduces the driving force for the CO formation reaction. However, detailed studies of this are still lacking in the literature.

3.1 Catalyst preparation methods

We have seen in the sections above and as evident in Table 3 that direct CO_2 hydrogenation to hydrocarbons always involves bifunctional catalyst systems, so in this section, the methods of preparation of these catalysts are discussed, with the intent to achieve varying degrees of contact between the two catalysts. Also, below in section 3.3, the importance of the proximity of the catalysts will be discussed. Most of the bifunctional catalysts are prepared by the solid mixing of methanol synthesis and hydrocarbon synthesis catalysts. Generally, this process is called granulation, which can be categorized into two parts, dry granulation and wet granulation. In the case of dry granulation, a mechanical compression can be used to mix the solid particles, while granulation with a liquid plays a role in facilitating the agglomeration.[236] As most of the studies in the case of bifunctional catalysts use a dry granulation process to prepare catalysts, only this method will be explained in detail here to keep this section brief.

A bifunctional catalyst was prepared using dry granule mixing, in which In_2O_3 and HZSM-5 were pressed and crushed to obtain 250 to 400 μm granule sizes and then both granule samples were mixed in an agate mortar. Further, the mixed sample was again pressed, crushed and sieved to obtain the above-mentioned particle size.[221] A similar method was used to prepare In_2O_3/SAPO-34 and In–Zr/SAPO-34 by the same group.[222] Another group prepared a mixed hybrid catalyst of In_2O_3/ZrO_2 and SAPO-34 by mixing these samples in a certain ratio. Then this mixed powder was compressed, crushed, and sieved to 10–20 mesh particles.[225] The In_2O_3/ZrO_2 sample was prepared by a deposition–precipitation method. Bifunctional catalysts were reported to be prepared by shaking In_2O_3–$ZnZrO_x$ and SAPO-34 granules in a vessel.[224] In_2O_3/$ZnZrO_x$ was synthesized using an impregnation method and $ZnZrO_x$ was prepared by a co-precipitation method. A tandem catalyst, namely $ZnZrO$/SAPO-34, was synthesized using physical mixing in which smaller size solid solutions of $ZnZrO$ were scattered on the outer surface of the zeolite and both components retained their individual structure.[227] Recently, a crystalline CuCe/SAPO-34 composite was prepared using a physical coating method.[231] In this process, the outside surface of SAPO-34 was covered with Cu/CeO_2, with the help of an alkaline-silica sol binder. Further, the sample was calcined at 823 K for 4 h. A core–shell structure of the (CuZnZr)CZZ@SAPO-34 composite catalyst was prepared with a physical coating method.[228] In this method, the outer surface of CuO–ZnO–ZrO_2 was covered with zeolite SAPO-34 with the help of an alkaline silica binder. Further, the catalyst was calcined at 773 K for 2 h.

3.2 Reaction mechanism and intermediates for direct CO_2 hydrogenation to hydrocarbons

One key challenge for the selective synthesis of hydrocarbons from CO_2 is the selection of a suitable CO_2-to-CH_3OH active catalyst that appropriately matches with the MTH reaction catalyst. As described above, bifunctional catalysts are effective for the synthesis of hydrocarbons. They are composed of a metal-oxide like In_2O_3–ZrO_2, ZnO–ZrO_2, Cr_2O_3, $ZnCrO_x$, $ZnGa_2O_4$ and $ZnAlO_x$ which could activate CO_2 and catalyze CO_2 to CH_3OH and/or DME in the temperature range of 573–673 K and zeolites such as HZSM, SAPO, and beta have been used to control the hydrocarbon selectivity due to their strong acidity and unique pore structure.[225,237,238] It could be possible that the active sites and the intermediates should be mostly the same in the bifunctional catalysts as for the individual catalysts when they are used separately to perform CH_3OH and hydrocarbon synthesis. However, the product selectivity and catalyst activity were found to be different when both catalyst components were combined and used as a bifunctional catalyst. Some groups have studied the reaction mechanism by DRIFT and DFT calculations.[141,230]

DFT calculations were carried out to study the catalytic cycle of CO_2 to CH_3OH over In_2O_3 oxygen vacancies as discussed earlier in this review.[221] Further the formed CH_3OH transfers to the zeolite where C–C coupling occurs at the acidic site of the zeolite and produces various hydrocarbons *via* the hydrocarbon-pool mechanism which is discussed earlier in section 2.2.1.2. The surface oxygen vacancies are increased by doping Zr into In_2O_3.[222] Similar observations were reported by Dang *et al.* after Zr doping into In_2O_3.[223] Later, the same group performed various experiments with an empty reactor, bare In_2O_3–$ZnZrO$ and SAPO-34 to explain the reaction mechanism of CO_2 hydrogenation over In_2O_3–$ZnZrO_x$/SAPO-34 catalysts under the same reaction conditions.[224] Over the In_2O_3–$ZnZrO$ catalyst, CH_3OH and CO were the major products. But after combination with the zeolite, the selectivity for CO decreased, and the selectivity for hydrocarbons increased. It was observed that the CH_xO species generated over In_2O_3–$ZnZrO_x$ further transferred to the zeolite for C–C coupling on the Brønsted acid sites to produce hydrocarbons.

Li *et al.* proposed a reaction mechanism based on *in situ* DRIFT spectroscopy coupled with a mass spectrometer and found mainly $HCOO*$ and CH_3O* intermediates on the surface of $ZnZrO$ but the IR studies showed a weak interaction of CH_3O* on $ZnZrO$ that favored the transfer of these species onto SAPO-34 for the formation of olefins.[227] It was concluded that the CH_3O*, $HCOO*$ species, and gas-phase CH_3OH were produced first *via* CO_2 hydrogenation on $ZnZrO$ and then the formed CH_3OH transferred to acidic sites of SAPO-34 for lower olefins production. The authors found that the CO selectivity was significantly suppressed and the CH_3OH selectivity was much higher in the case of a tandem catalyst compared with that for $ZnZrO$ alone. These results indicated an effective coupling of these reactions

(thermodynamic and kinetic coupling), where reactions over the tandem catalyst were more effective than the sum of reactions over individual catalysts (CO_2 to CH_3OH and MTH). Later, a similar mechanism was observed by the same group over a ZnZrO/HZSM-5 catalyst.[233] In this case, HCOO*, CHO*, and CH_3O* species were detected over the tandem catalysts during CO_2 hydrogenation where CH_3O* species most probably diffuse to zeolite HZSM-5 to make first light olefins and then aromatics from the lower olefins.

Liu *et al.* conducted *in situ* infrared (IR) spectroscopic measurements to propose a possible reaction mechanism for CO_2 hydrogenation on a $ZnGa_2O_4$ catalyst.[229] The authors demonstrated that the oxygen vacancy sites on $ZnGa_2O_4$ account for CO_2 activation to a CH_3OH intermediate and interaction with SAPO-34 can suppress the undesirable CO formation *via* the RWGS reaction, and was also responsible for the synthesis of hydrocarbons from CH_3OH. Carbonate species were observed on the pre-reduced $ZnGa_2O_4$ after the adsorption of CO_2 and after the introduction of H_2, HCOO* and CH_3O* were generated on the surface of $ZnGa_2O_4$ (Fig. 13). It was found that the –Zn–O– and –Ga–O– pairs were responsible for generating H species (H*) by activating H_2 and then these H species bind with activated CO_2 to form CH_3O* species. The CH_3O* species further formed CH_3OH that can be transferred into the pores of SAPO-34 and could produce lower olefins. The effect of oxygen-vacancies and water on CO_2 adsorption on the (111), (110), and (100) surfaces of $ZnGa_2O_4$ was studied using DFT slab calculations.[230] In some reports, the mesoporous $ZnGa_2O_4$ was found to be an effective photocatalyst for the photoreduction of CO_2 to CH_4.[239]

Ni *et al.* proposed a mechanism for CO_2 hydrogenation to aromatics over $ZnAlO_x$/H-ZSM-5 based on the catalytic results and DRIFTS studies.[232] According to this mechanism, surface formate species were formed on $ZnAlO_x$ and further hydrogenated to form CH_3O* species. Then, the methoxy species dissociated to intermediates including CH_3OH and DME which when transferred to H-ZSM-5 were further transformed to olefin intermediates. Finally, the formed olefins were converted to aromatics inside the micropores of H-ZSM-5.


Fig. 13 Possible mechanism of CO_2 conversion into hydrocarbons *via* CH_3OH intermediates over Zn–Ga–O catalysts. Reproduced from ref. 218 with permission from the Royal Society of Chemistry.

In addition, CO_2 hydrogenation over $ZnAlO_x$ generates more surface formate species compared to CO hydrogenation.

The mechanism of aromatics synthesis directly from CO_2 over Cr_2O_3/HZSM-5 was studied by *in situ* DRIFTS to gain more insights into the reaction pathway.[234] On Cr_2O_3, symmetric and asymmetric vibrations were observed related to HCOO* species which have been recognized as an intermediate for CH_3OH synthesis. Meanwhile in the case of Cr_2O_3/HZSM-5, the vibrations linked to HCOO* almost disappeared, but the CH_3O* vibrations on the other hand appeared, indicating the formation of C–C coupling after the addition of HZSM-5. In addition, the vibrations related to the benzene ring and the substituted benzene ring were also observed in the spectra. Thus, the DRIFTS findings confirmed that a CH_3OH-mediated pathway applies over the Cr_2O_3/HZSM-5 catalyst for CO_2 hydrogenation to aromatics. It was found that the selectivity for aromatics over H-ZSM-5 was lower than that for Cr_2O_3/HZSM-5 composites which was used for direct synthesis of aromatics from CO_2.

3.3 Proximity effect

The proximity and integration of the two-components play a crucial role in the catalytic performance of bifunctional catalysts for CO_2 hydrogenation. The effect of proximity and integration on product distribution has been studied in previous reports.[221,222,226,227,229,237,240] Fig. 14 and 15 show that there are three main methods to study the effect of proximity which include the following: (1) dual-bed mode in which the metal oxide and zeolite are positioned in series inside the reactor without mixing and separated by quartz sand; (2) granule mixing that could be obtained by the mixing of micrometer size granules of both components of a bifunctional catalyst. In some reports, quartz sand is also mixed as a third component to moderate the proximity, and (3) powder mixing (mortar mixing) in which both components are ground to nanometer size and mixed properly to increase their proximity. We have discussed more about granule and mortar mixing in section 3.1.

Gao *et al.* reported maximum conversion and selectivity for CO_2 and C_2–C_4 respectively over In_2O_3/ZSM-5 in the case of granule mixing whereas minimum in the case of mortar mixing, indicating that the proximity decreases the active sites for methanol synthesis as well as hydrocarbon synthesis (Fig. 14A).[221] In another experiment, the catalyst was packed in a dual-bed configuration in which two configurations were compared, one in which HZSM-5 was packed above the oxide and second below In_2O_3. In the first case, the authors found good selectivity for CH_4 (66.3%) and CH_3OH (31.8%) whereas the C_{5+} hydrocarbons selectivity was only 26.7%. However, in the latter case, the selectivity for CH_4 decreased to 4.5% while the selectivity for C_{5+} increased to 70.4%. The CO selectivity was found to have a maximum of 65% in the case of dual-bed packing.

Furthermore, in the case of granule stacking, the C_{5+} selectivity enhanced and the selectivity for CO (<45%) and CH_4
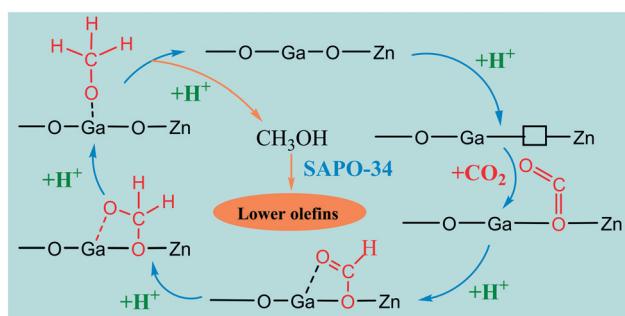
1686 | *Catal. Sci. Technol.*, 2021, **11**, 1665–1697

This journal is © The Royal Society of Chemistry 2021
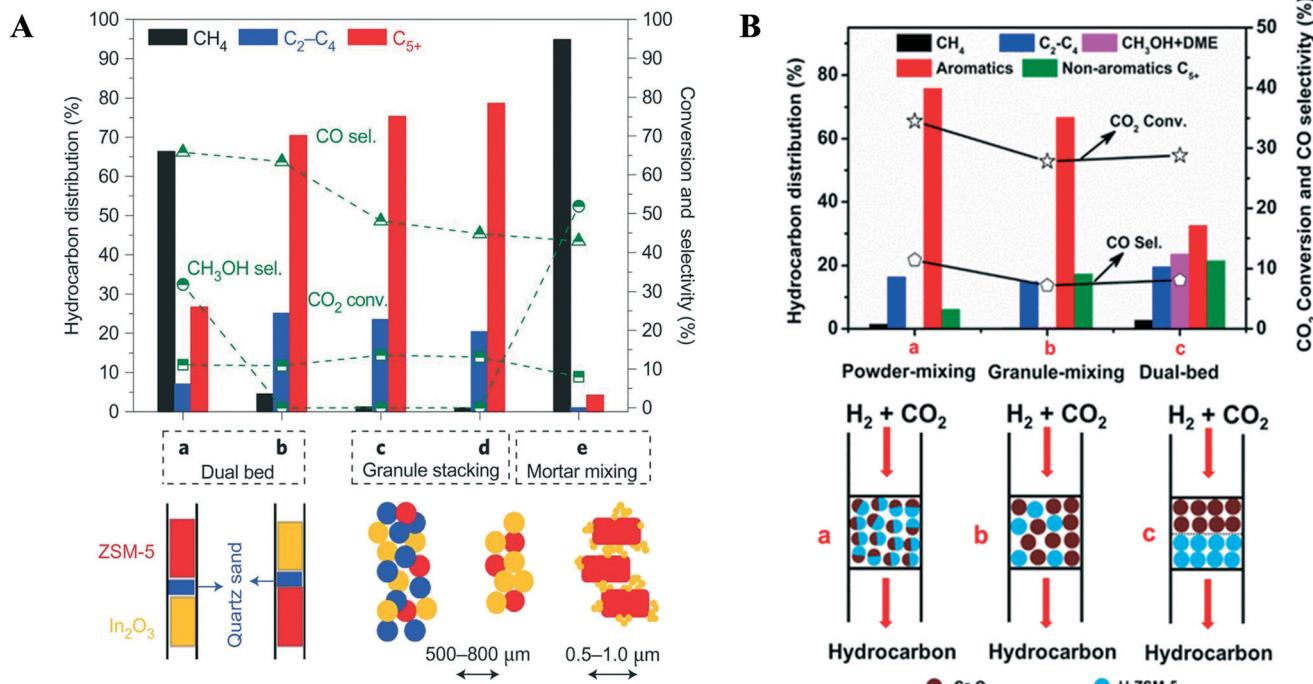
Fig. 14 Influence of the integration manner of the active components in various studies (A) over the In$_2$O$_3$/HZSM–5 composite. Reprinted with permission from ref. 221. (B) over Cr$_2$O$_3$/H-ZSM-5. "Reprinted (adapted) with permission from Y. Wang, L. Tan, M. Tan, P. Zhang, Y. Fang, Y. Yoneyama, G. Yang and N. Tsubaki, *ACS Catal.*, 2018, **9**, 895–901. Copyright (2019) American Chemical Society". (B) Over ZnZrO/SAPO. "Reprinted (adapted) with permission from Z. Li, J. Wang, Y. Qu, H. Liu, C. Tang, S. Miao, Z. Feng, H. An and C. Li, *ACS Catal.*, 2017, **7**, 8544–8548. Copyright (2017) American Chemical Society".

decreased significantly, whereas the CO$_2$ conversion only changed slightly. The catalyst performance was the same with and without addition of quartz sand in the case of granule

Fig. 15 Over ZnZrO/SAPO. "Reprinted (adapted) with permission from Z. Li, J. Wang, Y. Qu, H. Liu, C. Tang, S. Miao, Z. Feng, H. An and C. Li, *ACS Catal.*, 2017, **7**, 8544–8548. Copyright (2017) American Chemical Society".

stacking. Further, the distance between In$_2$O$_3$ and ZSM-5 was decreased by grinding them in an agate mortar into powder form to explore the effect of their intimate contact. In the case of mortar mixing, the much smaller In$_2$O$_3$ particles having a particle size of 10 nm were in a much closer contact with the 500–800 nm HZSM-5 particles. The authors found very low selectivity (4.2%) for C$_{5+}$ hydrocarbons and high selectivity for CH$_4$ (94.3%) among the hydrocarbons excluding alcohols and CH$_3$OH (51.9%) with 8% CO$_2$ conversion. The results suggested that close contact decreased the synergistic effect between In$_2$O$_3$ and ZSM-5 and caused a significant deactivation of HZSM-5. Similar observations were found over In–Zr/SAPO-34 and Na–Fe$_3$O$_4$/HZSM-5 catalysts,[237,241] whereas other studies suggest that it may occur due to the poisoning of the acid sites of the zeolite by In species.

ZnZrO/SAPO-34, Cr$_2$O$_3$/H-ZSM-5 and ZnZrO/H-ZSM-5 gave higher selectivity towards hydrocarbons when both components are packed *via* powder mixing.[227,233,240] The effect of ball milling and granule stacking styles of In$_2$O$_3$/ZrO$_2$ and SAPO-34 catalysts was studied.[225] It was found that the activity of the catalysts was reduced in the case of ball milling as it damaged the structure of the SAPO-34 zeolite, which was observed from characterization techniques. In addition, when the mixture of In$_2$O$_3$/ZrO$_2$ and SAPO-34 powder was packed in a granule stacking manner, the selectivity for light olefins was increased, due to a timely diffusion of CH$_3$OH into the zeolite to convert to hydrocarbons.
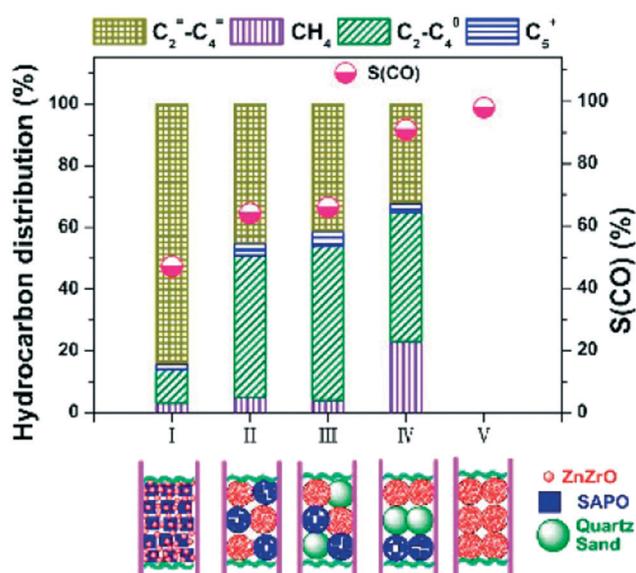
This journal is © The Royal Society of Chemistry 2021

Catal. Sci. Technol., 2021, **11**, 1665–1697 | **1687**

The best catalytic performance for aromatics production was found when Cr_2O_3 and ZSM-5 were in close proximity (Fig. 14B).[234] Further, the closeness of Cr_2O_3 and ZSM-5 was increased by ball milling and no change was observed in the selectivity for aromatics. When a prolonged distance was maintained between the two components it was difficult for the intermediate species formed on the metal oxide surface to reach ZSM-5 active sites to begin the subsequent MTA step. In the dual-bed configuration, the CH_3OH selectivity was high when the Cr_2O_3 catalyst was placed above the zeolite and quartz wool was loaded between them. Thus, the results suggested that the arrangement of Cr_2O_3 and ZSM-5 inside the reactor plays an important role in direct CO_2 conversion to aromatics or hydrocarbons.

The catalytic performance of a ZnZrO/SAPO-34 catalyst was determined by changing the two individual catalysts' positions and distance inside a tubular fixed bed reactor (Fig. 15).[227] The selectivity for lower olefins was decreased abruptly from 80% to 40%, whereas the selectivity for CO increased from 43% to 62% when the 250–450 nm granules of ZnZrO and zeolite were in mixed form in the reactor, compared to other integrated methods. No change was found in the results when quartz sand particles with the same size were mixed with ZnZrO and zeolite. This suggests that the spatial separation between ZnZrO and SAPO was the main factor influencing the selectivity. Further, when a quartz sand layer was situated between ZnZrO and SAPO-34 particles, the $C_2^=$–$C_4^=$ selectivity dropped sharply, and CO became the major product. The authors found that the excellent performance of the tandem catalyst was due to the effective synergy interaction between ZnZrO and SAPO-34.

4. Kinetic modeling

Detailed knowledge of the performance and mechanisms of CO_2 hydrogenation reactions can be obtained from kinetic modeling. The kinetic models can have widely different levels of detail and are mainly based on different approximations related to the rate determining steps and the nature of surface intermediates of the reaction.

4.1 Kinetics of CO_2 hydrogenation to methanol

In continuation of the discussion about the reaction intermediates and mechanisms related to copper-based and different oxide-based catalysts in sections 2.1.1 and 2.1.2, in this section, an overview of the kinetic models for the synthesis of methanol from CO_2 hydrogenation will be discussed in detail. Methanol is produced on an industrial scale from synthesis gas mixtures consisting of $CO/CO_2/H_2$ over commercial $Cu/ZnO/Al_2O_3$ catalysts under typical reaction conditions of 503–553 K and 5–12 MPa.[133] Kinetic modeling for methanol synthesis has been conducted for many years. Initially, most of the kinetic studies focused on macrokinetic modeling based on the Langmuir–Hinshelwood mechanism over Cu–Zn–Al catalysts. Later, the increasing efficiency of DFT and other electronic structure modeling

techniques has led to the development of sophisticated microkinetic models with the introduction of kinetic equations including concentration and temperature effects using the DFT results as an initiation point for the estimation of model parameters.

Different types of kinetic models for methanol synthesis have been reported in the literature.[242–245] Some older models have mostly focused on methanol synthesis from CO over copper-based catalysts, whereas newer studies focus mainly on direct hydrogenation of CO_2 to form methanol. Villa et al. used the Langmuir–Hinshelwood technique considering the non-dissociative adsorption of CO and H_2 to model the kinetics of methanol synthesis at low pressure from carbon monoxide and hydrogen over a $Cu/ZnO/Al_2O_3$ catalyst.[246] A kinetic model that quantitatively described the influence of concentration of carbon dioxide on methanol synthesis was introduced by Klier et al.[247] They proposed that the highest rate can be obtained by a balance between the promoting effect of CO_2 that can maintain the catalyst in an active state via its oxidizing ability and the decelerating effect from the strong adsorption of CO, when present at higher concentrations.[247] Later, a comprehensive kinetic study on methanol synthesis at low pressure utilizing CO, CO_2 and hydrogen over a $Cu/ZnO/Al_2O_3$ catalyst was introduced by Graaf et al.[248] which later has been refitted and reused by several other authors to understand their models with rates calculated under industrial conditions with commercially available catalysts.[100,247,249–251] Graaf et al.[248] explained their experimental results for methanol synthesis kinetics using a two-site Langmuir–Hinshelwood mechanism depending on dissociative hydrogen adsorption and three independent overall reactions: methanol synthesis from CO and CO_2 and the reverse water gas shift reaction. The results from the model suggested that methanol could be formed from both CO and CO_2, and that hydrogen was adsorbed dissociatively. One site was devoted to the competitive adsorption of CO and CO_2, while the other site was committed to the competitive adsorption of H_2 and water. The adsorption of methanol was supposed to be insignificant. The reactions were studied in a spinning basket reactor at a pressure of 15–50 bar and temperature of 483–518 K.[248,252,253]

A recent study by Diaz et al. shows the kinetics of CO_2 hydrogenation to methanol at atmospheric pressure utilizing a Pd–Cu–Zn/SiC catalyst. They developed three types of Langmuir–Hinshelwood (LH) kinetic models where the adsorption term was changed accordingly (competitive vs. two-site vs. three-site adsorption mechanisms). The hydrogenation of formate has been proposed as the rate determining step. The first model considered competitive adsorption of the reactants on the catalyst surface, the second model considered Pd and ZnO as two different adsorption sites and finally a three-site kinetic model was suggested where PdZn or PdCu along with ZnO had been considered as the adsorption sites. Finally, the proposed models were compared, and proper model differentiation was performed. It was established that the three-site LH kinetic model bestowed the minimum

1688 | Catal. Sci. Technol., 2021, **11**, 1665–1697

This journal is © The Royal Society of Chemistry 2021

unweighted residual sum of squares and satisfied all the confirmed restrictions and fitted well with the experimental results. Therefore, this was concluded to be the most suitable kinetic model.[254] The reaction rate equations for methanol synthesis from CO_2 and the RWGS reaction (eqn (8) and (9)) proposed by Díaz et al.[254] are as follows:

CO_2 hydrogenation:

$$r_{\text{MeOH-CO}_2} = \frac{k'_{\text{MeOH-CO}_2} \cdot K_{\text{CO}_2,\text{s}_1} \cdot K_{\text{H}_2,\text{s}_2} \cdot \frac{\left(P_{\text{CO}_2} \cdot P_{\text{H}_2}^3 - \frac{P_{\text{MeOH}} \cdot P_{\text{H}_2\text{O}}}{K_{\text{eqMeOH-CO}_2}}\right)}{P_{\text{H}_2}^2}}{D_{\text{MeOH-CO}_2}} \quad (8)$$

RWGS reaction:

$$r_{\text{RWGS}} = \frac{k'_{\text{RWGS}} \cdot K_{\text{CO}_2,\text{s}_3} \cdot \sqrt{K_{\text{H}_2,\text{s}_2}} \cdot \frac{P_{\text{CO}_2} \cdot P_{\text{H}_2} - \frac{P_{\text{CO}} \cdot P_{\text{H}_2\text{O}}}{K_{\text{eqRWGS}}}}{P_{\text{H}_2}^{0.5}}}{D_{\text{RWGS}}} \quad (9)$$

where the denominators of the rate equations refer to the adsorption terms as shown in Table 4.

As mentioned above, recent studies have focused more on microkinetic modeling for methanol synthesis from CO_2 hydrogenation considering various presumptions regarding the mechanism and the rate determining steps. A detailed mean-field microkinetic model for methanol synthesis and water–gas-shift reactions that included reaction intermediates e.g. HCOOH* and $CH_3O_2^*$ and allowed for the development of formic acid (HCOOH), formaldehyde (CH_2O), and methyl formate ($HCOOCH_3$) as byproducts has been considered by Grabow and Mavrikakis.[133] All the initial model parameters were deduced from periodic density functional theory (DFT) calculations on the Cu (111) surface and thereafter fitted to the experimental results performed under standard conditions using a $Cu/ZnO/Al_2O_3$ catalyst. It was observed that the WGS reaction mainly proceeds following the carboxyl pathway (that was explained above in sections 2.1.1. and 2.1.2) whereas both CO and CO_2 hydrogenation pathways are mostly operative for methanol synthesis.[133]

Indium oxide has been considered as a highly efficient catalyst for methanol synthesis by direct CO_2 hydrogenation as discussed in section 2.2. Pérez-Ramírez et al.[159] explained in detail the mechanistic and kinetic aspects of CO_2 hydrogenation on In_2O_3. Microkinetic modeling based on DFT simulations performed on $In_2O_3(111)$ supplied values for temperature and concentration-dependent rate expressions, which were shown to be in good agreement with the

experimental results. Microkinetic simulations were used to predict apparent activation energies and reaction orders and these agreed well with the experimental measurements. This is the only report, to date, on the kinetic modeling for CO_2 hydrogenation based on an indium oxide catalyst.[159] Another mean-field microkinetic model was used to forecast the reaction kinetics of different catalyst compositions on CO_2 hydrogenation, based on 33 reversible preliminary steps.[255] The model incorporates all the reaction pathways as calculated utilizing DFT without any assumptions on the rate determining step. First-principles multiscale modeling was achieved for a commercial-like catalyst (Zn_3O_3/Cu) and three other Cu/metal oxide-based catalysts (Cr_3O_3/Cu, Fe_3O_3/Cu, and Mg_3O_3/Cu). From the micro-kinetic modeling, methanol selectivity and conversion were acquired for each of the catalysts under various experimental conditions.[255] Apart from the well-reported static microkinetic models, a dynamic microkinetic model for methanol synthesis was proposed by Norskov et al. over a Cu/ZnO catalyst. The model contains the dynamic changes in particle morphology and the active surface area and also describes the kinetic behaviour under transient conditions.[249]

Having discussed both macro- as well as micro-kinetic modeling techniques for CO_2 hydrogenation to methanol, it is necessary to discuss the strengths and weaknesses of these modeling techniques. Macro-kinetic modeling deals with simple models built on power law kinetics or empirical Langmuir–Hinshelwood–Hougen–Watson (LHHW) kinetics predict reaction rates directly from the composition of the feed gas, temperature and pressure. Macrokinetic modeling is very practical and highly used in designing chemical reactors, quality control in catalyst synthesis, evaluating catalyst preferences and studies of catalyst deactivation. The models used in macro-kinetic calculations are therefore very robust for the fitting of kinetic data. However, the robustness that makes them so practical when used as empirical expressions makes them less useful for the determination of the mechanism of the reactions. These models do not explain the elementary reaction steps at the molecular level and different model formulations can often adequately describe the same experimental data. Therefore, a more comprehensive inspection of the reaction kinetics can be performed using microkinetic modeling, where an elementary reaction scheme and the molecular states of reactants and intermediates are utilized in simulating the

Table 4 Adsorption terms for the different types of models as reported by Díaz et al.[254]

Models	Conditions	Adsorption term
Competitive adsorption	$D_{\text{MeOH-CO}_2} = D_{\text{RWGS}} = D_\text{x}$ $\text{s}_1 = \text{s}_2 = \text{s}_3 = \text{s}$	$D_\text{x} = \left(1 + K_{\text{CO}_2,\text{s}} \cdot P_{\text{CO}_2} + \sqrt{K_{\text{H}_2,\text{s}}} \cdot P_{\text{H}_2}\right)^2$
Two-site mechanism	$D_{\text{MeOH-CO}_2} = D_{\text{RWGS}} = D_\text{x}$ $\text{s}_1 = \text{s}_3 = \text{s}$	$D_\text{x} = \left(1 + K_{\text{CO}_2,\text{s}} \cdot P_{\text{CO}_2}\right) \cdot \left(1 + \sqrt{K_{\text{H}_2,\text{s}}} \cdot P_{\text{H}_2}\right)$
Three-site mechanism	—	$D_{\text{MeOH-CO}_2} = \left(1 + K_{\text{CO}_2,\text{s}_1} \cdot P_{\text{CO}_2}\right) \cdot \left(1 + \sqrt{K_{\text{H}_2,\text{s}_2}} \cdot P_{\text{H}_2}\right)$ $D_{\text{RWGS}} = \left(1 + K_{\text{CO}_2,\text{s}_3} \cdot P_{\text{CO}_2}\right) \cdot \left(1 + \sqrt{K_{\text{H}_2,\text{s}_2}} \cdot P_{\text{H}_2}\right)$

s = active sites.

This journal is © The Royal Society of Chemistry 2021

Catal. Sci. Technol., 2021, 11, 1665–1697 | 1689

reaction at the molecular level.[256] Also, kinetic parameters in microkinetic models (like preexponential factors and activation energies) can be predicted from quantum mechanical modeling methods like DFT calculations. These aid in the identification of possible rate determining steps. The verification of microkinetic models depends on more elaborate surface measurement techniques and hence they can potentially make accurate predictions over a wide range of reaction conditions. Microkinetic modeling is computationally more demanding and hence not as robust as macrokinetic modeling. Hence both the modeling techniques have their importance in their own ways and are therefore considered significant in studying the kinetic modeling for catalytic hydrogenation reactions.

4.2 Kinetics of CO_2 hydrogenation from methanol to hydrocarbons

Section 2.2.1 introduced the basic conceptual mechanisms behind the MTH reactions; in this section, we discuss how they are formulated in terms of rate expressions with varying detail. Kinetic modeling of MTH reactions has been studied over many years mostly over ZSM-5 and SAPO. The incorporation of C_6^+ compounds in the models with the ZSM-5 zeolite marks the difference between the models based on ZSM-5 and SAPO.

Detailed kinetic models were formulated by Froment et al.[257,258] for the methanol to olefins (MTO) conversion over HZSM-5 catalysts with a Si/Al molar ratio of 200. The primary products (ethylene and propylene) formed from methanol and DME were modeled accurately using the Hougen–Watson model. The emergence of higher olefins was demonstrated with the help of the carbenium ion mechanism. The Evans–Polanyi relation was used to determine the activation energies of each step that considers the different energy levels of the carbenium ions and the olefin isomers.[257] In a continuation of this work, the authors tested eight kinetic models based on the fundamental steps for the conversion of methanol via dimethyl ether into olefins and determined 33 parameters. Nonlinear regression was used to minimize the function used for parameter estimation.[258] Zhou et al.[259] worked with ethylene, propylene, and n-butylene over the SAPO-34 catalyst at 723 K using a fixed-bed reactor with a weight hourly space velocity (WHSV) varying from 1 to 424 h^{-1}. The proposed kinetic model showed that the olefin concentrations were in equilibrium using a carbenium intermediate lump. The model was able to predict their results adequately.[259]

Gayubo et al. presented extensive modeling on MTO reaction kinetics with SAPO catalysts.[260–263] They proposed a kinetic model for the conversion of methanol to olefins over a SAPO-34 catalyst and further extended their studies on a SAPO-18 catalyst for a wide range of experimental conditions. Fig. 16 shows the kinetic reaction scheme for the methanol to olefins process that is used by Gayubo et al.[262] The kinetic model consists of three basic steps that develop gradually over time: an initiation period (formation of the active intermediate compounds), olefin formation, and finally deactivation stage (coke formation). Through this kinetic model, the authors predicted the experimental progress of the formation of olefins with time. Initially the production rate increases, later it passes through a maximum, where the concentration of the active intermediates reaches the maximum, followed by a reduction when deactivation causes a degeneration of the intermediates to form coke.[260–263] The same group also proposed a kinetic model including the effect of water on the MTG reaction kinetics on the HZSM-5 catalyst. They further extended the study by considering the effect of water in the kinetic model for catalyst deactivation.[264,265]

On the basis of the hydrocarbon pool mechanism (as explained in section 2.2.1.2), Kaarsholm et al.[266] proposed a model in which high molecular weight hydrocarbons were formed along with olefins inside the pores of the catalysts. The MTO reaction was studied for a phosphorus modified ZSM-5 catalyst in a fluidized bed reactor. The model involved 15 main reaction steps where, at equilibrium, all olefins are formed inside the pores of the catalyst. Fig. 17A shows the schematic for the reactions accounted for in this model by Kaarsholm et al.[266] This model fits well with the experimental data for the olefins but requires modifications in the case of paraffin and C_6^+ species (Fig. 17B). The olefinic species formed as products all through the temperature interval explored were well verified by the model.[266] Recently a new lumped kinetic model was established by Ryu et al.[267] with 9 reactions consisting of 7 lumps of products and intermediates that include methane, ethylene, propylene, butenes, propane, C_4 (that includes butane and 1,3-butadiene) and C_{5+} (including hydrocarbons with five or more carbon atoms and ethane) to investigate the catalytic activity of SAPO-34 for MTO reactions under various process conditions. This simple kinetic model is based on the hydrocarbon pool mechanism that has been developed from a detailed kinetic model by Bos et al.[268] The model is developed based on the assumption that all the reaction rate expressions are first order.[267]
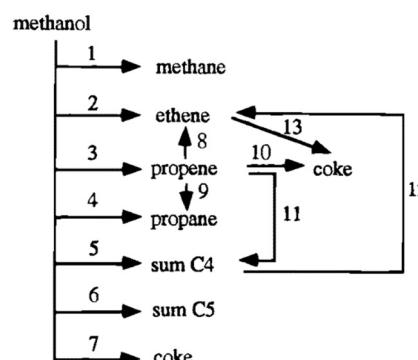
**Fig. 16** Kinetic scheme proposed by Bos et al.[268] for transformation of methanol on SAPO-34. Reprinted (adapted) with permission from A. G. Gayubo, A. T. Aguayo, A. E. Sánchez del Campo, A. M. Tarrío and J. Bilbao, Ind. Eng. Chem. Res., 2000, **39**, 292–300, Copyright (2000) American Chemical Society.

1690 | Catal. Sci. Technol., 2021, **11**, 1665–1697

This journal is © The Royal Society of Chemistry 2021
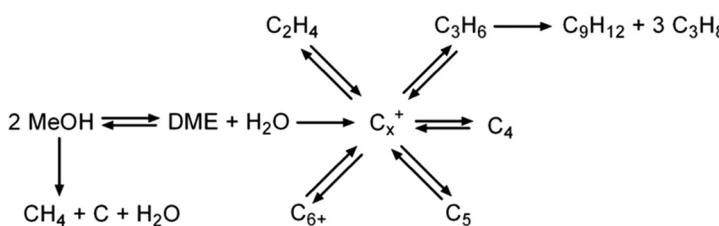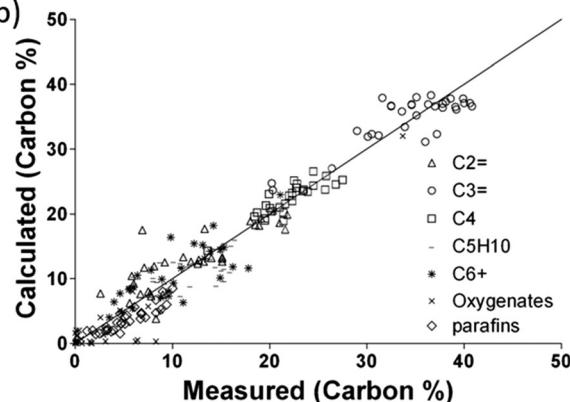
Fig. 17 (a) Schematic drawing of the kinetic model and (b) parity plot showing the comparison of the calculated product distribution to the measured data by Kaarsholm *et al.* Reprinted (adapted) with permission from M. Kaarsholm, B. Rafii, F. Joensen, R. Cenni, J. Chaouki and G. S. Patience, *Ind. Eng. Chem. Res.*, 2010, **49**, 29–38, Copyright (2010) American Chemical Society.

4.3 Kinetics of direct CO_2 hydrogenation using bifunctional catalysts

To increase the CO_2 conversion rate to methanol by coupling with MTO reactions, direct CO_2 hydrogenation using bifunctional catalysts has become recently prominent as described in section 3. But there are, to our knowledge, no kinetic modeling studies, as such, for direct CO_2 hydrogenation to hydrocarbons with methanol as an intermediate. It would seem possible to combine the standard models for CO_2 hydrogenation to methanol and MTO (as discussed in sections 4.1 and 4.2 in detail) together to describe the performance of the direct CO_2 hydrogenation procedure. However, it is noted from the experimental studies, as discussed in section 3.1, that with direct CO_2 hydrogenation, the performance of the combined catalyst was greater than the sum of the individual catalysts. Perhaps, this is due simply to coupling the reactions and its favourable effect on methanol synthesis thermodynamics perhaps, or there are other combined synergy effects of the catalysts. It was, for example, presumed that for Cr_2O_3/HZSM-5, this combination of catalysts allowed the surface diffusion of methanol intermediates from the oxide to the zeolite. A kinetic modeling study could be used to explore these possibilities and to identify possibly improved operating conditions for direct CO_2 hydrogenation.

5. Conclusion and future perspectives

Urgent action is needed in terms of decreasing CO_2 emissions in order to mitigate the challenges given by global warming. Currently, one promising action is to capture CO_2 and recycle it to useful chemicals and fuels. In this review, we have summarized the recent progress in producing chemicals and fuels, like methanol and hydrocarbons, by using CO_2 as a feedstock. The most studied reactions are the catalytic hydrogenation of CO_2 to methanol and hydrocarbons. In the case of indirect production of hydrocarbons, the CO_2 to methanol conversion is explored

on Cu, Pd, Pt, Zn, In, Ga, Ag, Au, ZnO, In_2O_3, Ga_2O_3 and ZrO_2. Methanol synthesis from CO_2 is facing some challenges such as the excessive formation of CO which affects the selectivity for the desired product. There are many aspects where future research could be focused, for example, increasing the yield of fuels and chemicals by catalyst development; the uncertainty about the intermediates on the surface of the catalysts; the exact role of support materials; mechanisms of catalyst deactivation; interface composition; structure of active sites if catalysts have more than one active site for example in the case of bimetallic catalysts and when the support material also contains an active site; and different types of modelling such as kinetic modelling.

In recent years, advanced developments have been made by various research groups by developing bifunctional catalysts to convert CO_2 to hydrocarbons and fuels. In the case of bifunctional catalysts, two different catalysts are combined to form hydrocarbons in a one stage process. The mechanism, preparation methods and proximity effects were discussed using various *in situ* experiments and DFT studies. It has been seen that the intimate contact between the catalysts could increase the selectivity for hydrocarbons but the mechanism for this is unclear as intimate intra-particle contact was found to be negative in a few studies. In a few studies, it was concluded that close contact helped to promote the timely diffusion of methanol into zeolites and this increased the selectivity for hydrocarbons while in other studies the zeolites were poisoned by the metal/metal-oxide catalyst used for methanol synthesis. Thus, it is difficult to say exactly what proximity between the catalyst materials is optimal for the highest selectivity and conversion. The thermodynamics and reaction kinetics are different for the reactions (CO_2 to methanol and MTH) as the active site needs different temperatures for the activation of CO_2 and C–C coupling. A mean temperature, that is somewhere between the temperature most often used and favorable for the individual methanol synthesis and MTH processes, was used in recent reports for the activation of the catalysts. However,

This journal is © The Royal Society of Chemistry 2021

Catal. Sci. Technol., 2021, **11**, 1665–1697 | **1691**

the temperature was found a limiting factor for bifunctional catalysts as higher temperature is favorable for the RWGS reaction and CO_2 activation whereas low temperature decreases the CO_2 conversion. Yet, studies have shown that the two reactions could be coupled efficiently to produce hydrocarbons from CO_2 in a single step. Moreover, it was noticed that the lifetime of zeolite catalysts in the MTH reaction could be slightly improved in the presence of H_2, CO_2 and H_2O co-feeds, which are the reactants and byproducts of the CO_2 to methanol reaction step. A suitable choice/modification of the zeolite catalyst could be used to steer the production of hydrocarbons of different carbon numbers.

Most of the studies reported that a decrease in the selectivity for CO and CH_4 could be achieved for bifunctional catalysts due to a synergetic interaction between both catalysts. But the mechanism and factors behind this are still unclear and deserve further research. However, bifunctional catalysts suffer from a low one-pass conversion efficiency and high selectivity towards CO in the case of direct synthesis. Also, the reported methanol selectivity in most studies for bifunctional systems is zero or very minimal and thus it can be concluded that for many systems it is possible to operate under conditions such that the rate of conversion of CO_2 and CO to methanol is limiting, whereas the conversion of methanol to hydrocarbons is relatively fast. Thus, it is possible for the equilibrium limitations for the methanol synthesis reaction to be avoided, which can be a factor allowing for somewhat lower selectivity for CO as compared to the process without further conversion of methanol to hydrocarbons. There is a gap in understanding of the mechanism after methanol synthesis and before C–C coupling in the case of bifunctional catalysts that needs to be addressed. For example, more than one intermediate is observed on the surface of catalysts but only one of them is likely responsible for forming the product, so it is unclear what the rest of the intermediates form and what/how they affect the selectivity and activity of the catalyst. In most cases, the selectivity for longer hydrocarbons is very low due to kinetic limitations of the C–C coupling. Efforts could focus to producing longer hydrocarbons from these bifunctional catalysts by modifications in catalyst structure and composition, changing the synthesis method of catalysts, and modifications in the packing method to obtain an efficient contact between both catalysts. We have assessed the reaction kinetics of both CO_2 to methanol and MTO reactions with a view of developing new kinetic models that couple these reactions and their catalysts for direct CO_2 hydrogenation to higher hydrocarbons with methanol as an intermediate, which warrants investigation.

Thus, we suggest that further research could emphasize the development of highly active catalysts for methanol synthesis as well as selective hydrocarbon synthesis and higher CO_2 conversion under industrially relevant conditions with better understanding of the fundamental activity–structure–composition relationship in bifunctional catalysts.

Conflicts of interest

There are no conflicts to declare.

Acknowledgements

References

1 J. Rogelj, M. Den Elzen, N. Höhne, T. Fransen, H. Fekete, H. Winkler, R. Schaeffer, F. Sha, K. Riahi and M. Meinshausen, *Nature*, 2016, **534**, 631–639.

2 S. J. Davis, K. Caldeira and H. D. Matthews, *Science*, 2010, **329**, 1330–1333.

3 G. Energy, *International Energy Agency: Paris, France*, 2018.

4 G. A. Olah, G. S. Prakash and A. Goeppert, *J. Am. Chem. Soc.*, 2011, **133**, 12881–12898.

5 S. Brynolf, M. Taljegard, M. Grahn and J. Hansson, *Renewable Sustainable Energy Rev.*, 2018, **81**, 1887–1905.

6 E. V. Kondratenko, G. Mul, J. Baltrusaitis, G. O. Larrazábal and J. Pérez-Ramírez, *Energy Environ. Sci.*, 2013, **6**, 3112–3135.

7 J. Hansson, R. Hackl, M. Taljegard, S. Brynolf and M. Grahn, *Front. Energy Res.*, 2017, **5**, 4.

8 K. M. K. Yu, I. Curcic, J. Gabriel and S. C. E. Tsang, *ChemSusChem*, 2008, **1**, 893–899.

9 D. Y. Leung, G. Caramanna and M. M. Maroto-Valer, *Renewable Sustainable Energy Rev.*, 2014, **39**, 426–443.

10 R. L. Newmark, S. J. Friedmann and S. A. Carroll, *Environ. Manage.*, 2010, **45**, 651–661.

11 C. M. Oldenburg, *Greenhouse Gases: Sci. Technol.*, 2012, **2**, 1–2.

12 W. Seifritz, *Nature*, 1990, **345**, 486–486.

13 S. C. Roy, O. K. Varghese, M. Paulose and C. A. Grimes, *ACS Nano*, 2010, **4**, 1259–1278.

14 E. Alper and O. Y. Orhan, *Petroleum*, 2017, **3**, 109–126.

15 S. E. Hosseini and M. A. Wahid, *Renewable Sustainable Energy Rev.*, 2016, **57**, 850–866.

16 M. Liu, Y. Yi, L. Wang, H. Guo and A. Bogaerts, *Catalysts*, 2019, **9**, 275.

17 M. Fujiwara, R. Kieffer, H. Ando and Y. Souma, *Appl. Catal., A*, 1995, **121**, 113–124.

18 S. Abelló and D. Montané, *ChemSusChem*, 2011, **4**, 1538–1556.

19 R.-P. Ye, J. Ding, W. Gong, M. D. Argyle, Q. Zhong, Y. Wang, C. K. Russell, Z. Xu, A. G. Russell and Q. Li, *Nat. Commun.*, 2019, **10**, 1–15.

20 H. Yang, C. Zhang, P. Gao, H. Wang, X. Li, L. Zhong, W. Wei and Y. Sun, *Catal. Sci. Technol.*, 2017, **7**, 4580–4598.

21 Z. Ma and M. D. Porosoff, *ACS Catal.*, 2019, **9**, 2639–2656.

22 M. M.-J. Li and S. C. E. Tsang, *Catal. Sci. Technol.*, 2018, **8**, 3450–3464.

23 I. U. Din, M. S. Shaharun, M. A. Alotaibi, A. I. Alharthi and A. Naeem, *J. CO2 Util.*, 2019, **34**, 20–33.

24 A. Álvarez, A. Bansode, A. Urakawa, A. V. Bavykina, T. A. Wezendonk, M. Makkee, J. Gascon and F. Kapteijn, *Chem. Rev.*, 2017, **117**, 9804–9838.

25 S. Dang, H. Yang, P. Gao, H. Wang, X. Li, W. Wei and Y. Sun, *Catal. Today*, 2019, **330**, 61–75.

26 M. Aresta, A. Dibenedetto and A. Angelini, *Chem. Rev.*, 2013, **114**, 1709–1742.

27 W. Li, H. Wang, X. Jiang, J. Zhu, Z. Liu, X. Guo and C. Song, *RSC Adv.*, 2018, **8**, 7651–7669.

28 V. Ipatieff and G. Monroe, *J. Am. Chem. Soc.*, 1945, **67**, 2168–2171.

29 M. Behrens, *Angew. Chem., Int. Ed.*, 2016, **55**, 14906–14908.

30 K.-i. Tominaga, Y. Sasaki, T. Watanabe and M. Saito, *Bull. Chem. Soc. Jpn.*, 1995, **68**, 2837–2842.

31 S. Bebelis, H. Karasali and C. Vayenas, *Solid State Ionics*, 2008, **179**, 1391–1395.

32 D. Theleritis, M. Makri, S. Souentie, A. Caravaca, A. Katsaounis and C. G. Vayenas, *ChemElectroChem*, 2014, **1**, 254–262.

33 M. Hoque and M. Guzman, *Materials*, 2018, **11**, 1990.

34 K. Li, B. Peng and T. Peng, *ACS Catal.*, 2016, **6**, 7485–7527.

35 M. Mikkelsen, M. Jørgensen and F. C. Krebs, *Energy Environ. Sci.*, 2010, **3**, 43–81.

36 S. G. Jadhav, P. D. Vaidya, B. M. Bhanage and J. B. Joshi, *Chem. Eng. Res. Des.*, 2014, **92**, 2557–2567.

37 J. Wu, M. Saito, M. Takeuchi and T. Watanabe, *Appl. Catal., A*, 2001, **218**, 235–240.

38 Y. Jiang, H. Yang, P. Gao, X. Li, J. Zhang, H. Liu, H. Wang, W. Wei and Y. Sun, *J. CO2 Util.*, 2018, **26**, 642–651.

39 C. Tisseraud, C. Comminges, A. Habrioux, S. Pronier, Y. Pouilloux and A. Le Valant, *Mol. Catal.*, 2018, **446**, 98–105.

40 Y. Yang, J. Evans, J. A. Rodriguez, M. G. White and P. Liu, *Phys. Chem. Chem. Phys.*, 2010, **12**, 9909–9917.

41 R. A. Köppel, C. Stöcker and A. Baiker, *J. Catal.*, 1998, **179**, 515–527.

42 A. García-Trenco, A. Regoutz, E. R. White, D. J. Payne, M. S. Shaffer and C. K. Williams, *Appl. Catal., B*, 2018, **220**, 9–18.

43 S. Li, Y. Wang, B. Yang and L. Guo, *Appl. Catal., A*, 2019, **571**, 51–60.

44 K. Sun, Z. Fan, J. Ye, J. Yan, Q. Ge, Y. Li, W. He, W. Yang and C.-j. Liu, *J. CO2 Util.*, 2015, **12**, 1–6.

45 R. Guil-López, N. Mota, J. Llorente, E. Millán, B. Pawelec, J. Fierro and R. Navarro, *Materials*, 2019, **12**, 3902.

46 R. Koeppel, A. Baiker and A. Wokaun, *Appl. Catal., A*, 1992, **84**, 77–102.

47 T. Fujitani, M. Saito, Y. Kanai, M. Takeuchi, K. Moriya, T. Watanabe, M. Kawai and T. Kakumoto, *Chem. Lett.*, 1993, **22**, 1079–1080.

48 M. Kilo, J. Weigel, A. Wokaun, R. Koeppel, A. Stoeckli and A. Baiker, *J. Mol. Catal. A: Chem.*, 1997, **126**, 169–184.

49 A. Erdöhelyi, M. Pásztor and F. Solymosi, *J. Catal.*, 1986, **98**, 166–177.

50 L. Fan and K. Fujimoto, *Appl. Catal., A*, 1993, **106**, L1–L7.

51 T. Fujitani, M. Saito, Y. Kanai, T. Watanabe, J. Nakamura and T. Uchijima, *Appl. Catal., A*, 1995, **125**, L199–L202.

52 X. Jiang, N. Koizumi, X. Guo and C. Song, *Appl. Catal., B*, 2015, **170**, 173–185.

53 M. R. Gogate and R. J. Davis, *Catal. Commun.*, 2010, **11**, 901–906.

54 E. L. Fornero, P. B. Sanguineti, D. L. Chiavassa, A. L. Bonivardi and M. A. Baltanás, *Catal. Today*, 2013, **213**, 163–170.

55 J. Słoczyński, R. Grabowski, P. Olszewski, A. Kozłowska, J. Stoch, M. Lachowska and J. Skrzypek, *Appl. Catal., A*, 2006, **310**, 127–137.

56 N. Pasupulety, H. Driss, Y. A. Alhamed, A. A. Alzahrani, M. A. Daous and L. Petrov, *Appl. Catal., A*, 2015, **504**, 308–318.

57 L. BASF, Germany, https://www.basf.com/global/en/who-we-are/history/chronology/1902-1924.html.

58 D. Sheldon, *Johnson Matthey Technol. Rev.*, 2017, **61**, 172–182.

59 M. Behrens, S. Zander, P. Kurr, N. Jacobsen, J. r. Senker, G. Koch, T. Ressler, R. W. Fischer and R. Schlögl, *J. Am. Chem. Soc.*, 2013, **135**, 6061–6068.

60 P. Davies, F. F. Snowdon, G. W. Bridger, D. O. Hughes and P. W. Young, *U.K. Pat.*, GB1010871, 1962.

61 J. T. Gallagher and J. M. Kidd, *U.K. Pat.*, GB 1159035, 1969.

62 F. Studt, M. Behrens, E. L. Kunkes, N. Thomas, S. Zander, A. Tarasov, J. Schumann, E. Frei, J. B. Varley and F. Abild-Pedersen, *ChemCatChem*, 2015, **7**, 1105–1111.

63 E. L. Kunkes, F. Studt, F. Abild-Pedersen, R. Schlögl and M. Behrens, *J. Catal.*, 2015, **328**, 43–48.

64 J. Liu, J. Shi, D. He, Q. Zhang, X. Wu, Y. Liang and Q. Zhu, *Appl. Catal., A*, 2001, **218**, 113–119.

65 T. Fujitani, M. Saito, Y. Kanai, T. Kakumoto, T. Watanabe, J. Nakamura and T. Uchijima, *Catal. Lett.*, 1994, **25**, 271–276.

66 C. Tisseraud, C. Comminges, S. Pronier, Y. Pouilloux and A. Le Valant, *J. Catal.*, 2016, **343**, 106–114.

67 T. Lunkenbein, J. Schumann, M. Behrens, R. Schlögl and M. G. Willinger, *Angew. Chem., Int. Ed.*, 2015, **54**, 4544–4548.

68 H. Lei, R. Nie, G. Wu and Z. Hou, *Fuel*, 2015, **154**, 161–166.

69 F. Liao, Y. Huang, J. Ge, W. Zheng, K. Tedsree, P. Collier, X. Hong and S. C. Tsang, *Angew. Chem., Int. Ed.*, 2011, **50**, 2162–2165.

70 J. Sun, G. Yang, Q. Ma, I. Ooki, A. Taguchi, T. Abe, Q. Xie, Y. Yoneyama and N. Tsubaki, *J. Mater. Chem. A*, 2014, **2**, 8637–8643.

71 S. Kuld, M. Thorhauge, H. Falsig, C. F. Elkjær, S. Helveg, I. Chorkendorff and J. Sehested, *Science*, 2016, **352**, 969–974.

72 J. Toyir, R. Miloua, N. Elkadri, M. Nawdali, H. Toufik, F. Miloua and M. Saito, *Phys. Procedia*, 2009, **2**, 1075–1079.

73 O. Martin, C. Mondelli, D. Curulla-Ferré, C. Drouilly, R. Hauert and J. Pérez-Ramírez, *ACS Catal.*, 2015, **5**, 5607–5616.

74 M. Behrens, F. Studt, I. Kasatkin, S. Kühl, M. Hävecker, F. Abild-Pedersen, S. Zander, F. Girgsdies, P. Kurr and B.-L. Kniep, *Science*, 2012, **336**, 893–897.

75 S. A. Kondrat, P. J. Smith, J. H. Carter, J. S. Hayward, G. J. Pudge, G. Shaw, M. S. Spencer, J. K. Bartley, S. H. Taylor and G. J. Hutchings, *Faraday Discuss.*, 2017, **197**, 287–307.

76 N. Mota, R. Guil-Lopez, B. Pawelec, J. Fierro and R. Navarro, *RSC Adv.*, 2018, **8**, 20619–20629.

77 R. Gaikwad, A. Bansode and A. Urakawa, *J. Catal.*, 2016, **343**, 127–132.

This journal is © The Royal Society of Chemistry 2021

Catal. Sci. Technol., 2021, **11**, 1665–1697 | 1693

78 B. Tidona, C. Koppold, A. Bansode, A. Urakawa and P. R. von Rohr, *J. Supercrit. Fluids*, 2013, **78**, 70–77.

79 A. Bansode and A. Urakawa, *J. Catal.*, 2014, **309**, 66–70.

80 C. Li, X. Yuan and K. Fujimoto, *Appl. Catal., A*, 2014, **469**, 306–311.

81 J. Słoczyński, R. Grabowski, A. Kozłowska, P. Olszewski, J. Stoch, J. Skrzypek and M. Lachowska, *Appl. Catal., A*, 2004, **278**, 11–23.

82 R. Raudaskoski, M. V. Niemelä and R. L. Keiski, *Top. Catal.*, 2007, **45**, 57–60.

83 J. Toyir, P. R. r. de la Piscina, J. L. G. Fierro and N. s. Homs, *Appl. Catal., B*, 2001, **29**, 207–215.

84 J. Toyir, P. R. r. de la Piscina, J. L. G. Fierro and N. s. Homs, *Appl. Catal., B*, 2001, **34**, 255–266.

85 M. Lachowska and J. Skrzypek, *React. Kinet. Catal. Lett.*, 2004, **83**, 269–273.

86 X.-M. Liu, G. Lu and Z.-F. Yan, *Appl. Catal., A*, 2005, **279**, 241–245.

87 J. B. Wang, H.-K. Lee and T.-J. Huang, *Catal. Lett.*, 2002, **83**, 79–86.

88 Z.-s. Hong, Y. Cao, J.-f. Deng and K.-n. Fan, *Catal. Lett.*, 2002, **82**, 37–44.

89 X. An, J. Li, Y. Zuo, Q. Zhang, D. Wang and J. Wang, *Catal. Lett.*, 2007, **118**, 264–269.

90 Y. Liu, Y. Zhang, T. Wang and N. Tsubaki, *Chem. Lett.*, 2007, **36**, 1182–1183.

91 F. Arena, K. Barbera, G. Italiano, G. Bonura, L. Spadaro and F. Frusteri, *J. Catal.*, 2007, **249**, 185–194.

92 X. Guo, D. Mao, S. Wang, G. Wu and G. Lu, *Catal. Commun.*, 2009, **10**, 1661–1664.

93 X. Guo, D. Mao, G. Lu, S. Wang and G. Wu, *J. Catal.*, 2010, **271**, 178–185.

94 E. Frei, A. Schaadt, T. Ludwig, H. Hillebrecht and I. Krossing, *ChemCatChem*, 2014, **6**, 1721–1730.

95 L. Li, D. Mao, J. Yu and X. Guo, *J. Power Sources*, 2015, **279**, 394–404.

96 L. Angelo, K. Kobl, L. M. M. Tejada, Y. Zimmermann, K. Parkhomenko and A.-C. Roger, *C. R. Chim.*, 2015, **18**, 250–260.

97 T. Witoon, J. Chalorngtham, P. Dumrongbunditkul, M. Chareonpanich and J. Limtrakul, *Chem. Eng. J.*, 2016, **293**, 327–336.

98 S. Kattel, B. Yan, Y. Yang, J. G. Chen and P. Liu, *J. Am. Chem. Soc.*, 2016, **138**, 12440–12450.

99 L. Angelo, M. Girleanu, O. Ersen, C. Serra, K. Parkhomenko and A.-C. Roger, *Catal. Today*, 2016, **270**, 59–67.

100 J.-F. o. Portha, K. Parkhomenko, K. Kobl, A.-C. c. Roger, S. Arab, J.-M. Commenge and L. Falk, *Ind. Eng. Chem. Res.*, 2017, **56**, 13133–13145.

101 X.-L. Liang, X. Dong, G.-D. Lin and H.-B. Zhang, *Appl. Catal., B*, 2009, **88**, 315–322.

102 S. E. Collins, M. A. Baltanás and A. L. Bonivardi, *J. Catal.*, 2004, **226**, 410–421.

103 S. E. Collins, J. J. Delgado, C. Mira, J. J. Calvino, S. Bernal, D. L. Chiavassa, M. A. Baltanás and A. L. Bonivardi, *J. Catal.*, 2012, **292**, 90–98.

104 X. Zhou, J. Qu, F. Xu, J. Hu, J. S. Foord, Z. Zeng, X. Hong and S. C. E. Tsang, *Chem. Commun.*, 2013, **49**, 1747–1749.

105 J. Qu, X. Zhou, F. Xu, X.-Q. Gong and S. C. E. Tsang, *J. Phys. Chem. C*, 2014, **118**, 24452–24466.

106 H. Bahruji, M. Bowker, G. Hutchings, N. Dimitratos, P. Wells, E. Gibson, W. Jones, C. Brookes, D. Morgan and G. Lalev, *J. Catal.*, 2016, **343**, 133–146.

107 A. Ota, E. L. Kunkes, I. Kasatkin, E. Groppo, D. Ferri, B. Poceiro, R. M. N. Yerga and M. Behrens, *J. Catal.*, 2012, **293**, 27–38.

108 Y. Hartadi, D. Widmann and R. J. Behm, *ChemSusChem*, 2015, **8**, 456–465.

109 Y. Hartadi, D. Widmann and R. J. Behm, *Phys. Chem. Chem. Phys.*, 2016, **18**, 10781–10791.

110 F. Studt, I. Sharafutdinov, F. Abild-Pedersen, C. F. Elkjær, J. S. Hummelshøj, S. Dahl, I. Chorkendorff and J. K. Nørskov, *Nat. Chem.*, 2014, **6**, 320–324.

111 C. Shao, L. Fan, K. Fujimoto and Y. Iwasawa, *Appl. Catal., A*, 1995, **128**, L1–L6.

112 T. Iizuka, M. Kojima and K. Tanabe, *J. Chem. Soc., Chem. Commun.*, 1983, 638–639.

113 T. Inoue, T. Iizuka and K. Tanabe, *Appl. Catal.*, 1989, **46**, 1–9.

114 H. Kusama, K. K. Bando, K. Okabe and H. Arakawa, *Appl. Catal., A*, 2001, **205**, 285–294.

115 H. Zhan, F. Li, P. Gao, N. Zhao, F. Xiao, W. Wei, L. Zhong and Y. Sun, *J. Power Sources*, 2014, **251**, 113–121.

116 I. Kasatkin, P. Kurr, B. Kniep, A. Trunschke and R. Schlögl, *Angew. Chem., Int. Ed.*, 2007, **46**, 7324–7327.

117 M. Behrens, *J. Catal.*, 2009, **267**, 24–29.

118 I. Sharafutdinov, C. F. Elkjær, H. W. P. de Carvalho, D. Gardini, G. L. Chiarello, C. D. Damsgaard, J. B. Wagner, J.-D. Grunwaldt, S. Dahl and I. Chorkendorff, *J. Catal.*, 2014, **320**, 77–88.

119 Y. Hartadi, D. Widmann and R. J. Behm, *J. Catal.*, 2016, **333**, 238–250.

120 J. Xiao and T. Frauenheim, *J. Phys. Chem. C*, 2013, **117**, 1804–1808.

121 K. Larmier, W. C. Liao, S. Tada, E. Lam, R. Verel, A. Bansode, A. Urakawa, A. Comas-Vives and C. Copéret, *Angew. Chem., Int. Ed.*, 2017, **56**, 2318–2323.

122 S.-i. Fujita, M. Usui, H. Ito and N. Takezawa, *J. Catal.*, 1995, **157**, 403–413.

123 L. Gao and C. Au, *J. Catal.*, 2000, **189**, 1–15.

124 Y. Yang, D. Mei, C. H. Peden, C. T. Campbell and C. A. Mims, *ACS Catal.*, 2015, **5**, 7328–7337.

125 M. D. Porosoff, B. Yan and J. G. Chen, *Energy Environ. Sci.*, 2016, **9**, 62–73.

126 Y.-F. Zhao, Y. Yang, C. Mims, C. H. Peden, J. Li and D. Mei, *J. Catal.*, 2011, **281**, 199–211.

127 J. Tabatabaei, B. Sakakini and K. Waugh, *Catal. Lett.*, 2006, **110**, 77–84.

128 Y. Yang, C. A. Mims, R. S. Disselkamp, J.-H. Kwak, C. H. Peden and C. Campbell, *J. Phys. Chem. C*, 2010, **114**, 17205–17211.

1694 | *Catal. Sci. Technol.*, 2021, **11**, 1665–1697

This journal is © The Royal Society of Chemistry 2021

129 S. Kattel, P. J. Ramírez, J. G. Chen, J. A. Rodriguez and P. Liu, *Science*, 2017, **355**, 1296–1299.

130 F. Arena, G. Italiano, K. Barbera, S. Bordiga, G. Bonura, L. Spadaro and F. Frusteri, *Appl. Catal., A*, 2008, **350**, 16–23.

131 Y. Yang, C. A. Mims, D. Mei, C. H. Peden and C. T. Campbell, *J. Catal.*, 2013, **298**, 10–17.

132 H. Nakatsuji and Z. M. Hu, *Int. J. Quantum Chem.*, 2000, **77**, 341–349.

133 L. Grabow and M. Mavrikakis, *ACS Catal.*, 2011, **1**, 365–384.

134 X. Zhang, J.-X. Liu, B. Zijlstra, I. A. Filot, Z. Zhou, S. Sun and E. J. Hensen, *Nano Energy*, 2018, **43**, 200–209.

135 K. Chen, H. Fang, S. Wu, X. Liu, J. Zheng, S. Zhou, X. Duan, Y. Zhuang, S. C. E. Tsang and Y. Yuan, *Appl. Catal., B*, 2019, **251**, 119–129.

136 E. Lam, K. Larmier, P. Wolf, S. Tada, O. V. Safonova and C. Copéret, *J. Am. Chem. Soc.*, 2018, **140**, 10530–10535.

137 W. Wang, Y. Zhang, Z. Wang, J.-m. Yan, Q. Ge and C.-j. Liu, *Catal. Today*, 2016, **259**, 402–408.

138 Q. Sun, J. Ye, C. j. Liu and Q. Ge, *Greenh Gases*, 2014, **4**, 140–144.

139 J. Ye, Q. Ge and C.-j. Liu, *Chem. Eng. Sci.*, 2015, **135**, 193–201.

140 J. Ye, C. Liu and Q. Ge, *J. Phys. Chem. C*, 2012, **116**, 7817–7825.

141 J. Ye, C. Liu, D. Mei and Q. Ge, *ACS Catal.*, 2013, **3**, 1296–1306.

142 O. Martin, A. J. Martín, C. Mondelli, S. Mitchell, T. F. Segawa, R. Hauert, C. Drouilly, D. Curulla-Ferré and J. Pérez-Ramírez, *Angew. Chem., Int. Ed.*, 2016, **55**, 6261–6265.

143 T.-y. Chen, C. Cao, T.-b. Chen, X. Ding, H. Huang, L. Shen, X. Cao, M. Zhu, J. Xu and J. Gao, *ACS Catal.*, 2019, **9**, 8785–8797.

144 W. Luo, W. Xie, M. Li, J. Zhang and A. Züttel, *J. Mater. Chem. A*, 2019, **7**, 4505–4515.

145 J. Ye, C.-j. Liu, D. Mei and Q. Ge, *J. Catal.*, 2014, **317**, 44–53.

146 N. Rui, Z. Wang, K. Sun, J. Ye, Q. Ge and C.-j. Liu, *Appl. Catal., B*, 2017, **218**, 488–497.

147 J. Wang, G. Li, Z. Li, C. Tang, Z. Feng, H. An, H. Liu, T. Liu and C. Li, *Sci. Adv.*, 2017, **3**, e1701290.

148 L. Yao, X. Shen, Y. Pan and Z. Peng, *J. Catal.*, 2019, **372**, 74–85.

149 N. Akkharaphatthawon, N. Chanlek, C. K. Cheng, M. Chareonpanich, J. Limtrakul and T. Witoon, *Appl. Surf. Sci.*, 2019, **489**, 278–286.

150 J. L. Snider, V. Streibel, M. A. Hubert, T. S. Choksi, E. Valle, D. C. Upham, J. Schumann, M. S. Duyar, A. Gallo and F. Abild-Pedersen, *ACS Catal.*, 2019, **9**, 3399–3412.

151 M. S. Frei, C. Mondelli, R. García-Muelas, K. S. Kley, B. Puértolas, N. López, O. V. Safonova, J. A. Stewart, D. C. Ferré and J. Pérez-Ramírez, *Nat. Commun.*, 2019, **10**, 1–11.

152 Y.-L. Men, Y. Liu, Q. Wang, Z.-H. Luo, S. Shao, Y.-B. Li and Y.-X. Pan, *Chem. Eng. Sci.*, 2019, **200**, 167–175.

153 H. Jiang, J. Lin, X. Wu, W. Wang, Y. Chen and M. Zhang, *J. CO2 Util.*, 2020, **36**, 33–39.

154 A. R. Richard and M. Fan, *ACS Catal.*, 2017, **7**, 5679–5692.

155 A. R. Richard and M. Fan, *Fuel*, 2018, **222**, 513–522.

156 M. Chen, J. Xu, Y.-M. Liu, Y. Cao, H.-Y. He and J.-H. Zhuang, *Appl. Catal., A*, 2010, **377**, 35–41.

157 D. Liu, Y. Men, J. Wang, G. Kolb, X. Liu, Y. Wang and Q. Sun, *Int. J. Hydrogen Energy*, 2016, **41**, 21990–21999.

158 C. Rameshan, H. Lorenz, L. Mayr, S. Penner, D. Zemlyanov, R. Arrigo, M. Haevecker, R. Blume, A. Knop-Gericke and R. Schlögl, *J. Catal.*, 2012, **295**, 186–194.

159 M. S. Frei, M. Capdevila-Cortada, R. García-Muelas, C. Mondelli, N. López, J. A. Stewart, D. C. Ferré and J. Pérez-Ramírez, *J. Catal.*, 2018, **361**, 313–321.

160 K. K. Ghuman, T. E. Wood, L. B. Hoch, C. A. Mims, G. A. Ozin and C. V. Singh, *Phys. Chem. Chem. Phys.*, 2015, **17**, 14623–14635.

161 L. B. Hoch, T. E. Wood, P. G. O'Brien, K. Liao, L. M. Reyes, C. A. Mims and G. A. Ozin, *Adv. Sci.*, 2014, **1**, 1400013.

162 A. Tsoukalou, P. M. Abdala, D. Stoian, X. Huang, M.-G. Willinger, A. Fedorov and C. R. Müller, *J. Am. Chem. Soc.*, 2019, **141**, 13497–13505.

163 T. Bielz, H. Lorenz, W. Jochum, R. Kaindl, F. Klauser, B. Klotzer and S. Penner, *J. Phys. Chem. C*, 2010, **114**, 9022–9029.

164 A. Posada-Borbón and H. Grönbeck, *Phys. Chem. Chem. Phys.*, 2019, **21**, 21698–21708.

165 C. D. Chang and A. J. Silvestri, *J. Catal.*, 1977, **47**, 249–259.

166 C. D. Chang, *Catal. Rev.: Sci. Eng.*, 1983, **25**, 1–118.

167 C. D. Chang, *Catal. Today*, 1992, **13**, 103–111.

168 I. Yarulina, A. D. Chowdhury, F. Meirer, B. M. Weckhuysen and J. Gascon, *Nat. Catal.*, 2018, **1**, 398.

169 U. Olsbye, S. Svelle, M. Bjørgen, P. Beato, T. V. Janssens, F. Joensen, S. Bordiga and K. P. Lillerud, *Angew. Chem., Int. Ed.*, 2012, **51**, 5810–5831.

170 F. J. Keil, *Microporous Mesoporous Mater.*, 1999, **29**, 49–66.

171 P. Tian, Y. Wei, M. Ye and Z. Liu, *ACS Catal.*, 2015, **5**, 1922–1938.

172 V. Van Speybroeck, K. De Wispelaere, J. Van der Mynsbrugge, M. Vandichel, K. Hemelsoet and M. Waroquier, *Chem. Soc. Rev.*, 2014, **43**, 7326–7357.

173 E. Kianfar, S. Hajimirzaee, S. S. Musavian and A. S. Mehr, *Microchem. J.*, 2020, 104822.

174 W. Wang and M. Hunger, *Acc. Chem. Res.*, 2008, **41**, 895–904.

175 W. Wang, M. Seiler and M. Hunger, *J. Phys. Chem. B*, 2001, **105**, 12553–12558.

176 X. Wu, S. Xu, W. Zhang, J. Huang, J. Li, B. Yu, Y. Wei and Z. Liu, *Angew. Chem., Int. Ed.*, 2017, **56**, 9039–9043.

177 J. Li, Z. Wei, Y. Chen, B. Jing, Y. He, M. Dong, H. Jiao, X. Li, Z. Qin and J. Wang, *J. Catal.*, 2014, **317**, 277–283.

178 A. D. Chowdhury, K. Houben, G. T. Whiting, M. Mokhtar, A. M. Asiri, S. A. Al-Thabaiti, S. N. Basahel, M. Baldus and B. M. Weckhuysen, *Angew. Chem., Int. Ed.*, 2016, **55**, 15840–15845.

179 R. Dessau and R. LaPierre, *J. Catal.*, 1982, **78**, 136–141.

180 I. M. Dahl and S. Kolboe, *J. Catal.*, 1994, **149**, 458–464.

181 B. Arstad and S. Kolboe, *J. Am. Chem. Soc.*, 2001, **123**, 8137–8138.

This journal is © The Royal Society of Chemistry 2021

Catal. Sci. Technol., 2021, **11**, 1665–1697 | **1695**

182 S. Svelle, F. Joensen, J. Nerlov, U. Olsbye, K.-P. Lillerud, S. Kolboe and M. Bjørgen, *J. Am. Chem. Soc.*, 2006, **128**, 14770–14771.

183 A. Hwang and A. Bhan, *Acc. Chem. Res.*, 2019, **52**, 2647–2656.

184 S. Kim, G. Park, M. H. Woo, G. Kwak and S. K. Kim, *ACS Catal.*, 2019, **9**, 2880–2892.

185 S. S. Arora, Z. Shi and A. Bhan, *ACS Catal.*, 2019, 6407–6414.

186 Y. Bhawe, M. Moliner-Marin, J. D. Lunn, Y. Liu, A. Malek and M. Davis, *ACS Catal.*, 2012, **2**, 2490–2495.

187 G. Sastre, *Front. Chem. Sci. Eng.*, 2016, **10**, 76–89.

188 X. Li and J. Jiang, *Phys. Chem. Chem. Phys.*, 2018, **20**, 14322–14330.

189 S. Teketel, M. W. Erichsen, F. L. Bleken, S. Svelle, K. P. Lillerud and U. Olsbye, *Catalysis*, 2014, **26**, 179–217.

190 S. Lee and M. Choi, *J. Catal.*, 2019, **375**, 183–192.

191 F. Goodarzi, I. P. Herrero, G. N. Kalantzopoulos, S. Svelle, A. Lazzarini, P. Beato, U. Olsbye and S. Kegnæs, *Microporous Mesoporous Mater.*, 2020, **292**, 109730.

192 S. S. Arora, D. L. Nieskens, A. Malek and A. Bhan, *Nat. Catal.*, 2018, **1**, 666–672.

193 S. Senger and L. Radom, *J. Am. Chem. Soc.*, 2000, **122**, 2613–2620.

194 R. Gounder and E. Iglesia, *J. Catal.*, 2011, **277**, 36–45.

195 X. Zhao, J. Li, P. Tian, L. Wang, X. Li, S. Lin, X. Guo and Z. Liu, *ACS Catal.*, 2019, **9**, 3017–3025.

196 L. Smith, A. Cheetham, R. Morris, L. Marchese, J. Thomas, P. Wright and J. Chen, *Science*, 1996, **271**, 799–802.

197 J. C. Siria, M. Duran, A. Lledos and J. Bertran, *J. Am. Chem. Soc.*, 1987, **109**, 7623–7629.

198 I. G. Economou, *Ind. Eng. Chem. Res.*, 2002, **41**, 953–962.

199 A. T. Aguayo, A. G. Gayubo, A. M. Tarrío, A. Atutxa and J. Bilbao, *J. Chem. Technol. Biotechnol.*, 2002, **77**, 211–216.

200 A. Zachariou, A. Hawkins, D. Lennon, S. F. Parker, S. K. Matam, C. R. A. Catlow, P. Collier, A. Hameed, J. McGregor and R. F. Howe, *Appl. Catal., A*, 2019, **569**, 1–7.

201 F. Magzoub, X. Li, J. Al-Darwish, F. Rezaei and A. A. Rownaghi, *Appl. Catal., B*, 2019, **245**, 486–495.

202 H. Hernando, C. Ochoa-Hernández, M. Shamzhy, I. Moreno, J. Fermoso, P. Pizarro, J. M. Coronado, J. Čejka and D. P. Serrano, *Catal. Sci. Technol.*, 2019, **9**, 789–802.

203 R. Bingre, R. Li, Q. Wang, P. Nguyen, T. Onfroy and B. Louis, *Catalysts*, 2019, **9**, 545.

204 A. D. Chowdhury, I. Yarulina, E. Abou-Hamad, A. Gurinov and J. Gascon, *Chem. Sci.*, 2019, **10**, 8946–8954.

205 Y. Shen, T. T. Le, D. Fu, J. E. Schmidt, M. Filez, B. M. Weckhuysen and J. D. Rimer, *ACS Catal.*, 2018, **8**, 11042–11053.

206 M. Choi, K. Na, J. Kim, Y. Sakamoto, O. Terasaki and R. Ryoo, *Nature*, 2009, **461**, 246.

207 W. Dai, G. Wu, L. Li, N. Guan and M. Hunger, *ACS Catal.*, 2013, **3**, 588–596.

208 B. P. Hereijgers, F. Bleken, M. H. Nilsen, S. Svelle, K.-P. Lillerud, M. Bjørgen, B. M. Weckhuysen and U. Olsbye, *J. Catal.*, 2009, **264**, 77–87.

209 D. Chen, K. Moljord, T. Fuglerud and A. Holmen, *Microporous Mesoporous Mater.*, 1999, **29**, 191–203.

210 H.-G. Jang, H.-K. Min, J. K. Lee, S. B. Hong and G. Seo, *Appl. Catal., A*, 2012, **437**, 120–130.

211 R. Khare, D. Millar and A. Bhan, *J. Catal.*, 2015, **321**, 23–31.

212 M. Li, Y. Zhang, Y. Luo and X. Shu, *Catal. Commun.*, 2019, **132**, 105805.

213 J. Zhang, H. Zhang, X. Yang, Z. Huang and W. Cao, *J. Nat. Gas Chem.*, 2011, **20**, 266–270.

214 M. Fujiwara, H. Ando, M. Tanaka and Y. Souma, *Appl. Catal., A*, 1995, **130**, 105–116.

215 K. Fujimoto and T. Shikada, *Appl. Catal.*, 1987, **31**, 13–23.

216 T. Inui, T. Takeguchi, A. Kohama and K. Tanida, *Energy Convers. Manage.*, 1992, **33**, 513–520.

217 T. Inui, *Catal. Today*, 1996, **29**, 329–337.

218 R. Diercks, J. D. Arndt, S. Freyer, R. Geier, O. Machhammer, J. Schwartze and M. Volland, *J. Chem. Technol. Biotechnol.*, 2008, **31**, 631–637.

219 A. Corma, F. Melo, L. Sauvanaud and F. Ortega, *Catal. Today*, 2005, **107**, 699–706.

220 Y.-J. Lee, S.-C. Baek and K.-W. Jun, *Appl. Catal., A*, 2007, **329**, 130–136.

221 P. Gao, S. Li, X. Bu, S. Dang, Z. Liu, H. Wang, L. Zhong, M. Qiu, C. Yang and J. Cai, *Nat. Chem.*, 2017, **9**, 1019–1024.

222 P. Gao, S. Dang, S. Li, X. Bu, Z. Liu, M. Qiu, C. Yang, H. Wang, L. Zhong and Y. Han, *ACS Catal.*, 2017, **8**, 571–578.

223 S. Dang, P. Gao, Z. Liu, X. Chen, C. Yang, H. Wang, L. Zhong, S. Li and Y. Sun, *J. Catal.*, 2018, **364**, 382–393.

224 S. Dang, S. Li, C. Yang, X. Chen, X. Li, L. Zhong, P. Gao and Y. Sun, *ChemSusChem*, 2019, **12**, 3582–3591.

225 J. Gao, C. Jia and B. Liu, *Catal. Sci. Technol.*, 2017, **7**, 5602–5607.

226 J. Wang, A. Zhang, X. Jiang, C. Song and X. Guo, *J. CO2 Util.*, 2018, **27**, 81–88.

227 Z. Li, J. Wang, Y. Qu, H. Liu, C. Tang, S. Miao, Z. Feng, H. An and C. Li, *ACS Catal.*, 2017, **7**, 8544–8548.

228 J. Chen, X. Wang, D. Wu, J. Zhang, Q. Ma, X. Gao, X. Lai, H. Xia, S. Fan and T.-S. Zhao, *Fuel*, 2019, **239**, 44–52.

229 X. Liu, M. Wang, C. Zhou, W. Zhou, K. Cheng, J. Kang, Q. Zhang, W. Deng and Y. Wang, *Chem. Commun.*, 2018, **54**, 140–143.

230 C. Jia, W. Fan, X. Cheng, X. Zhao, H. Sun, P. Li and N. Lin, *Phys. Chem. Chem. Phys.*, 2014, **16**, 7538–7547.

231 M. Sedighi and M. Mohammadi, *J. CO2 Util.*, 2019, **35**, 236–244.

232 Y. Ni, Z. Chen, Y. Fu, Y. Liu, W. Zhu and Z. Liu, *Nat. Commun.*, 2018, **9**, 1–7.

233 Z. Li, Y. Qu, J. Wang, H. Liu, M. Li, S. Miao and C. Li, *Joule*, 2019, **3**, 570–583.

234 Y. Wang, L. Tan, M. Tan, P. Zhang, Y. Fang, Y. Yoneyama, G. Yang and N. Tsubaki, *ACS Catal.*, 2018, **9**, 895–901.

235 Y. Wei, C. Yuan, J. Li, S. Xu, Y. Zhou, J. Chen, Q. Wang, L. Xu, Y. Qi and Q. Zhang, *ChemSusChem*, 2012, **5**, 906–912.

236 S. Shanmugam, *BioImpacts*, 2015, **5**, 55.

237 J. Wei, Q. Ge, R. Yao, Z. Wen, C. Fang, L. Guo, H. Xu and J. Sun, *Nat. Commun.*, 2017, **8**, 15174.

1696 | *Catal. Sci. Technol.*, 2021, **11**, 1665–1697

This journal is © The Royal Society of Chemistry 2021

238 X. Wang, G. Yang, J. Zhang, S. Chen, Y. Wu, Q. Zhang, J. Wang, Y. Han and Y. Tan, *Chem. Commun.*, 2016, **52**, 7352–7355.

239 S. C. Yan, S. X. Ouyang, J. Gao, M. Yang, J. Y. Feng, X. X. Fan, L. J. Wan, Z. S. Li, J. H. Ye and Y. Zhou, *Angew. Chem., Int. Ed.*, 2010, **49**, 6400–6404.

240 K. Cheng, W. Zhou, J. Kang, S. He, S. Shi, Q. Zhang, Y. Pan, W. Wen and Y. Wang, *Chem*, 2017, **3**, 334–347.

241 J. Zecevic, G. Vanbutsele, K. P. de Jong and J. A. Martens, *Nature*, 2015, **528**, 245–248.

242 T. Askgaard, J. Norskov, C. Ovesen and P. Stoltze, *J. Catal.*, 1995, **156**, 229–242.

243 K. V. Bussche and G. Froment, *J. Catal.*, 1996, **161**, 1–10.

244 J. Skrzypek, M. Lachowska and H. Moroz, *Chem. Eng. Sci.*, 1991, **46**, 2809–2813.

245 H.-W. Lim, M.-J. Park, S.-H. Kang, H.-J. Chae, J. W. Bae and K.-W. Jun, *Ind. Eng. Chem. Res.*, 2009, **48**, 10448–10455.

246 P. Villa, P. Forzatti, G. Buzzi-Ferraris, G. Garone and I. Pasquon, *Ind. Eng. Chem. Process Des. Dev.*, 1985, **24**, 12–19.

247 K. Klier, V. Chatikavanij, R. Herman and G. Simmons, *J. Catal.*, 1982, **74**, 343–360.

248 G. Graaf, E. Stamhuis and A. Beenackers, *Chem. Eng. Sci.*, 1988, **43**, 3185–3195.

249 C. Ovesen, B. Clausen, J. Schiøtz, P. Stoltze, H. Topsøe and J. K. Nørskov, *J. Catal.*, 1997, **168**, 133–142.

250 P. Rasmussen, P. Holmblad, T. Askgaard, C. Ovesen, P. Stoltze, J. Nørskov and I. Chorkendorff, *Catal. Lett.*, 1994, **26**, 373–381.

251 P. Rasmussen, M. Kazuta and I. Chorkendorff, *Surf. Sci.*, 1994, **318**, 267–280.

252 G. Graaf, P. Sijtsema, E. Stamhuis and G. Joosten, *Chem. Eng. Sci.*, 1986, **41**, 2883–2890.

253 G. Graaf, H. Scholtens, E. Stamhuis and A. Beenackers, *Chem. Eng. Sci.*, 1990, **45**, 773–783.

254 J. Díez-Ramírez, J. Díaz, F. Dorado and P. Sánchez, *Fuel Process. Technol.*, 2018, **173**, 173–181.

255 M. Huš, D. Kopač, N. S. Štefančič, D. L. Jurković, V. D. Dasireddy and B. Likozar, *Catal. Sci. Technol.*, 2017, **7**, 5900–5913.

256 A. G. Hansen, W. J. van Well and P. Stoltze, *Top. Catal.*, 2007, **45**, 219–222.

257 T.-Y. Park and G. F. Froment, *Ind. Eng. Chem. Res.*, 2001, **40**, 4172–4186.

258 T.-Y. Park and G. F. Froment, *Ind. Eng. Chem. Res.*, 2001, **40**, 4187–4196.

259 H. Zhou, Y. Wang, F. Wei, D. Wang and Z. Wang, *Appl. Catal., A*, 2008, **348**, 135–141.

260 A. Gayubo, A. Aguayo, A. Alonso and J. Bilbao, *Ind. Eng. Chem. Res.*, 2007, **46**, 1981–1989.

261 A. Gayubo, A. Aguayo, A. Alonso, A. Atutxa and J. Bilbao, *Catal. Today*, 2005, **106**, 112–117.

262 A. G. Gayubo, A. T. Aguayo, A. E. Sánchez del Campo, A. M. Tarrío and J. Bilbao, *Ind. Eng. Chem. Res.*, 2000, **39**, 292–300.

263 A. G. Gayubo, A. T. Aguayo, M. Castilla, M. Olazar and J. Bilbao, *Chem. Eng. Sci.*, 2001, **56**, 5059–5071.

264 A. G. Gayubo, A. T. Aguayo, A. L. Morán, M. Olazar and J. Bilbao, *AIChE J.*, 2002, **48**, 1561–1571.

265 A. G. Gayubo, A. T. Aguayo, M. Castilla, A. L. Moran and J. Bilbao, *Chem. Eng. Commun.*, 2004, **191**, 944–967.

266 M. Kaarsholm, B. Rafii, F. Joensen, R. Cenni, J. Chaouki and G. S. Patience, *Ind. Eng. Chem. Res.*, 2010, **49**, 29–38.

267 M.-K. Lee, J. Kim, J.-H. Ryu, Y.-S. Yoon, C.-U. Kim, S.-Y. Jeong and I.-B. Lee, *Ind. Eng. Chem. Res.*, 2019, **58**, 13227–13238.

268 A. R. Bos, P. J. Tromp and H. N. Akse, *Ind. Eng. Chem. Res.*, 1995, **34**, 3808–3816.

This journal is © The Royal Society of Chemistry 2021

Catal. Sci. Technol., 2021, **11**, 1665–1697 | 1697